FORMATION OF MICROPOROSITY
IN
CASTINGS

by

Ronald A. Entwistle, B. Sc.
Queen's University, Kingston,
(1974)

A thesis submitted to the Faculty of Graduate Studies
and Research in partial fulfilment of the
requirements for the degree of
Master of Engineering

Department of Metallurgical Engineering,
McGill University,
Montreal, Canada.

August 1976

ABSTRACT

An investigation on microporosity in castings was carried out on an Al - 4.5% Cu alloy system. The amount, type and distribution of microporosity in ingots, cast both in air and various levels of vacuum, is presented, with a standard density technique employed as the major experimental method to quantitatively measure microporosity.

Results indicate there is a distribution of porosity within every ingot; a distribution, that is reproducible and dependent upon the casting conditions. For the gas levels 0.02 - 0.46 ml H_2/100 gm Al (S.T.P.), superheat and mould temperature were found to affect the distribution and amount of porosity the most.

Macro and microexamination revealed information regarding the nature of porosity. Ingots displaying a fine grain structure exhibited fine interdendritic porosity, while ingots of a coarser grained structure showed a layer type which was intergranular in nature.

An analysis comparing porosity to various solidification parameters, such as dendrite arm spacings and local solidification times are presented. The results indicate that porosity is only a function of these variables for a fine grain structure where the porosity was fine and interdendritic in nature.

RESUME

Nous avons étudié la microporosité dans les pièces couleés en alliage Al-4.5%Cu. Nous avons utilisé une technique standard, pour mesurer la densité, comme méthode expérimentale principale pour mesurer la microporosité. Nous présentons des résultats sur le taux, le type et la distribution de la microporosité dans les lingots coulés dans l'atmosphère ambiante et sous vide à différents veaux.

Les résultats indiquent que la porosité est distribuée dans tous les lingots d'une façon reproductible et dépendante des conditions de couleé.

Quand le niveau de gaz se situe entre 0.02 et 0.46 ml H_2/100 gm Al (S.T.P.)les effets de la surchauffe et de la température du moule sont les plus prononcés.

La micro et la macroexamination révèlent la nature de la porosité. Les lingots d'une structure à grain fin présentent une porosité fine et dentrique, tandis que les lingots d'une structure à gros grains présentent une porosité intergranulaire et arrangeé en couches.

Nous avons comparé la porosité à différentes paramètres della solidification comme l'espace entre dendrites et le temps de solidification local. Cette analyse montre que la porosité dépend de ces paramètres seulement quand il s'agit d'une structure à grain fin où la porosité est fine et interdentrique.

ACKNOWLEDGEMENTS

The author would like to thank Dr. J. E. Gruzleski for the immense help and guidance which has helped very much.

Also thanks are due to Dr. W. M. Williams and other members of the staff of the Department of Mining and Metallurgical Engineering for creating the atmosphere which made this work easier.

The assistance of Mr. M. Knoepful for his technical knowledge and Mr. R. Barnhurst for his assistance in the casting experiments are greatly appreciated.

The author also wishes to thank Mr. B. Altshuller and Mr. I. Amey of Alcan International Ltd., Kingston, for their sincere help, particularly in supplying the gas and spectrographic analyses.

Thanks to all others for their assistance, it was greatly appreciated.

TABLE OF CONTENTS

Page

ABSTRACT i

RESUME ii

ACKNOWLEDGEMENTS iii

TABLE OF CONTENTS iv

LIST OF FIGURES vii

LIST OF TABLES xv

CHAPTER I. INTRODUCTION 1

1.1 DESCRIPTION 1

1.2 THEORY OF MICROPORE FORMATION 9

1.2.1 Heterogeneous Nucleation 10
1.2.2 Homogeneous Nucleation 12

1.2.2.1 Gas Nucleation 15
1.2.2.2 Nucleation - A feeding problem 16

1.3 PAST EXPERIMENTAL RESEARCH 23

1.3.1 Freezing Range 26
1.3.2 Gas Content 29
1.3.3 Solidification Rates 31
1.3.4 Pressure 33

1.4 AIMS OF THE PRESENT INVESTIGATION ...34

CHAPTER II. EXPERIMENTAL PROCEDURE 36

2.1 AIR MELT EXPERIMENTS 38

2.1.1 Alloy Preparation 38
2.1.2 Melting Apparatus 39
2.1.3 Moulds 41
2.1.4 Casting Procedure 41
2.1.5 Sampling 43

2.2 VACUUM MELT EXPERIMENTS 45

2.2.1 Melting Equipment 45
2.2.2 Vacuum Casting Unit 47
2.2.3 Vacuum Casting 49

Page

2.3 DENSITY AND METALLOGRAPHIC ANALYSIS .54

2.3.1 Density Measurement 54
2.3.2 Metallographic Analysis 60
2.3.3 Scanning Electron Microscopy .63
2.3.4 Computer Modelling 64

CHAPTER III. RESULTS 65

3.1 TREATMENT OF EXPERIMENTAL DATA 65

3.2 POROSITY DISTRIBUTION PROFILES 67

3.2.1 Air Castings 67
3.2.2 Vacuum Castings 80

3.3 RELATIONSHIP OF POROSITY TO STRUCTURE 96

3.3.1 Macrostructure 96
3.3.2 Microstructure 99

3.4 INFLUENCE OF SOLIDIFICATION PARAMETERS 109

3.4.1 Secondary Dendrite Arm Spacings 110
3.4.2 Local Solidification Time ...114

CHAPTER IV. DISCUSSION 123

4.1 MICROPOROSITY 123

4.1.1 Suitability of Al-4.5% Cu to the study 124
4.1.2 Sampling Techniques for Microporosity 128

4.2 RELATIONSHIP OF POROSITY TO STRUCTURE 132

4.2.1 Air Castings 133
4.2.2 Vacuum Casting 142

4.3 EFFECT OF CASTING VARIABLES ON PORE FORMATION 147

4.3.1 Initial Gas Content 147
4.3.2 Solidification Rates 150
4.3.3 Applied Pressures 151

Page

4.4 HETEROGENEOUS AND/OR HOMOGENEOUS NUCLEATION OF PORES 153

CHAPTER V. CONCLUSIONS AND SUGGESTIONS FOR FUTURE WORK 157

REFERENCES 162

APPENDIX 165

LIST OF FIGURES

		Page
FIGURE 1.1	Examples of porosity (a) gas porosity (b) shrinkage porosity	2
FIGURE 1.2	Effect of porosity on mechanical properties: (a) external defect (b) internal defect	3
FIGURE 1.3	Solidification of a Short Freezing Range Alloy: (a) start of solidification (b) intermediate time in solidification (c) end of solidification	6
FIGURE 1.4	Solidification of a Long Freezing Range Alloy: (a) start of solidification (b) settling of grains (c) end of solidification	7
FIGURE 1.5	Microporosity in Al - 4.5% Cu. Porosity exists in $CuAl_2$ region of cast. Unetched (X170)	8
FIGURE 1.6	Examples of Heterogeneous Nucleation (a) entrapment of air in cast stream (b) evolution off mould wall (c) nucleation of pore on inclusions	11
FIGURE 1.7	Homogeneous Nucleation	13
FIGURE 1.8	Feeding Mechanisms in Open Topped Ingots	18
FIGURE 1.9	Feeding of Liquid Metal into an Interdendritic Channel	20
FIGURE 1.10	Schematic of Burst Feeding [12,21]	24
FIGURE 1.11	Schematic of Solid Feeding [12,21]	25
FIGURE 1.12	Mg-Zn phase diagram	28
FIGURE 2.1	Al-Cu phase diagram	37

Page

FIGURE 2.2 Moulds Used in Experiments
(a) Cylindrical Mould
(b) "Ransley" Mould
(c) Spectrographic Mould 44

FIGURE 2.3 Vacuum Furnace Induction Unit
(a) Control Panel
(b) Vacuum Chamber 46

FIGURE 2.4 Mould Heater Unit 48

FIGURE 2.5 Vacuum Experimental Set-up 50

FIGURE 2.6 Sectioning of Ingot for Density Measurements 55

FIGURE 2.7 Density Apparatus 57

FIGURE 3.1 Typical porosity result in an ingot where porosity is given for every nodal point. Pouring temperature 700°C (973K), Mould temperature 25°C (298K), Hydrogen concentration 0.19 ml H_2/100 gm Al (S.T.P.), Atmospheric pressure 66

FIGURE 3.2 Porosity profile of ingot shown in Figure 3.1. In producing this graph, three assumptions were made:
1) porosity at the mould wall is zero
2) values of porosity are those at the centre of each individual sample
3) linearity of porosity exists between samples 71

FIGURE 3.3 Effect of mould temperature on porosity distribution in an atmospheric cast ingot poured at low superheat. Pouring temperature 700°C (973K), Hydrogen concentration 0.19 ml H_2/100 gm Al (S.T.P.), Mould temperature 70°C (343K) 72

FIGURE 3.4 Effect of mould temperature on porosity distribution in an atmospheric cast ingot poured at low superheat. Pouring temperature 700°C (973K), Hydrogen concentration 0.19 ml H_2/100 gm Al (S.T.P.), Mould temperature 240°C (513K) 73

Page

FIGURE 3.5 Effect of gas content on porosity distribution in an atmospheric cast ingot poured at low superheat. Pouring temperature 700°C (973K), Mould temperature 25°C (298K), Hydrogen concentration 0.30 ml H_2/100 gm Al (S.T.P.) 74

FIGURE 3.6 Porosity profile of atmospheric cast ingot poured at a high superheat. Pouring temperature 825°C (1098K), Mould temperature 25°C (298K), Hydrogen concentration 0.46 ml H_2/100 gm Al (S.T.P.) 75

FIGURE 3.7 Effect of mould temperature on porosity distribution in an atmospheric cast ingot poured at high superheat. Pouring temperature 825°C (1098K), Mould temperature 250°C (523K), Hydrogen concentration 0.46 ml H_2/100 gm Al (S.T.P.) 76

FIGURE 3.8 Effect of mould temperature on porosity distribution in an atmospheric cast ingot poured at high superheat. Pouring temperature 825°C (1098K), Mould temperature 400°C (673K), Hydrogen concentration 0.46 ml H_2/100 gm Al (S.T.P.) 77

FIGURE 3.9 Effect of very high superheats on porosity distribution in an atmospheric cast ingot. Pouring temperature 950°C (1223K), Mould temperature 250°C (523K), Hydrogen concentration 0.45 ml H_2/100 gm Al (S.T.P.) 78

FIGURE 3.10 Effect of grain refining on porosity distribution in an atmospheric cast ingot poured at high superheat. Pouring temperature 825°C (1098K), Mould temperature 250°C (523K), Hydrogen concentration 0.23 ml H_2/100 gm Al (S.T.P.) 79

Page

FIGURE 3.11 Vacuum degassing of hydrogen from Al - 4.5% Cu. Melt temperature 700°C (973K), Pressure over melt 0.25 torr (44.4Pa), Area to volume ratio of liquid bath 81

FIGURE 3.12 Effect of reduced gas content on porosity distribution in an ingot cast under atmospheric pressure. Pouring temperature 700°C (973K), Mould temperature 200°C (473K), Hydrogen concentration 0.02 ml H_2/100 gm Al (S.T.P.) 88

FIGURE 3.13 Effect of reduced pressure on porosity distribution in a cast ingot poured at low superheat. Pouring temperature 700°C (973K), Mould temperature 275°C (548K), Hydrogen concentration 0.07 ml H_2/100 gm Al (S.T.P.), Pressure over cast 0.20 torr (26.6Pa) 89

FIGURE 3.14 Effect of reduced pressure on porosity distribution. Pouring temperature 700°C (973K), Mould temperature 300°C (573K), Hydrogen concentration 0.03 ml H_2/100 gm Al (S.T.P.), Pressure over cast 1.50 torr (200 Pa), Mean porosity 0.7% 90

FIGURE 3.15 Effect of pressure on porosity distribution. Pouring temperature 700°C (973K), Mould temperature 280°C (553K), Hydrogen concentration 0.03 ml H_2/100 gm Al (S.T.P.), Pressure over cast 760 torr (101.3KPa), Mean porosity 0.5% .91

FIGURE 3.16 Effect of reduced pressure on porosity distribution in an ingot poured at high superheat. Pouring temperature 825°C (1098K), Mould temperature 275°C (548K), Hydrogen concentration o.14 ml H_2/100 gm Al (S.T.P.), Pressure over cast 100 torr (13.3KPa) 92

Page

FIGURE 3.17 Porosity distribution in an ingot poured at high superheat. Pouring temperature 825°C (1098K), Mould temperature 275°C (548K), Hydrogen concentration 0.14 ml H_2/100 gm Al (S.T.P.), Pressure over cast 760 torr (101.3 KPa) 93

FIGURE 3.18 Effect of mould temperature on porosity distribution in an ingot poured under reduced pressure. Pouring temperature 700°C (973K), Hydrogen concentration 0.02 ml H_2/100 gm Al (S.T.P.), Pressure over cast 0.20 torr (26.6Pa), Mould temperature 90°C (363K), Mean porosity 0.4% 94

FIGURE 3.19 Effect of mould temperature on porosity distribution in an ingot poured under reduced pressure. Pour temperature 700°C (973K), Hydrogen concentration 0.02 ml H_2/100 gm Al (S.T.P.), Pressure over cast 0.20 torr (26.6Pa), Mould temperature 525°C (798K), Mean porosity 0.5% 95

FIGURE 3.20 Porous ingot surface of ingot described in Figure 3.19 (X3/4) 100

FIGURE 3.21 Fine columnar and equiaxed structure, typical of ingots that displayed low amounts of porosity. Pour temperature 700°C (973K), Mould temperature 200°C (473K), Hydrogen concentration 0.02 ml H_2/100 gm Al (S.T.P.), Pressure over cast 760 torr (101.3KPa) (X3/4) ... .100

FIGURE 3.22 Micrograph of an atmospheric cast ingot showing a high degree of layer porosity. Pouring temperature 950°C (1223K), Mould temperature 250°C (523K). Unetched (X20) 101

FIGURE 3.23 Micrograph of a region of layer porosity showing its intergranular nature. Pouring temperature 950°C (1223K), Mould temperature 250°C (523K). Dilute Keller's etch (X40) 102

Page

FIGURE 3.24 Macrostructure of an atmospheric cast ingot exhibiting coarse equiaxed grains in the centre. Pouring temperature 825°C (1098K), Mould temperature 25°C (298K). 0.1% NaOH etch (X9/10) 103

FIGURE 3.25 Macrostructure of an atmospheric cast ingot exhibiting coarse columnar grains. Pouring temperature 950°C (1098K), Mould temperature 250°C (523K), 0.1% NaOH etch (X9/10) 103

FIGURE 3.26 Macrostructure of a vacuum cast ingot exhibiting higher porosity in regions of smaller equiaxed grains. Pouring temperature 700°C (973K), Mould temperature 300°C (573K), Hydrogen concentration 0.03 ml H_2/100 gm Al (S.T.P.), Pressure over cast 0.20 torr (26.6Pa) 104

FIGURE 3.27 Microstructure of a vacuum cast ingot showing fine interdendritic porosity. Unetched (X170) 105

FIGURE 3.28 Microstructure of an atmospheric cast ingot showing fine interdendritic porosity in the direction of the heat flow, Unetched (X170).....106

FIGURE 3.29 Scanning electron micrographs of a "hot tear" region showing the dendritic lining of the pore a) X84 b) X168 107

FIGURE 3.30 Scanning electron micrograph of a "gas type" pore a) X 42 b) X 168 108

FIGURE 3.31 Percent porosity as a function of secondary dendrite arm spacing. Secondary dendrite arm spacing measurements appear in Table 3.6 116

FIGURE 3.32 Percent porosity as a function of secondary dendrite arm spacing for ingot which displayed a fine grain structure 117

FIGURE 3.33 Percent porosity as a function of local solidification time (31). Pouring temperature 700°C (973K), Mould temperature 25°C (298K) 118

Page

FIGURE 3.34 Local Solidification Time as a function of position in the mould. Pouring temperature 700°C (973K), Mould temperature 25°C (298K) 119

FIGURE 3.35 Local Solidification Time as a function of position in the mould. Pouring temperature 950°C (1223K), Mould temperature 25°C (298K) 120

FIGURE 3.36 Percent porosity versus Solidification Time for various fraction solids. Pouring temperature 700°C (973K), Mould temperature 25°C (298K) 121

FIGURE 3.37 Percent porosity versus Solidification Time for various fractions solids. Pouring temperature 950°C (1223K), Mould temperature 25°C (298K) 122

FIGURE 4.1 Solubility of hydrogen in solid and liquid aluminum 125

FIGURE 4.2 Effect of thermal conductivity on the solidification of a metal 126

FIGURE 4.3 Effect of freezing range on the solidification of a metal 127

FIGURE 4.4 Sectioning of a cylindrical ingot to obtain a representative sample for the measurement of porosity 130

FIGURE 4.5 Sectioning of various types of ingots to obtain a representative sample for the measurement of porosity 131

FIGURE 4.6 Schematic illustration of the development of columnar grains in an ingot 136

FIGURE 4.7 Expected porosity profile of an ingot which solidified in a manner similar to that shown in Figure 4.6 138

FIGURE 4.8 Schematic illustration of development of equiaxed grains in the centre of an ingot 140

Page

FIGURE 4.9 Expected porosity profile of an ingot which solidified in a manner similar to that shown in Figure 4.8 141

FIGURE 4.10 Schematic of equiaxed grains settling both in air and vacuum at various levels of gas concentration 146

FIGURE 4.11 Critical gas content to nucleate a pore and the rate of solidification required to form a shrinkage or gas type pore 149

FIGURE 4.12 Macrostructure of vacuum cast ingot where the top froze over. Pouring temperature 700°C (973K), Mould temperature 275°C (548K), Hydrogen concentration 0.07 ml H_2/100 gm Al (S.T.P.), Pressure over cast 0.20 torr (26.6Pa) 154

LIST OF TABLES

Page

TABLE 1.1 Minimum temperature gradients required to reduce porosity in various alloys 32

TABLE 2.1 Materials used in Investigation 40

TABLE 2.2 Air Casting Experiments 42

TABLE 2.3 Vacuum Casting Experiments 51

TABLE 2.4 Gas and Spectrographic Analysis 53

TABLE 2.5 Calibration of Density Apparatus 59

TABLE 2.6 Effect of Segregation in Al-4.5% Cu 61

TABLE 3.1 Mean Values of Porosity in Air Castings..68

TABLE 3.2 Mean Values of Porosity in Vacuum Castings 82

TABLE 3.3 Effect of Initial Gas Content on Porosity 84

TABLE 3.4 Effect of Pressure on Mean Porosity 86

TABLE 3.5 Grain Structure of the Castings 97

TABLE 3.6 Dendrite Arm Spacings
Air Melts 111
Vacuum Melts 112

TABLE 3.7 Secondary Dendrite Arm Spacings as a function of Local Solidification Time 113

CHAPTER I

INTRODUCTION

1.1 DESCRIPTION

Microporosity occurs as fine holes or pores distributed within a material, and as will be discussed later, it is the result of either gas rejection, unfed shrinkage or a combination of both. It also is a common short range phenomenon in cast metals, extending over distances the order of the grain or dendrite size.

Micropores originate during solidification, and their shape in the cast product (Figures 1.1a,b) will be of a form determined by gas rejection and/or poor feeding. A shrinkage cavity will appear as a jagged hole or spongy area lined with dendrites while a gas cavity will appear as a spherical, flattened or elongated hole.

It is generally assumed that microporosity [1,17] can be deleterious to the mechanical properties of various alloys, but as yet there has been no safe minimum amount established. These voids will affect the mechanical properties because they behave as stress raisers (Figures 1.2a,b), and, in critically loaded sections, will seriously affect the strengths of the section. The effects are similar to

Figure 1.1 Examples of porosity.

(a) Gas porosity in an Al alloy die cast. (9.0% Si, 3.5% Cu, rest Al)

(b) Shrinkage porosity in an Mg alloy weld joint. (10% Al, 1.0% Zn, 0.02% Mn, rest Mg).

Source - Metals Handbook Volume 7.

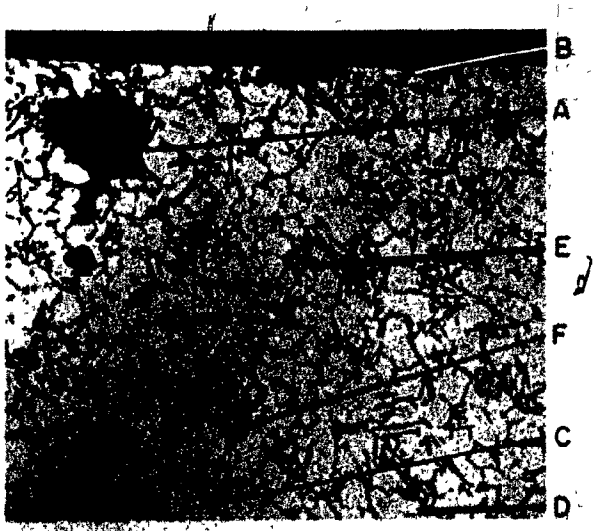

0.5% hydrofluoric acid • 130×

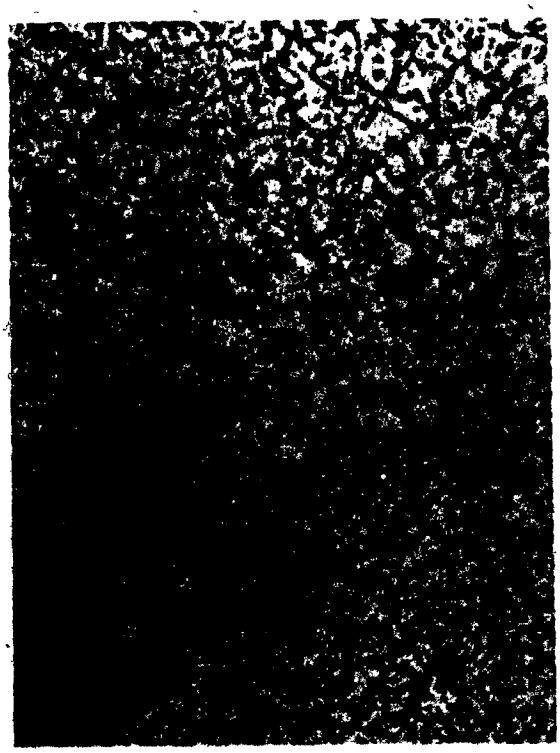

Phospho-picral etchant (121) 65×

Figure 1.2 Effect of porosity on mechanical properties

(a) external defect

(b) internal defect

STRESS RAISERS

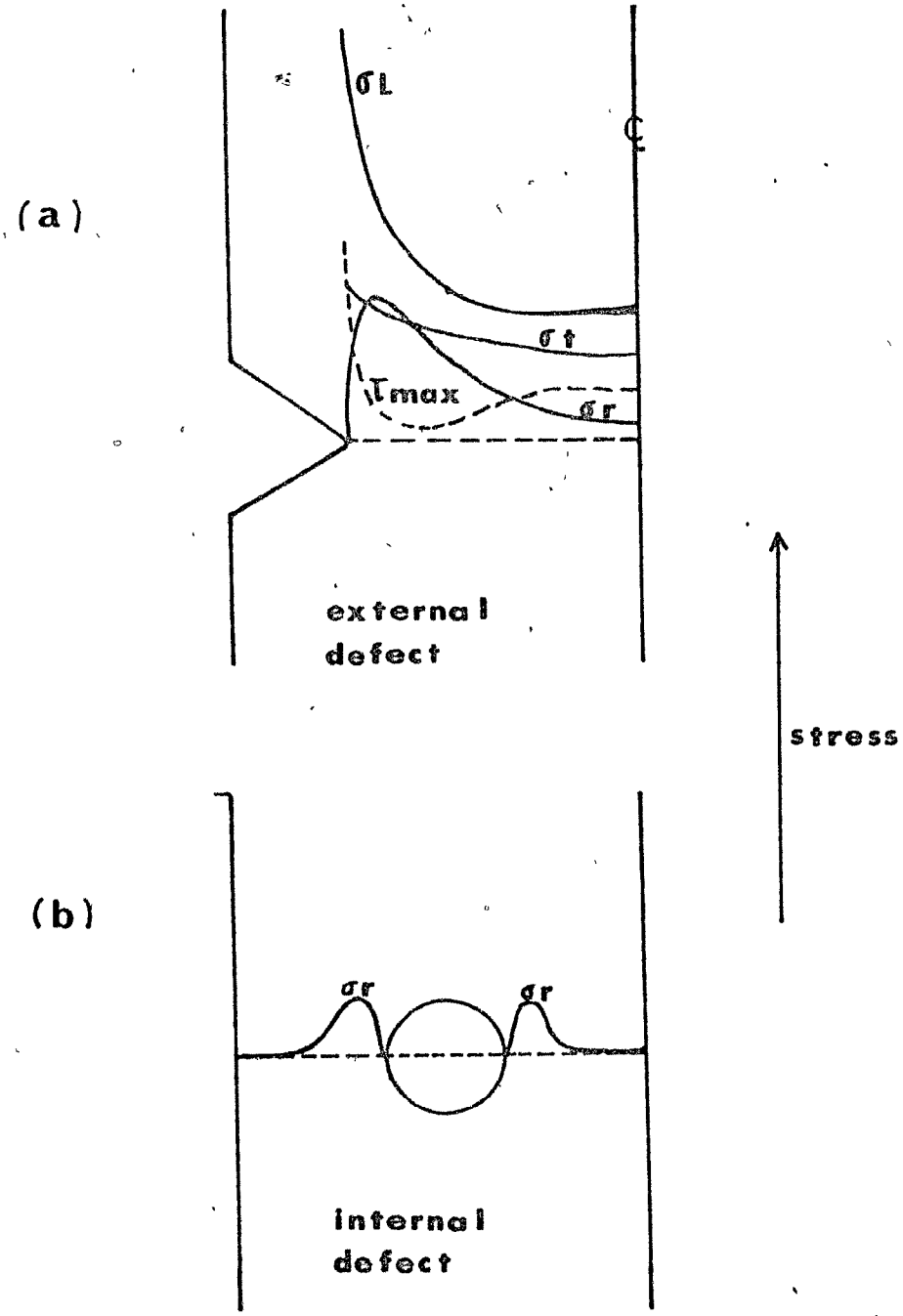

those occurring at an external defect or notch (Figures 1.2a). In this case, the longitudinal and tangential normal stresses (σ_L & σ_T) and the maximum shear stress (λ_{max}) peak at the root of the notch, while the radial stress (σ_r) peaks below the root of the notch. A more severe notch will tend to intensify these maxima. In the case of an internal defect or micropore (Figure 1.2b), the stresses will peak slightly away from the edge of the defect and then drop off rapidly.

Under static loading, the highly stressed metal will yield plastically at the defect passing high stresses to other parts of the section until failure occurs. With fatigue loading, the material will be stressed below its elastic limit and yielding will occur on a much smaller scale. A crack will then be initiated before the stress pattern can change to relieve the concentrated stresses.

Past research [2-5] on microporosity has shown that it does not occur in all metal and alloy systems. The presence and amount of microporosity appears to depend on the mode of freezing, ie. whether the alloy has a short or long freezing range. Microporosity is not a problem for metals and alloys of short freezing ranges because they solidify as illustrated in Figure 1.3. After casting into the mould, solidification begins with the formation of tiny

crystallites (chill zone) at the mould wall. Then the most favourably oriented crystals will grow rapidly into the melt forming a uniform front: the rate of movement and direction of this front being proportional to the rate of heat extraction. For a certain temperature gradient in the cast, the depth of this front will depend on the degree of undercooling and the freezing range. Although microporosity is not usually a problem in these alloy systems, a common defect is typically gross shrinkage porosity or "pipe" which occurs in the last area to solidify.

Microporosity will be common in long freezing range alloys because of the system's mode of solidification (Figure 1.4). Solidification again commences with the formation of a chill zone; however, the front of solidification will be more uneven, with solid dendrite arms protruding into the liquid. The tips of the arms will be at the liquidus temperature with the roots at the eutectic temperature. The length of these arms will be proportional to the temperature gradient. Microporosity that occurs will be in these roots, because as the arms grow further out, they cut off feed metal and allow pore formation in the eutectic areas. This is supported by Figure 1.5 which illustrates that porosity is associated with the eutectic regions in Al-4.5%Cu alloy.

Figure 1.3 Solidification of a Short Freezing Range Alloy

(a) start of solidification

(b) intermediate time in solidification

(c) end of solidification

SOLIDIFICATION OF A SHORT FREEZING RANGE ALLOY

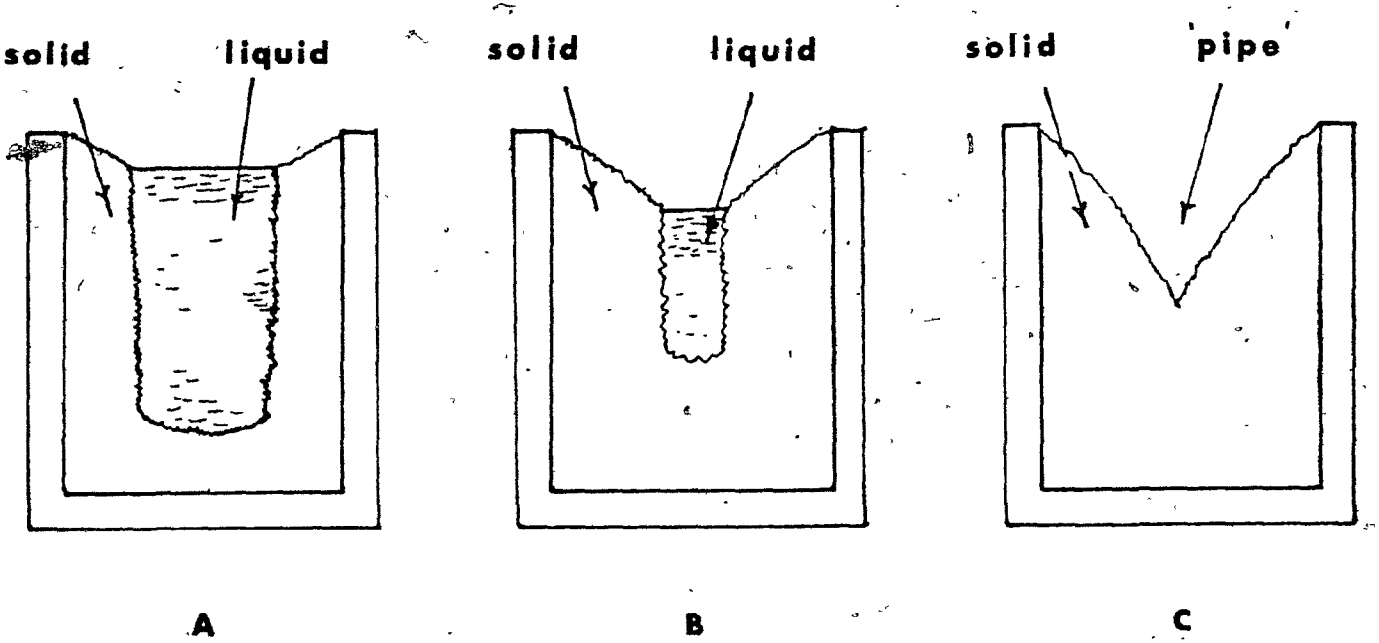

Figure 1.4 Solidification of a Long Freezing Range Alloy

(a) start of solidification

(b) settling of grains

(c) end of solidification

SOLIDIFICATION OF A LONG FREEZING RANGE ALLOY

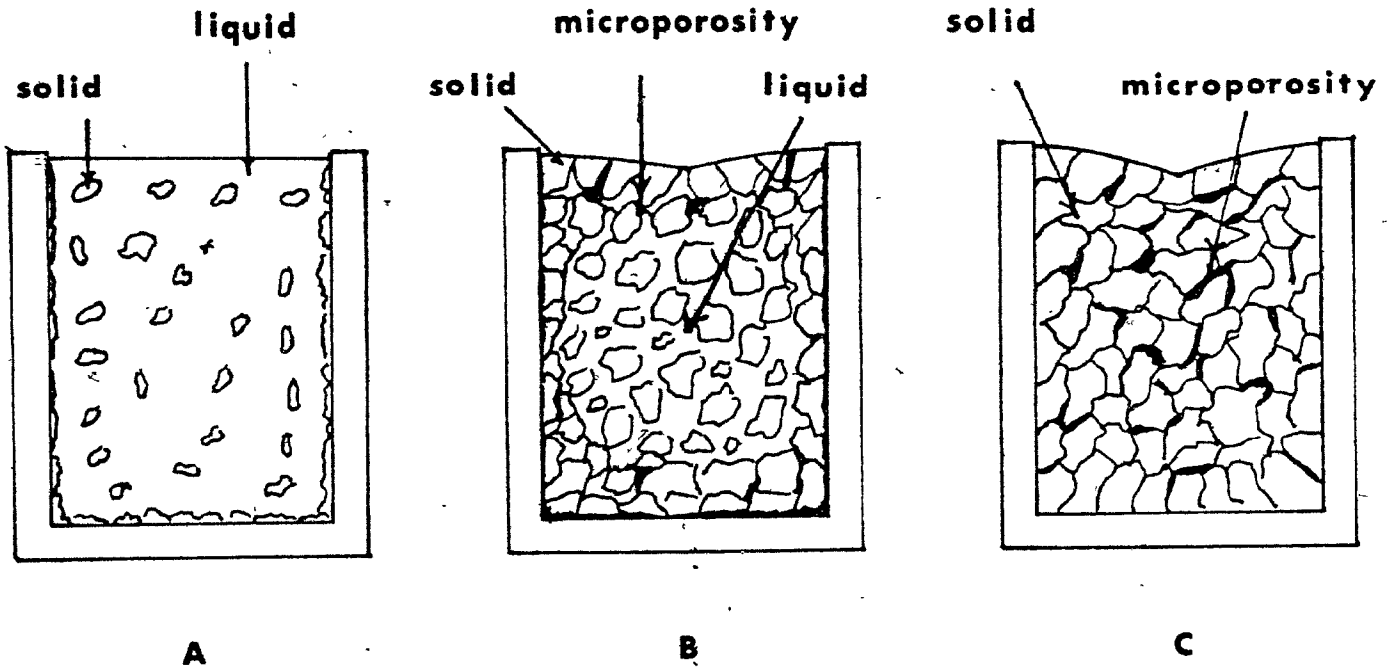

Figure 1.5 Microporosity in Al - 4.5% Cu. Porosity exists in $CuAl_2$ region of cast. Unetched x 170

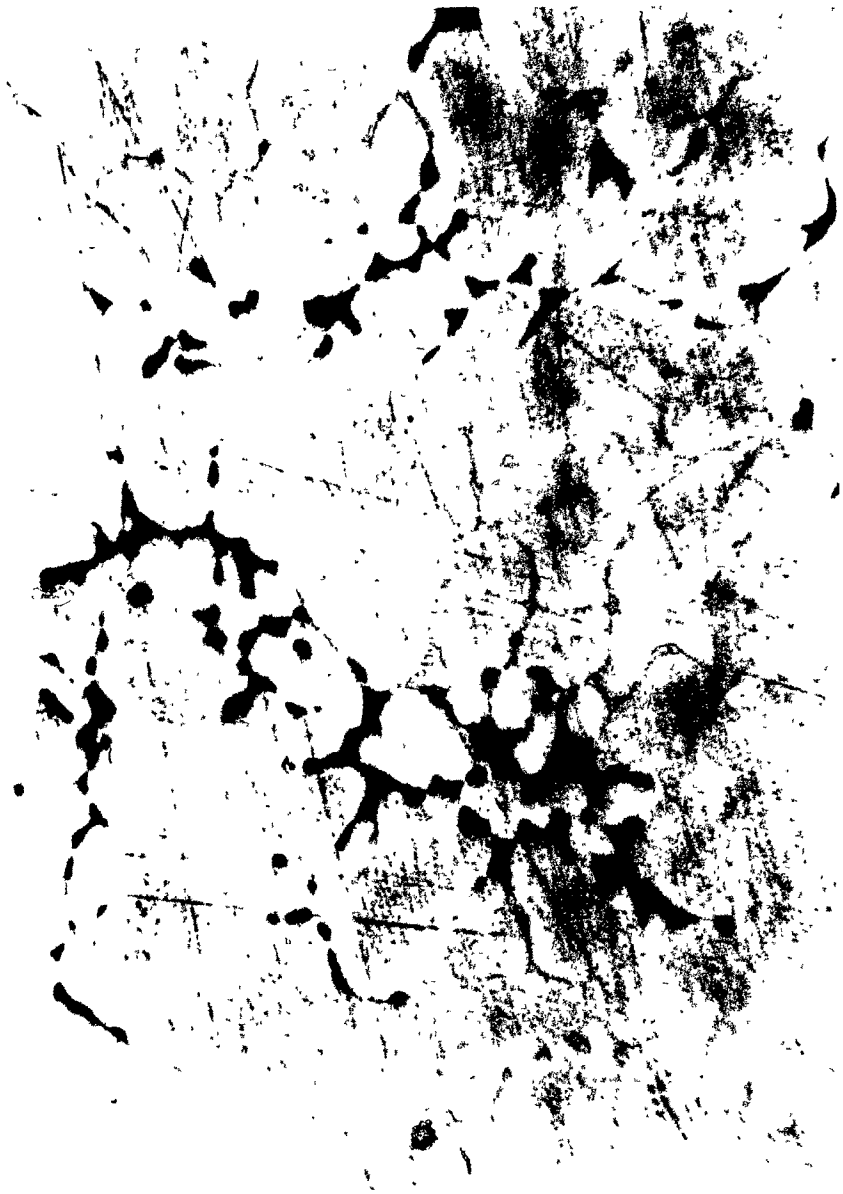

1.2 THEORY OF MICROPORE FORMATION

The driving forces for micropore formation (dissolved gas or shrinkage) have been extensively debated. Quantitative treatment of the problem considers gas bubbles and shrinkage cavities simply as pores without reference to their specific origin.

Pore formation is possible by a mechanism of nucleation, either heterogeneous or homogeneous. In heterogeneous nucleation pores are formed by foreign nuclei (air bubbles, inclusions) and in homogeneous nucleation pores are formed without the aid of any nucleus.

Pores may nucleate at any time in the solidification process. The time at which they form will, however, determine their shape in the final cast. Pores formed early in solidification will most likely have time to escape (Appendix 1) leaving no trace in the final product while pores formed late in solidification will freeze in the solid in their original form. Pores formed at intermediate times will solidify into the solid in a different form from the original. For example, a pore created as a gas bubble at the bottom of the mould may finally appear in the top of the solidified cast as a shrinkage type pore due to its interference with a shrinkage pore during flotation.

1.2.1 Heterogeneous Nucleation

Heterogeneous nucleation as illustrated in Figure 1.6 is most important during the early stages of solidification although there is evidence that it can also be important during the final stages [7]. Examples of heterogeneous nucleation during the early stages of solidification are the entrapment of bubbles in the liquid stream and gas evolution by materials (eg. water vapour in sand moulds). This type of nucleation has been termed non-nucleation by Campbell [7]. Those pores formed early in solidification will be governed by the equation below:

$$Pi - Pe = \frac{2\gamma}{r} \qquad (1.1)$$

where Pi and Pe are the internal and external pressures respectively on a pore of radius r, and γ is the gas-liquid surface tension. If the radius of the pore created by heterogeneous nucleation is less than r the pore will disappear whereas if the pore radius is greater than r, the pore will grow. A pore of radius exactly equal to r will remain and act as a pore nucleus for further pore formation.

Another common type of pore formation by heterogeneous nucleation is the nucleation of pores on inclusions

Figure 1.6 Examples of Heterogeneous Nucleation

a) entrapment of air in cast stream

b) evolution off mould wall

c) nucleation of pore on inclusions

HETEROGENEOUS

NUCLEATION

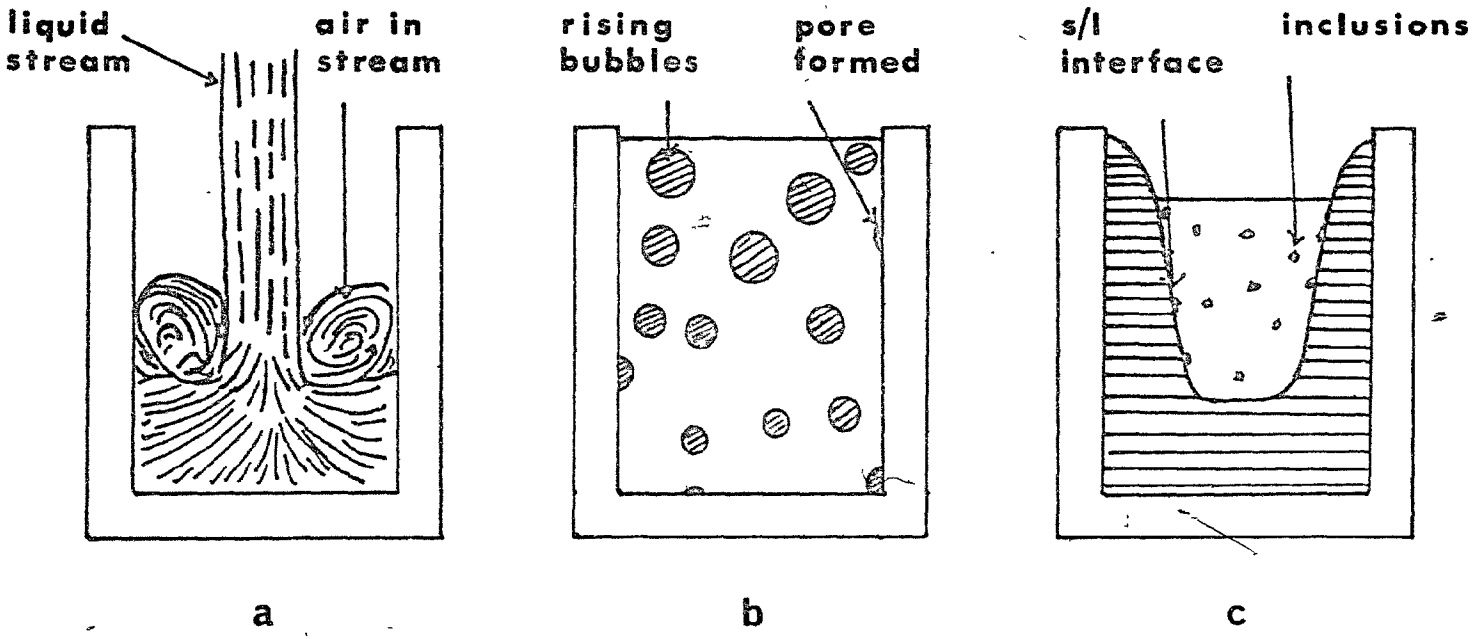

that exist in the melt. This type of pore formation is also possible late in solidification and occurs in the mushy zone; for example, when Al_2O_3 inclusions are swept out in front of the advancing solid-liquid front.

1.2.2 Homogeneous Nucleation

At a time in solidification when pockets of liquid metal are completely surrounded by solid, pore formation must take place by homogeneous nucleation if no nuclei are present.

Shrinkage and gas rejection are believed to be the principal driving forces of nucleation and growth of such a pore. To originate a pore in the liquid phase, a force must be supplied to overcome the forces that would collapse a void. As mentioned in the previous section, Equation 1.1 holds here.

$$Pi - Pe = \frac{2\gamma}{r} \qquad (1.1)$$

Previous work [6,8] shows that Pi (internal pressure) is the sum of the pressures : Pg, the equilibrium gas pressure and Ps, the shrinkage pressure. The external pressure, Pe, is the sum of the pressures : Patm, the atmospheric pressure and Pm, the pressure due to the metallostatic head. As illustrated in Figure 1.7, equation 1.1 can be rewritten as[25]:

Figure 1.7 Homogeneous Nucleation

HOMOGENEOUS

NUCLEATION

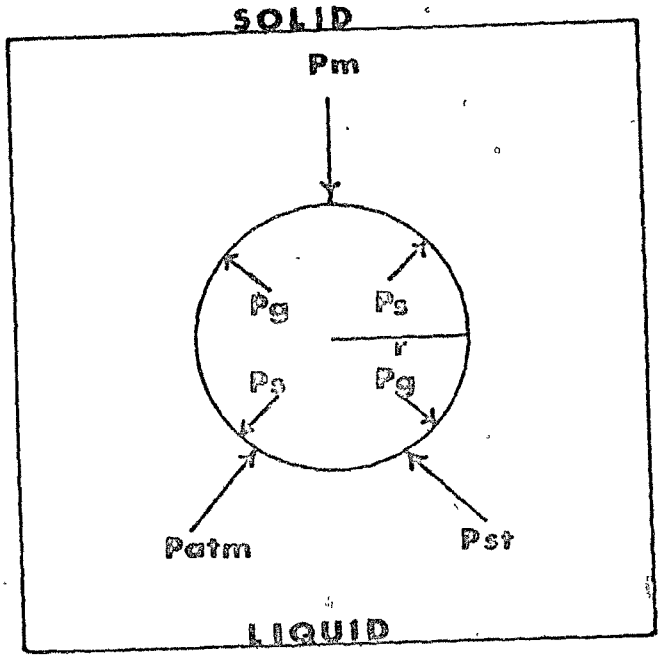

LIQUID SURROUNDED BY SOLID

FOR PORE FORMATION

$$Pg + Ps - (Patm + Pm) \geqq Pst$$

$$Pg + Ps - (Patm + Pm) = \frac{2\gamma}{r} \qquad (1.2)$$

Since a pore cannot develop from zero radius due to the fact that at zero radius the surface tension term ($\frac{2\gamma}{r}$) approaches infinity, some other mechanism must explain the growth of a pore from zero radius to a finite size r. In heterogeneous nucleation, pores of radius r are brought in from outside which is not possible in homogeneous nucleation. However, a hydrogen pore of finite radius can spring into a size r due to build-up and interaction of gas molecules in a localized region of the liquid. Once formed, the pores will be governed by the pressure relationship above.

For a specific location in the mould the atmospheric pressure, metallostatic head and $\frac{2\gamma}{r}$ factor will be essentially constant and the conditions for pore nucleation are given by:

$$Pg + Ps = P^* \qquad (1.3)$$

where P^* is the initial pressure required to nucleate a void. Thus nucleation of a pore can be looked on as the result involving either gas nucleation, unfed shrinkage or a combination of the both.

1.2.2.1 Gas Nucleation

Gas nucleation of a pore occurs because Pg rises due to the rejection of gas at the solid-liquid interface. The growth of a pore by the rejection of gas is a diffusion process. The rate controlling step will be either the rate of gas rejection at the solid-liquid interface or the rate of gas precipitation into the cavity. Assuming no diffusion of the gas in the solid and that the concentration gradient at the S/L interface is small, then Pg in the liquid can be referred to as the equilibrium gas pressure. This Pg is the total pressure of all the gases and vapours in equilibrium with the liquid. For a diatomic gas such as H_2 in aluminum, it can be easily calculated since

$$Pg = (Co/K)^2 \qquad (1.4)$$

where Co is the initial content of H_2 in aluminum and K is Sievert's gas constant [26]. In more complicated systems, such as ferrous materials, the equilibrium gas pressure can be calculated as the sum of the pressures of CO, CO_2, H_2, N_2 gases as well as SO_2, H_2S, H_2O, Fe (vapour).

To decrease the Pg, and make gas nucleation more difficult, Co, the initial gas content in the liquid must be

decreased. Many processes employ this principle to decrease pore formation. Standard techniques [9,10] used are flux additions, flushing with inert gases and vacuum treatment.

1.2.2.2 Nucleation - A feeding problem

Pore formation can also be seen as a feeding problem. As solidification proceeds the shrinkage pressure, Ps, increases as feeding of liquid metal through the dendrite mesh becomes more difficult. The feeding problem develops in many ways and on different size scales.

Figure 1.8 is a diagram illustrating the solidification of a long freezing range alloy at time "t". The ingot has three main regions : solid, liquid and mush. The mush consists of a mixture of solid dendrites and liquid metal, and is typically several centimetres in thickness. Liquid metal surrounds the dendrite mesh and exists in the interdendritic regions which are channels of the order of 10^{-2} cm. in size[11]. It is in these areas that the major solute and gas rejection occurs.

To reduce this Ps term, feeding of liquid metal through the dendrite mesh must be accomplished. For the last twenty to thirty years, it has been widely accepted[2,4,12]

that there are three mechanisms of feeding which will operate : liquid feeding, mass feeding and interdendritic feeding. Two others, burst and solid, have been envisaged[12] and deserve mention.

Liquid feeding is the macroscopic movement of liquid metal to the solid-liquid interface to supply a reservoir of liquid metal. In metal and alloys of short freezing range it is the only type which is assumed to occur. Liquid feeding is the best understood of all feeding mechanisms and a comprehensive review of this subject to 1959 has been compiled by Wallace[13]. Absence of this type of feeding leads to porosity in the last areas to freeze where the casting simply runs out of liquid metal (Figure 1.3). Hot-topping is the usual procedure used to achieve a constant supply of liquid metal and hence promote liquid feeding.

Mass feeding is the macroscopic movement of mush, and occurs in long freezing range alloys (Figure 1.4). This movement usually occurs up to the point at which the mush is 35% solid, but measurements have shown it to be effective even to 68% solid[15], at which point the dendrite mesh forms a coherent network (Figure 1.8). Early research focussed on this type of feeding as being one of the most important in reducing the microporosity. It has been found that poor mass

Figure 1.8 Feeding Mechanisms in Open Topped Ingots

FEEDING MECHANISMS IN OPEN TOPPED INGOTS

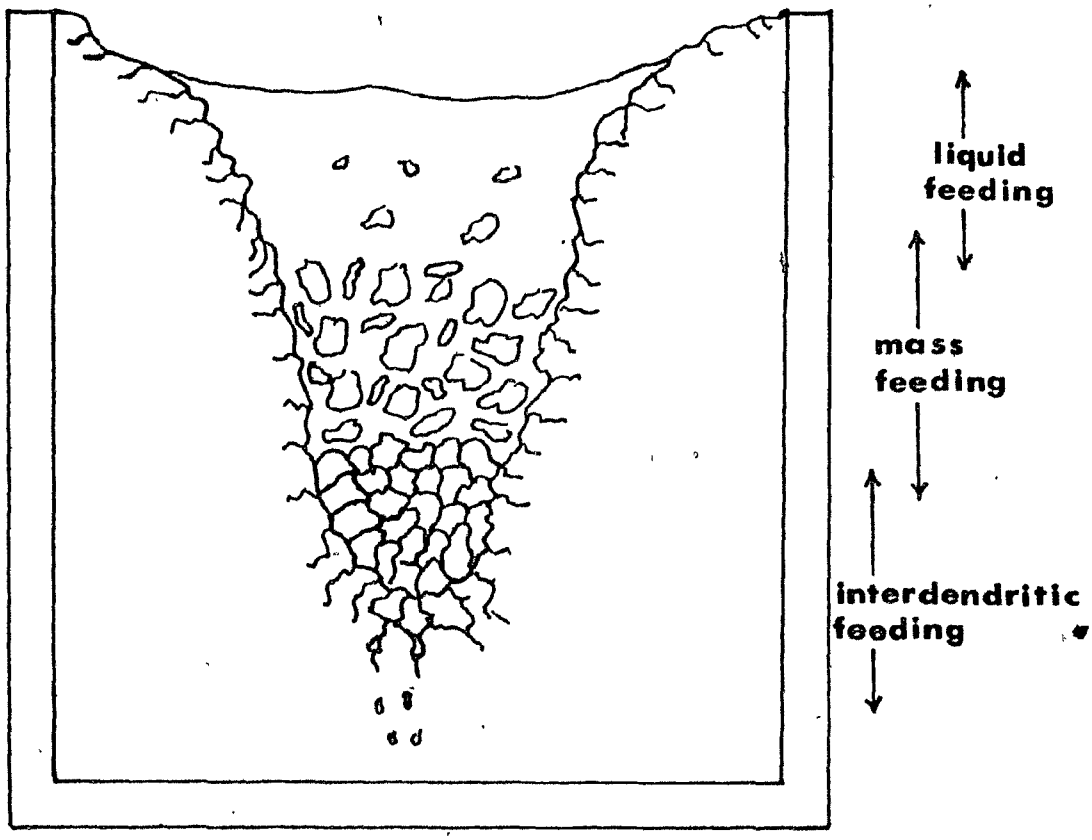

feeding can lead to blocking of feeding channels on the macroscopic scale. This type of feeding must be highly dependant on such variables as the primary dendrite arm spacing and the dimensions of the casting. Mass feeding of grain refined ingots should be easier than feeding of an ingot with long columnar grains, since the flow of liquid metal between smaller equiaxed grains is easier than down long channels between columnar grains.

At a later stage in the solidification process, when liquid and mass feeding are no longer possible, feeding of liquid metal through the interdendritic channels (Figure 1.8) becomes important. Limited experimental data[15] is available on interdendritic feeding and research has generally been approached from a theoretical point of view.

The first attempt at an analysis was made by Allen[14] in 1932. He considered the possibility of feeding liquid metal into an interdendritic channel (Figure 1.9) of radius r and length L. To prevent pore formation the rate of liquid metal flow down the channel must equal the rate of movement of the solid-liquid interface due to solidification. The rate of the liquid metal flow down the channel is $\Delta P/\mu L$, where ΔP is the pressure drop between the tip and opening of the channel, μ is the viscosity of the liquid metal and

Figure 1.9 Feeding of Liquid Metal into an Interdendritic Channel

FEEDING OF LIQUID METAL INTO A CHANNEL

NO PORE FORMATION IF $$\frac{\Delta P}{\mu L'} \geq \frac{\alpha\, dm}{dt} \qquad (1.5)$$

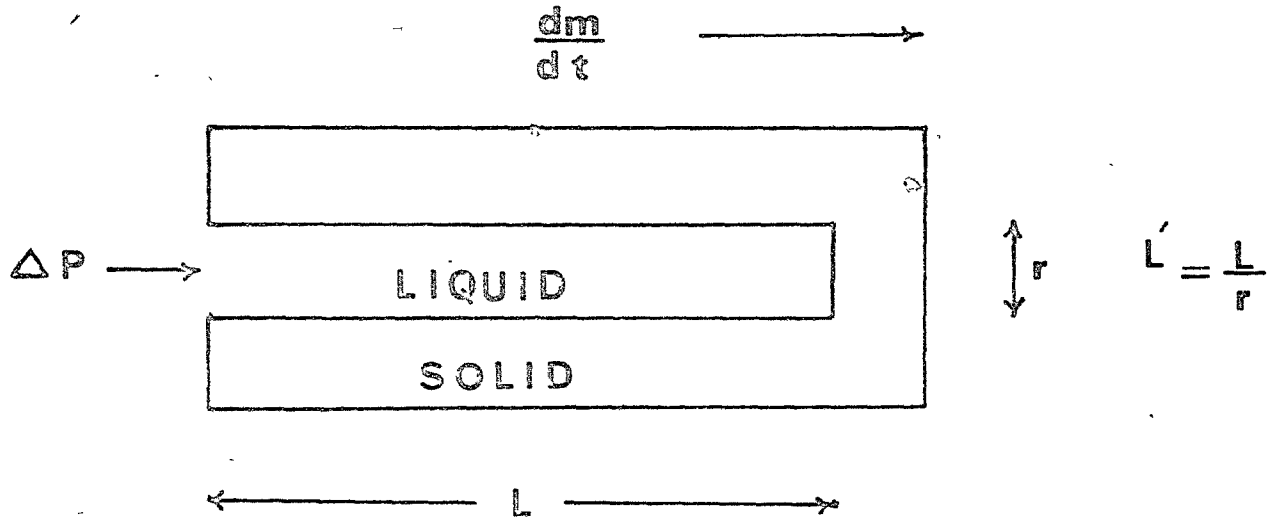

L' is a dimensionless number equal to r/L. The rate of contraction is $\propto dm/dt$ where α is the volume contraction and dm/dt is the rate of solidification. To prevent pores from forming

$$\frac{\Delta P}{\mu L'} \geq \alpha \frac{dm}{dt} \qquad (1.5)$$

If gas rejection is neglected, a pressure Ps due to shrinkage will develop where :

$$Ps = \alpha \mu L' \quad (dm/dt) \qquad (1.6)$$

Therefore if the pressure supplied at the channel opening is less than Ps (pressure due to shrinkage), a pore will nucleate. However for the case of centreline shrinkage in a cyclinder Equation 1.6 is a relatively simple approach and other more complicated analysis have been attempted[15,16] as :

$$Ps = \frac{32 \mu \beta \lambda^2 L^2}{r^4} \qquad (1.7)$$

where $\beta = \alpha/1-\alpha$ (α is the volume contraction)

μ = viscosity of the liquid metal

$\lambda = K' (Tm - To) \rho s H \sqrt{\pi \alpha'}$

K' = mould thermal conductivity

Tm, To = melting point of metal, ambient temperature respectively

H = latent heat of fusion

α' = mould thermal diffusivity

ρs = density of the solid

L = casting length

r = radius of liquid channel

In cases of dendritic solidification of long freezing range alloys, researchers [15,16] have taken into account the factors t = "tortuosity factor" to account for the fact that liquid flow channels are not straight and smooth, and, n = "number of flow channels per unit cross-section of cylinder". Equation 1.7 can than be developed as :

$$Ps = \frac{32\mu\rho\lambda^2 L^2}{r^4} \times \left(\frac{t^{2*}}{R^2 n}\right) \qquad (1.8)$$

where R equals the radius of the cylinder.

Hence in interdendritic feeding, the magnitude of Ps and thus nucleation is dependent on :

1) rate of solidification

2) characteristics of the interdendritic channel

When the dendrite mesh has developed to the point where pockets of liquid metal are left in the solidified cast, then the only way possible to feed liquid metal into these areas is by burst feeding [12]. This occurs when liquid metal bursts through a solid skin to feed a liquid pool and is possible because the strength of the solidified metal is low (Figure 1.10).

Another possible feeding mechanism which has been proposed is solid feeding. It has been dealt with in detail elsewhere[12,21], and was introduced to denote the inward movement of the solidified outer shell of the cast to compensate for solidification shrinkage. As illustrated in Figure 1.11, to prevent pore formation the solid shell must contract and the liquid must expand. The resulting cast will have no pores, but will be highly stressed.

1.3 PAST EXPERIMENTAL RESEARCH

A review of the literature has shown that while several theoretical approaches to the problem of microporosity have been taken, there is a lack of concrete experimental evidence to prove or disprove any given theory.

Most experimental research to date has regarded

Figure 1.10 Schematic of Burst Feeding [12,21]

SCHEMATIC REPRESENTATION OF BURST FEEDING

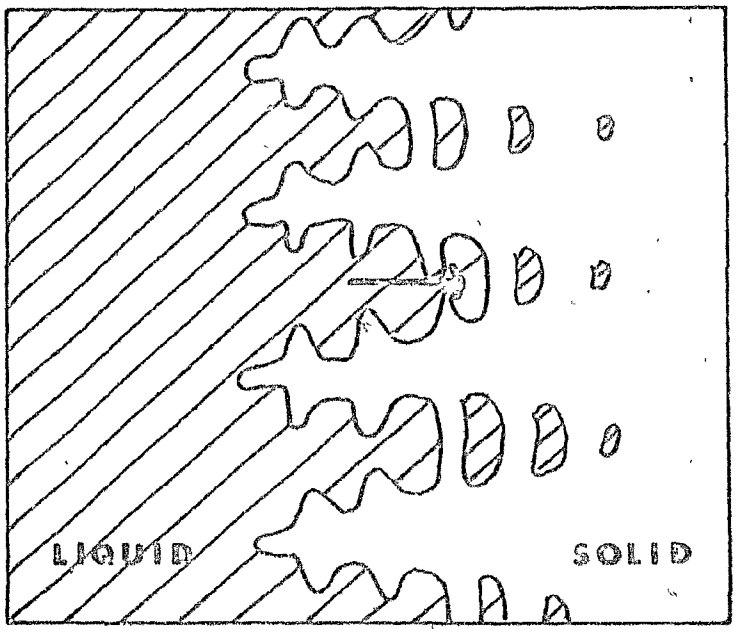

Figure 1.11 Schematic of Solid Feeding [12,21].
Liquid expands to accomodate solidification shrinkage (b) thus creating a lower internal pressure. Solid contracts due to pressure differential (c).

SOLID FEEDING OF CASTINGS

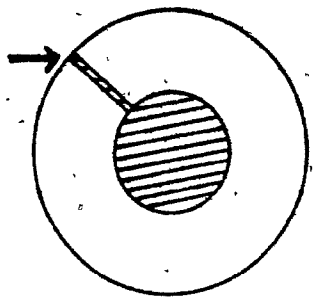

feeding of liquid

(a)

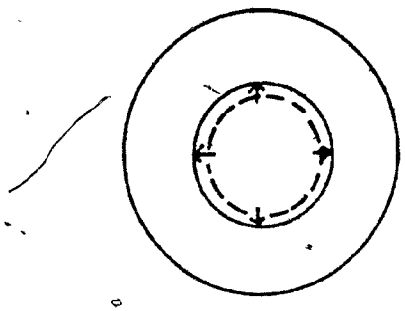

liquid expansion

(b)

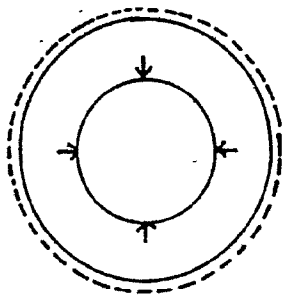

solid contraction

(c)

the problem with consideration of one of four variables :

1) Effect of the freezing range (3,5,6,17,18)

2) Effect of initial gas content (6,10,19,21,22)

3) Solidification Rates (7,22,23)

4) Effect of Pressure over the solidifying cast (19,24)

1.3.1 Freezing Range

The freezing range under equilibrium conditions is defined as the difference between the liquids and solidus temperatures. Whittenberger and Rhines (6) stated that for 14 alloy systems investigated, there is a linear relationship between freezing range and percent porosity. Others have also reported that porosity increases in steels as the carbon content rises from 0.2 to 0.46 %C.

One of the difficulties in relating porosity to freezing range is that under the non-equilibrium conditions of solidification, the actual freezing range is greater than that predicted by the equilibrium phase diagram. Non-equilibrium conditions which have been shown to be applicable (17,18) to metal casting, are the assumptions of

no diffusion in the solid, and complete diffusion in the liquid on a microscale. If no macrosegregation occurs, the actual volume of residual liquid in the interdendritic spaces at some temperature is given by :

$$fl = \left[\frac{(dT/dCl)\ Co}{T_F - T} \right]^{1/1-K} \qquad (1.9)$$

where Co is the initial solute concentration, dT/dCl is the slope of the liquidus, K is the partition ratio and T_F is the freezing point of the solvent. Equation 1.9 predicts the presence of eutectic at very small solute concentrations. The freezing range is then actually $T_l - T_e$ instead of $T_l - T_s$ where:

T_l = temperature of liquidus

T_s = temperature of solidus

T_e = temperature of eutectic

On this basis it would appear that a better relationship than freezing range versus porosity, is one which compares the freezing range-composition relation to the porosity-composition relationship. Experimental results (17) indicate this to be so, for example, in Zn - Mg alloys (Figure 1.12) there is no porosity up to 3% Zn, a peak at 6% Zn and no porosity at compositions greater than 9% Zn.

Figure 1.12 Mg - Zn phase diagram

Mg-Zn Magnesium-Zinc

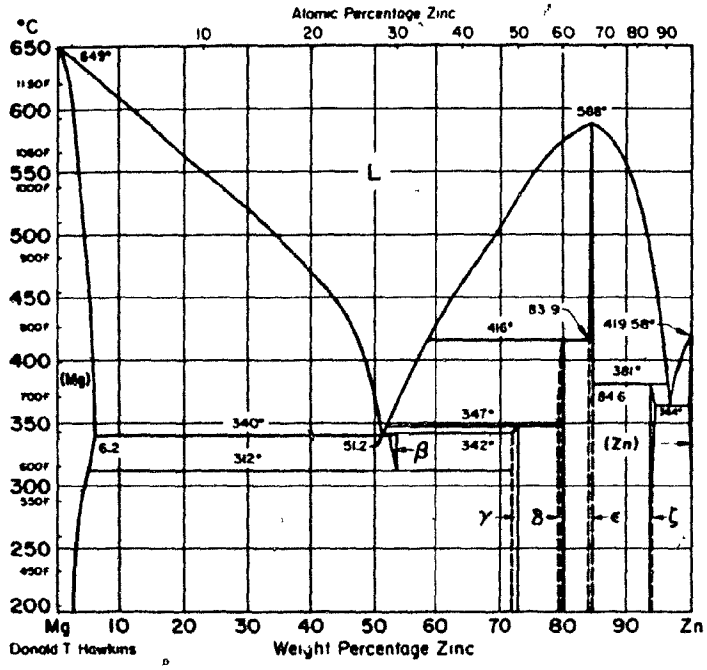

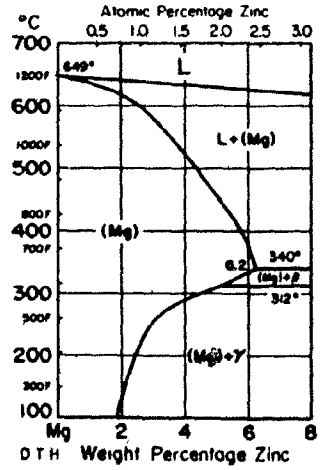

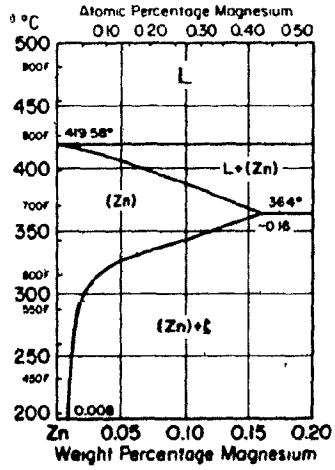

1.3.2 Gas Content

When considering the effect of gas content on pore formation, researchers usually have chosen systems in which gas analysis is simple (H_2 in aluminum alloys). Although porosity in steel has been investigated extensively[7], the effect of gas content on systems such as steel has been neglected because the several gases in solution complicate the analysis.

Uram et al [19] found, in pure aluminum at its melting point, that under atmospheric conditions, porosity versus initial gas content is possibly a linear relationship. They also reported that a critical gas content is required to nucleate a void.

Chamberlain and Sulzer [20], casting aluminum alloys in sand moulds, found similar results. Porosity is directly related to the initial gas content, and as the gas content decreased from 0.35 ml H_2 / 100 gm Al (S.T.P.) to 0.15 ml H_2 / 100 gm Al (S.T.P.) the porosity decreased.

Whittenberger and Rhines [6] in 1952 published one of the most important papers on the topic. They viewed the formation of casting porosity as a nucleation and growth process with solidification shrinkage and gas precipitation as co-operative driving forces. Experimental evidence

evaluating the individual contribution of each force confirms that microporosity is nucleated by gas precipitation. They demonstrated that in degassed alloys which shrink on solidification (Al - 4.5% Cu) no porosity existed, and they also showed that porosity could exist in gas containing alloys (Bi - Sb) which expand on solidification. The important conclusion was that unfed shrinkage could not nucleate porosity alone, but porosity could be nucleated by gas without shrinkage. However, although gas alone could nucleate a pore, the growth and final shape and size was due to unfed shrinkage [21,22].

Campbell (21) attempted to evaluate the shrinkage pressure theoretically and found that homogeneous nucleation of a pore by shrinkage was impossible since the shrinkage stress in the liquid is at least an order of magnitude smaller than the fracture stress of the liquid. Thus in the absence of gas, some other form of heterogeneous or non-nucleation process should be responsible for the creation of pores in unfed regions of castings. In principle he concluded that sound castings were possible even in the absence of good feeding.

Nishi and Kurobuchi [22] examined the conditions for pore formation in unidirectionally solidified Al - 4.0% Cu alloys. They found that the critical gas content for pore

formation was approximately 0.15 ml H_2 / 100 gm Al (S.T.P.). However, once a pore formed, the shape of a shrinkage or gas pore was dependent upon the initial gas content and solidification rates. At solidification speeds of 3,6,12 and 60 cm/hr, the critical gas levels to form a gas pore instead of a shrinkage type pore were 0.22, 0.26, 0.34 and 0.41 ml H_2 / 100 gm Al (S.T.P.) respectively.

1.3.3 Solidification Rates

Mahadevan et al [23] studied the influence of solidification gradients (fraction solid / cm) on casting soundness in Al - 4.5% Cu alloys. They concluded that the porosity decreased linearly as the log of the solidification gradients (maximum and average) increased. Similar results were obtained with the use of metallic or non-metallic chills. The relationships between amount of porosity and solidification gradients were expressed in the form of simple linear equations.

Many authors deal with the minimum temperature gradient required for the elimination of porosity in any alloy. Results have been quoted and are presented in Table 1.1. Recent work by Nishi et al [22] has shown the influence of

Table 1.1

Reported values of the minimum temperature gradient to reduce porosity in various alloys [17].

Material	Minimum Gradient (°C / cm)	Freezing Range (Non Equilibrium)
Al - 4.5 Cu	5 - 13	100
Al - 7 Mg	1	70
Cu 85 - Sn 5	8	130
88 Cu-8Sn-4Zn	1 - 3	130
88 Cu-10Sn-2Zn	25	160
0.3C Steel		
(plates)	1 - 2	40
(bars)	6 - 12	40

solidification speeds on pore formation in unidirectionally solidified alloys. The higher the speed, the higher the gas level must be to form a gas bubble type pore in lieu of a shrinkage type pore. Although solidification rates do not affect pore nucleation, they can affect the growth.

1.3.4 Pressure

Pressure applied to a solidifying ingot is important because it can increase the gas solubility in the solid, hinder pore formation and compress existing pores.

Uram et al [19] illustrated how applied pressure can affect the amount of "gas type" micropores in aluminum castings. They found that as the applied pressure increased, the dependency of porosity on initial gas content decreased, and the critical gas content for pore formation increased. Although the applied pressures might affect the "shrinkage type" pores by forcing liquid metal through the narrow feed channels, this was found not the case, primarily because the applied pressure used was too low (17 atmospheres (1722.1 KPa)).

Other work [24] considered the influence of a reduced pressure. In an aluminum alloy, the effect of reducing the head and keeping the initial gas content constant results

in the highest porosity with the lowest pressure. A relatively sound cast at 1 atm (101.3 KPa) became an unsound cast (gas type macropores) at 22 torr (2.9 KPa). The solidification of the same alloy at 90 torr (11.9 KPa)[24] with different gas contents yielded results which followed the preceding findings by Uram et al[19]. Porosity decreased with initial gas content, but this relationship was more sensitive to gas content and the critical gas level for pore formation was less.

1.4 AIMS OF THE PRESENT INVESTIGATION

As has been mentioned, microporosity is generally found in alloys that solidify over a wide range of temperatures. Many have regarded the problem qualitatively as being caused by shrinkage, gas, or a combination of both; yet there has been little experimental or analytical work done to discover the relative contributions of shrinkage, or gas in the formation of pores. There has also been very little quantitative research to ascertain the influence of various processing variables on microporosity.

With this in mind the chief aim of this present investigation was to study quantitatively the distribution of micropores in an ingot. It was considered at the outset that

the questions to be answered were:

1) Does microporosity follow a reproducible pattern?

2) What are the relevant variables and how do they quantitatively affect pore formation?

3) Is it possible to predict the amount of microporosity in an ingot?

CHAPTER II

EXPERIMENTAL PROCEDURE

Microporosity in castings was investigated with reference to the influence of relevant variables on its distribution. An Al - 4.5 % Cu alloy (Figure 2.1), was chosen for several reasons ; it solidifies over a long range of temperatures ($100^{o}C$, 100K); it has only one gas in solution of any importance to its casting operation (hydrogen); and much previous research on microporosity used this alloy.

Castings were made in air at atmospheric pressure to show which variables affect the distribution of porosity (pouring temperature, mould temperature, hydrogen concentration), and further to serve as standards of porosity for comparison to later experiments in vacuum. Some of these air melts were grain refined using a standard Al - Ti - B grain refiner. All experiments with relevant details are listed in Tables 2.2 and 2.3.

Since previous research (Section 1.3) showed that initial gas content and pressure over the solidifying cast can affect microporosity, castings were made at various levels of vacuum to measure the effect of these two variables. Vacuum degassing of H_2 from aluminum melts has already been

Figure 2.1 Al - Cu phase diagram

Al — Cu

PHASE DIAGRAM

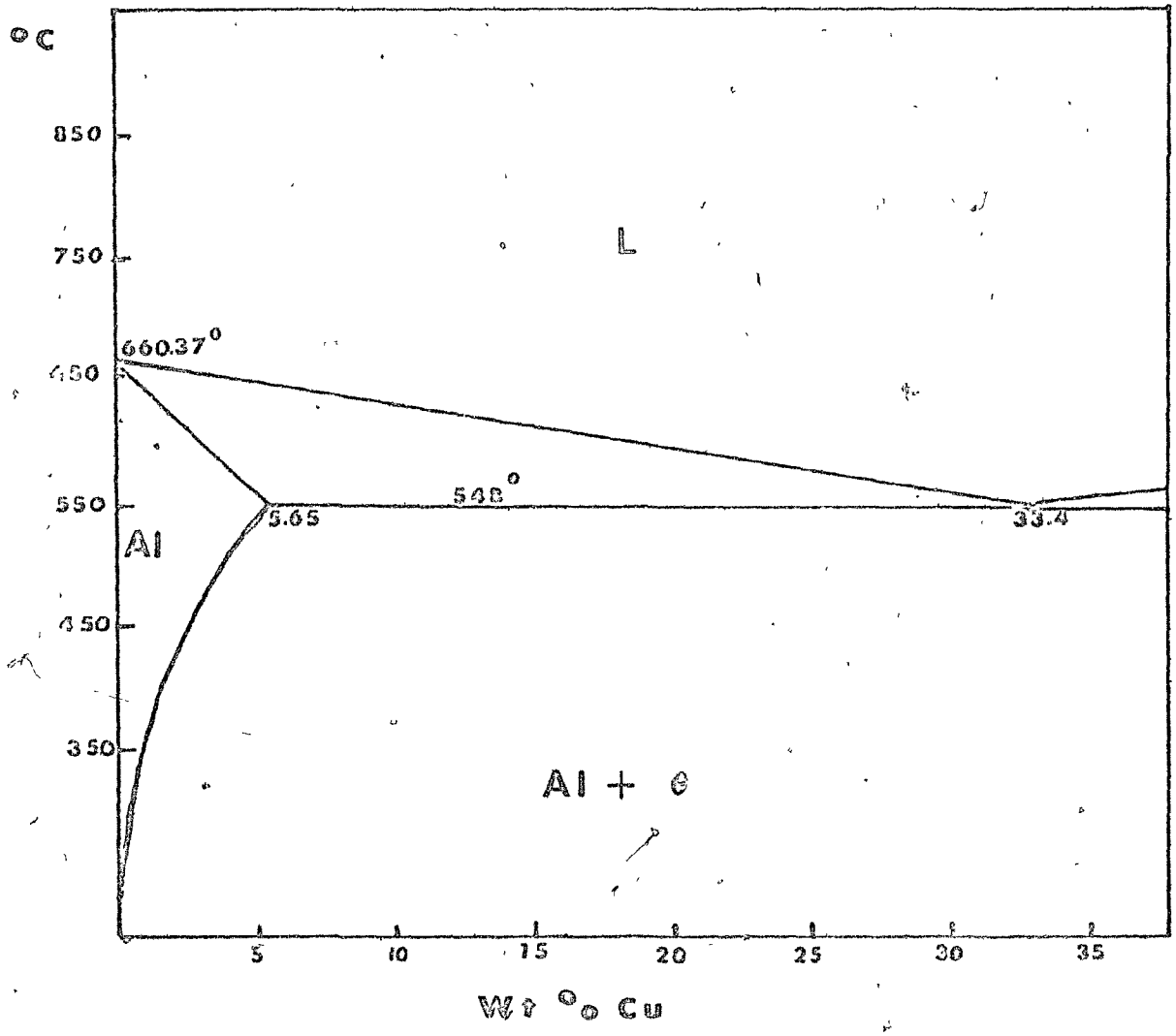

shown to reduce the gas content rapidly, even at low vacuum levels, eg. 1 torr (133.3Pa) [35]. The effective head pressure (Equation 1.2) can also be altered by the use of a vacuum; for example, a decrease in chamber pressure from 760 torr (101.3 KPa) to 0.25 torr (33.33 Pa) represents a 3000 fold decrease. The details of the air and vacuum casting experiments are listed in Tables 2.2 and 2.3 respectively.

Each experiment produced cylindrical castings of dimensions 4" (100 mm) high by 3 3/4" (93.8 mm) diameter. The castings were examined both quantitatively and qualitatively with a standard density technique employed as a quantitative measure, and macroetching and various other metallographic techniques as a qualitative measure. Also, for each experimental run, either in air or in vacuum, a spectrographic sample was taken for analysis of composition, and a "Ransley mould" sample was taken for later gas analysis by an established sub-fusion technique [25].

2.1 AIR MELT EXPERIMENTS

2.1.1 Alloy Preparation

To prepare the alloy, aluminum of commercial purity grade (Table 2.1) was melted in an induction furnace, and held at 100°C superheat to avoid excessive gas pick-up.

Electrolytic tough pitch copper (Table 2.1) was then charged to the melt, with efficient mixing of the alloy accomplished by the inductive stirring. Each melt was typically in the range of 14 - 16 Kg. in weight.

2.1.2 Melting Apparatus

A Tocco Meltmaster, 150 KVA, 400V, 3000 Hz induction unit was employed for this investigation. The unit consisted of a recrystallized alumina crucible packed inside an induction coil capable of handling melts of aluminum up to 120 Kg . The alumina crucible was 197 mm. in diameter with a depth of 356 mm.

Temperature was monitored using chromel-alumel thermocouples sheathed in double bore alumina tubes of bore diameter 2.7 mm which were in turn protected by a single bore alumina tube of inner diameter 2.8 mm, which was closed at one end.

During each experiment, once temperature was attained, temperature control was accomplished by keeping the power constant to the furnace. This enabled control to the nearest $\pm$ 10° C (10K).

Table 2.1

Materials used in Investigation

Material	Analysis	Source
Aluminum (commercial grade)	0.11% Fe, 0.09 Si 0.01% Zn, rest Al (Cu,Mg,Ni,Ti,Cr) 0.01%	Alcan International Ltd.
Copper (electrolytic tough pitch)	0.015-0.030% O (45) ½ p.p.m. H_2 metallic impurities 0.003	Canadian Copper Refiners Ltd.
Hycor TA530 Crucible	90% Al_2O_3 10% SiO_2	Engineering Ceramics Co. Ltd.
Aluminum Grain Refiner	5.8% Ti, 1.1% B, rest Al	Alcan International Ltd.

2.1.3 Moulds

Casting were made into cylindrical steel moulds of 3 3/4 inches (93.8 mm) diameter by 4 inches (100 mm) high (Figure 2.2). The thickness of the mould wall and baseplate was ¼ inches (12.6 mm). Before casting, each mould was cleaned to remove iron oxide, dried to remove moisture and then preheated to the desired temperature from heat supplied by the melt surface.

2.1.4 Casting Procedure

As outlined in Table 2.2, the air melt experiments consisted of holding each melt at 700°C (973K), 825°C (1098K) and 950°C (1223K) and casting into steel moulds preheated at either 25°C (298K), 70°C (343K) and 250°C (523K). In one case, for a pouring temperature of 825°C (1098K), a casting was made into a mould held at 400°C (673K). All castings were allowed to air cool before being removed from the steel moulds.

The grain refining experiments were basically similar. Once the alloy attained a temperature of 825°C (1098K), the grain refiner (Table 2.1) was added to the

Table 2.2
Air Casting Experiments

Experiment Number	Type of Experiment	Melt Temp °C (K)	Superheat °C (K)	Mould Temp °C (K)
A11	Non - Grain Refined	700 (973)	50	25 (298)
A12		700 (973)	50	25 (298)
A13		700 (973)	50	70 (343)
A14		700 (973)	50	240 (513)
A21		825 (1098)	175	25 (298)
A22		825 (1098)	175	70 (343)
A23		825 (1098)	175	250 (523)
A24		825 (1098)	175	400 (673)
A31	Grain Refined	950 (1223)	300	25 (298)
A32		950 (1223)	300	70 (343)
A33		950 (1223)	300	250 (523)
A41		825 (1098)	175	25 (298)
A42		825 (1098)	175	70 (343)
A43		825 (1098)	175	250 (523)

molten bath to bring the titanium and boron contents to 0.21% and 0.04% respectively. To minimize the fading effect of the grain refiner, castings were immediately poured at 825°C (1098K) into steel moulds held at 25°C (298K), 70°C (343K) and 250°C (523K).

For each pouring temperature, either grain refined or not, samples were cast for gas and spectrographic analysis as described below. Results of these casts appear in Table 2.4.

2.1.5 Sampling

Gas analysis samples were cast in specially prepared graphite "Ransley Moulds" [25] (Figure 2.2). These moulds allowed for a rapidly solidified sample free of pore formation. To determine the gas content, a standard sub-fusion extraction method was employed with results reported on a volume basis : ml / 100 gm Al at S.T.P.

A standard disc type steel mould (Figure 2.2) was fabricated for casting of spectrographic samples. In order to obtain quantitative results, the sample was prepared in the same chemical and physical form as the

Figure 2.2 Moulds Used in Experiment

(a) Cylindrical Mould

(b) Ransley Mould

(c) Spectrographic Mould

A

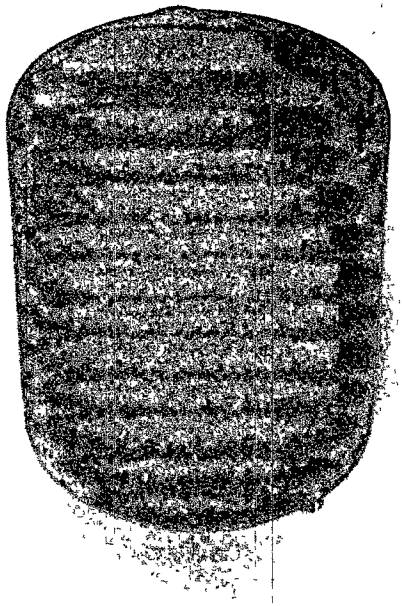

B

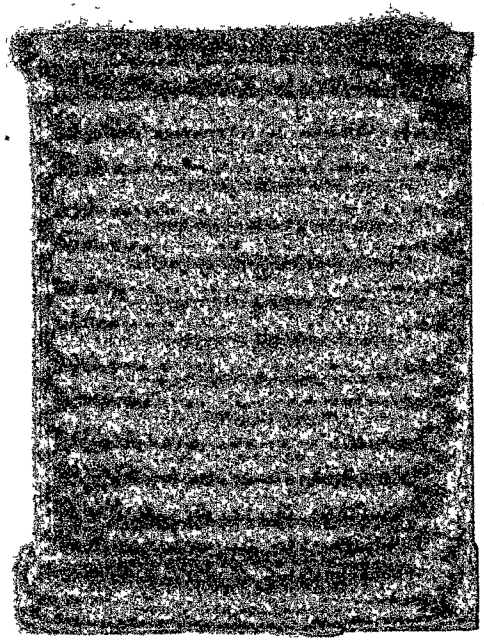

C

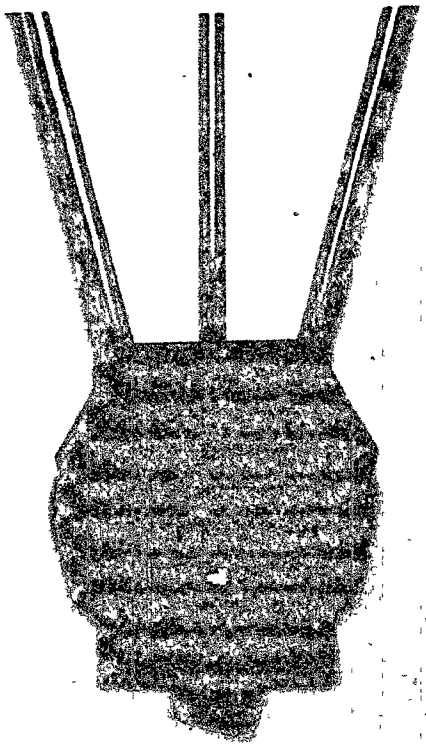

standard [32]. The concentration of alloying elements (Cu) and impurities (Fe, Si, Mg etc.) was determined to the nearest 0.01wt% with the aluminum content calculated by difference.

All gas and spectrographic analyses (Table 2.4) were performed by The Aluminum Company of Canada Ltd., Research Centre, Kingston.

2.2 VACUUM MELT EXPERIMENTS

2.2.1 Melting Equipment

The vacuum melting and casting experiments were carried out in the vacuum induction melting assembly shown in Figure 2.3. The unit consisted of a 150 KVA 400V, 3000 Hz induction furnace coupled with a 2260 l vacuum chamber. The recrystallized alumina crucible was similar to that used in the air melt except that it was packed inside an induction coil capable now of handling melts to 150 Kg. The pumping unit for the chamber consisted of a 300 C.F.M. (8.5×10^3 l/min) mechanical pump in series with 1300 C.F.M. (3.68×10^4 l/min) Roots blower. Temperature control and monitoring made use of a chromel-alumel thermocouple as was used in the air melts. This connected to a chart

Figure 2.3 Vacuum Furnace Induction Unit

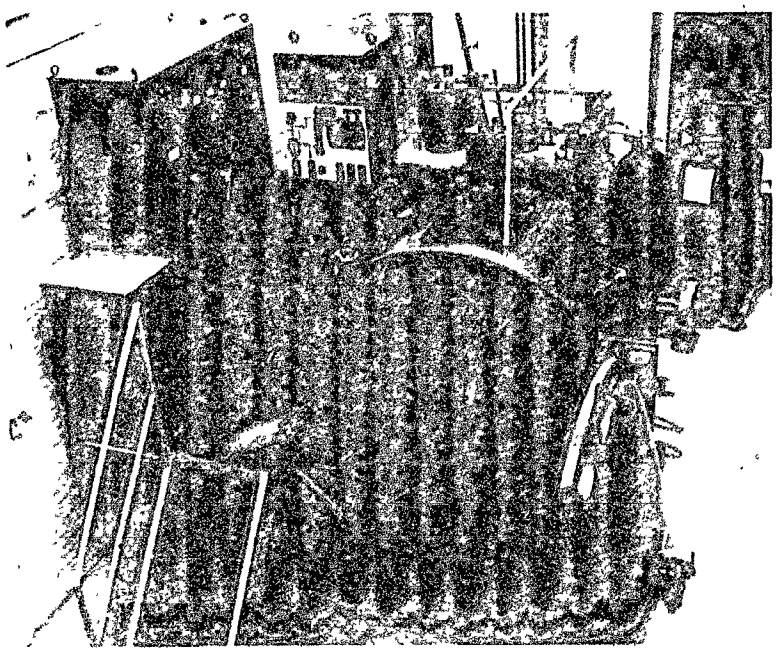

recorder through vacuum seals in the chamber wall.

2.2.2 Vacuum Casting Unit

An assembly was designed to vacuum cast the Al - 4.5% Cu alloy into preheated moulds as shown in Figure 2.4. The set-up of the assembly was such that the molten stream flowed through a preheated tundish into a steel mould positioned on a turn-table. This steel mould sat in a mould heater capable of holding four steel moulds and of revolving below the tundish. The tundish was capable of channeling a molten stream of 6" (150 mm.) to 1" (25mm.), and consists of a 10Ω resistance heated coil, which in turn was connected to a 150V, 10 amp variac through sealed power leads in the chamber wall.

In order that the castings could be made into moulds at varying temperatures a unit, previously mentioned, was built. This unit was designed such that castings could be poured into four steel moulds during any experiment without breaking vacuum. The apparatus (Figure 2.4) had four independently controlled resistance (14Ω) furnaces embedded in silica sand, and contained in a steel cylinder of 9" (228 mm.) height by 23" (585 mm.) diameter. Refractory cement covered the top (25 mm.) of the cylinder to both cut

Figure 2.4 Mould Heater Unit

MOULD HEATER UNIT

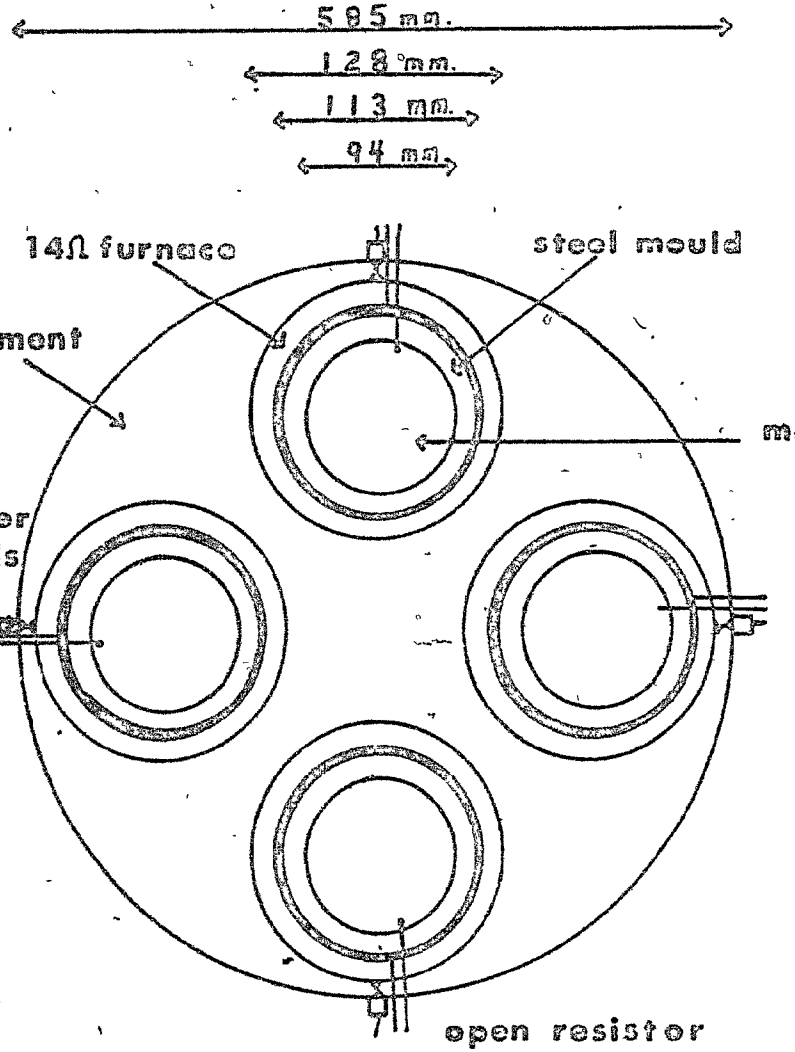

TOP VIEW

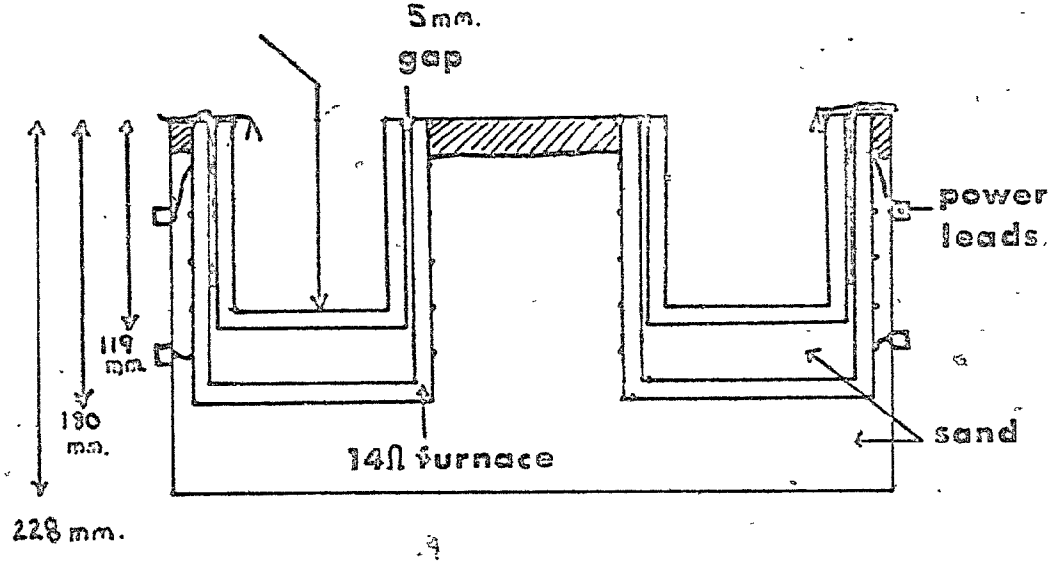

SIDE VIEW

down on the heat loss from the furnaces and to prevent the metal splashing during the casting and shorting out the wiring of the resistance furnaces. Each mould heater had its own (Figure 2.5) power leads connected to 150V, 10 amp variacs, chromel alumel thermocouple, and open resistor protuding $\frac{1}{2}$" (1.25mm.) into the steel mould. The open resistor consisted of two bare steel wires attached to a source measuring resistance. As the mould filled with molten metal, this metal rose and surrounded the steel wires creating a closed circuit of finite resistance. This signalled that pouring should end. The same steel moulds were used in vacuum as in air. These fitted in the mould heaters with a 5 mm. clearance.

This entire unit was enclosed inside the vacuum chamber, and power to the moulds as well as temperature could be monitored very closely throughout the experiment without breaking vacuum. The temperature of the moulds could be controlled easily within the range of 50°C (323K) to 600°C (873K) $\pm$ 5°C (5K).

2.2.3 Vacuum Casting

The vacuum experimental series (Table 2.3) was performed to make castings under various levels of vacuum

Figure 2.5 Vacuum Experimental Set-up

VACUUM EXPERIMENTAL SET-UP

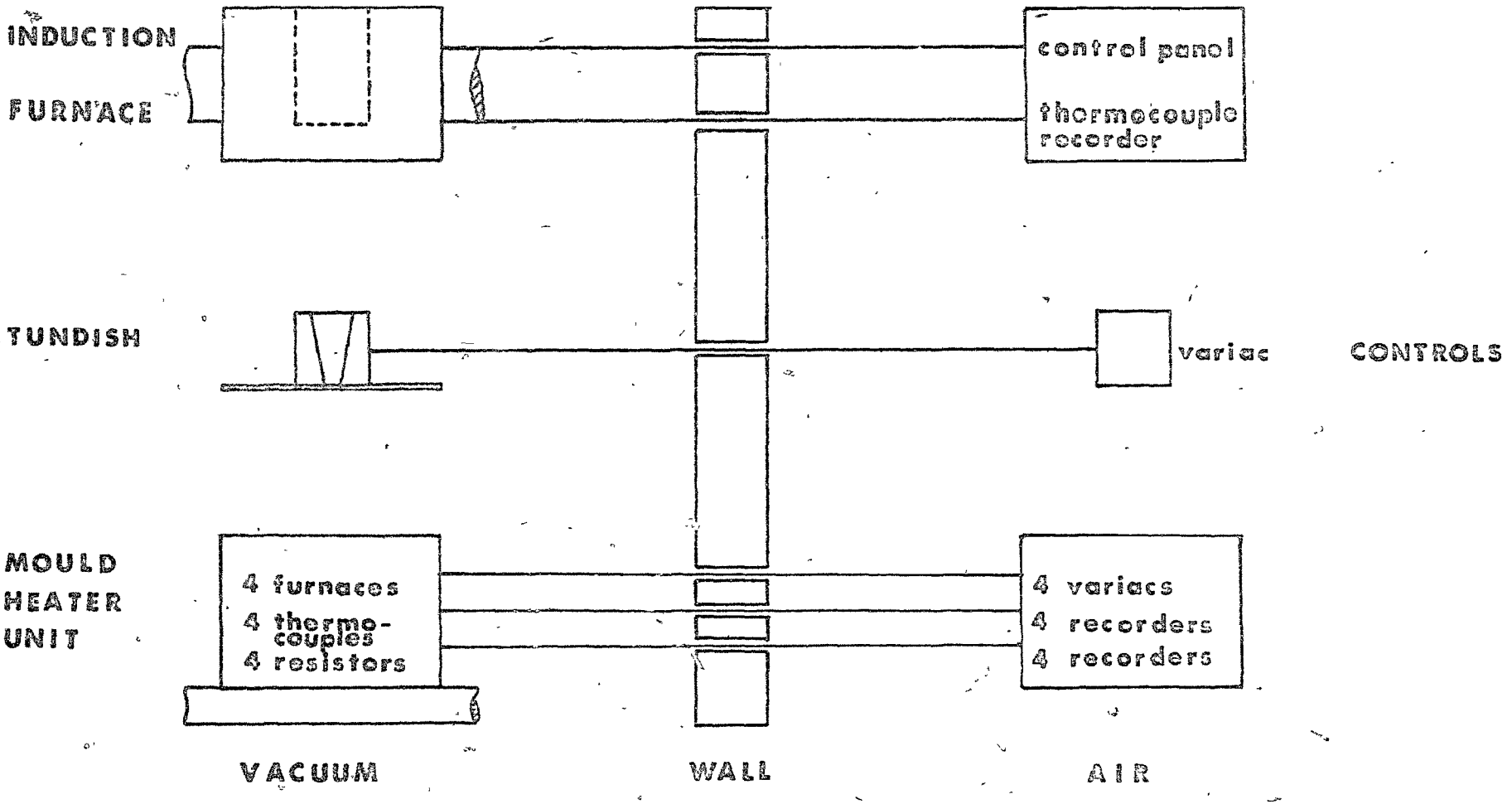

Table 2.3

Vacuum Casting Experiments

Experiment Number	Time of Degassing (minutes)	Pouring Temp. oC (K)	Mould Temp. oC (K)	Pressure on Casting Torr (Pascals)
V11	10*	700 (973)	275 (548)	0.20 (26.6)
V12		700 (973)	275 (548)	760 (1.01×10^5)
V21	50*	700 (973)	200 (473)	0.20 (26.6)
V22		700 (973)	370 (643)	0.20 (26.6)
V23		700 (973)	300 (573)	1.50 (200)
V24		700 (973)	280 (553)	760 (1.01×10^5)
V31	90*	700 (973)	30 (303)	0.20 (26.6)
V32		700 (973)	300 (573)	0.20 (26.6)
V33		700 (973)	300 (573)	1.50 (200)
V34		700 (973)	200 (473)	760 (1.01×10^5)
V41	120*	700 (973)	90 (363)	0.20 (26.6)
V42		700 (973)	120 (393)	0.20 (26.6)
V43		700 (973)	250 (523)	0.20 (26.6)
V44		700 (973)	525 (798)	0.20 (26.6)
V51	90**	825 (1098)	275 (548)	0.35 (46.7)
V52		835 (1098)	275 (548)	1.40 (187)
V53		825 (1098)	275 (548)	100 (1.33×10^4)
V54		825 (1098)	275 (548)	760 (1.01×10^5)

* Degassed at 700°C (973K) and 0.20 torr (26.6Pa)

** Degassed at 825°C (1098K) and 0.35 torr (46.7Pa)

and gas content. Alloy preparation was similar to that used in air melts, and after alloying each melt of Al - 4.5% Cu was degassed at 700°C (973K) and 0.25 torr (33.3Pa) chamber pressure with the times of degassing at the reduced pressure given in Table 2.3.

Once the vacuum degassing step was completed, the casting procedure followed one of two types. The first procedure was that of casting at various levels of vacuum into moulds held at the same temperature to examine the effect of external pressure on microporosity distribution. Four moulds were heated to a steady - state temperature, and a cast into the first mould was made after the degassing operation, at the pressure of the degassing. Before the next cast, air was admitted to the chamber, and the second cast was made at the new pressure. The pressure was again raised for the third cast, and finally the fourth cast was performed at atmospheric pressure. Samples for gas and spectrographic analysis were then taken at atmospheric pressure after the final cast.

The second procedure followed that of casting at one vacuum level into moulds at different temperatures to examine the effect of solidification rate on microporosity distributions at these reduced pressures. The four moulds

Table 2.4

Gas and Spectrographic Analysis

Experimental Number	Type of Experiment	Alloy Composition wt %					Initial Gas Content ml H_2/100 gm Al (S.T.P.)
		% Cu	%Fe	%Si	%Ti	%B	
A1 *	Air	5.00	0.12	0.09	-	-	0.19
A12		4.86	0.12	0.08	-	-	0.30
A2		4.29	0.12	0.07	-	-	0.46
A3		4.26	0.12	0.08	-	-	0.45
A4**		4.02	0.11	0.13	0.21	0.04	0.23
V1	Vacuum	4.68	0,13	0.08	-	-	0.07
V2		4.47	0.13	0.09	-	-	0.07
V3		4.68	0.13	0.09	-	-	0.02
V4		4.57	0.13	0.09	-	-	0.02
V5		4.51	0.11	0.11	-	-	0.14

* A1 represents A11, A13, A14, casts (Table 2.2)

** 0.1 wt % Ni and 0.1 wt % Zn present

were heated to four temperatures between 90°C (363K) to 525°C (798K) as given in Table 2.3. After degassing for 120 minutes, castings were made at 0.25 torr (33.3Pa) pressure into the four moulds, and each casting was allowed to solidify in vacuum. After solidification, the chamber was brought to atmospheric pressure so that gas and spectrographic samples could be taken.

2.3 DENSITY AND METALLOGRAPHIC ANALYSIS

The experiments outlined in Tables 2.2 and 2.3 produced castings of Al - 4.5% Cu which were prepared for further quantitative and qualitative analysis by metallographic and density techniques. The ingots were sectioned as illustrated in Figure 2.6. The centreline slice was cut into cubes according to the grid outlined, so that they could be quantitatively analysed by the density technique. Opposite the centreline slice, the left face was used for macroexamination while the right face yielded samples for microexamination.

2.3.1 Density Measurement

The quantitative analysis of microporosity was

Figure 2.6 Sectioning of Ingot for Density Measurements

SECTIONING PROCEDURE

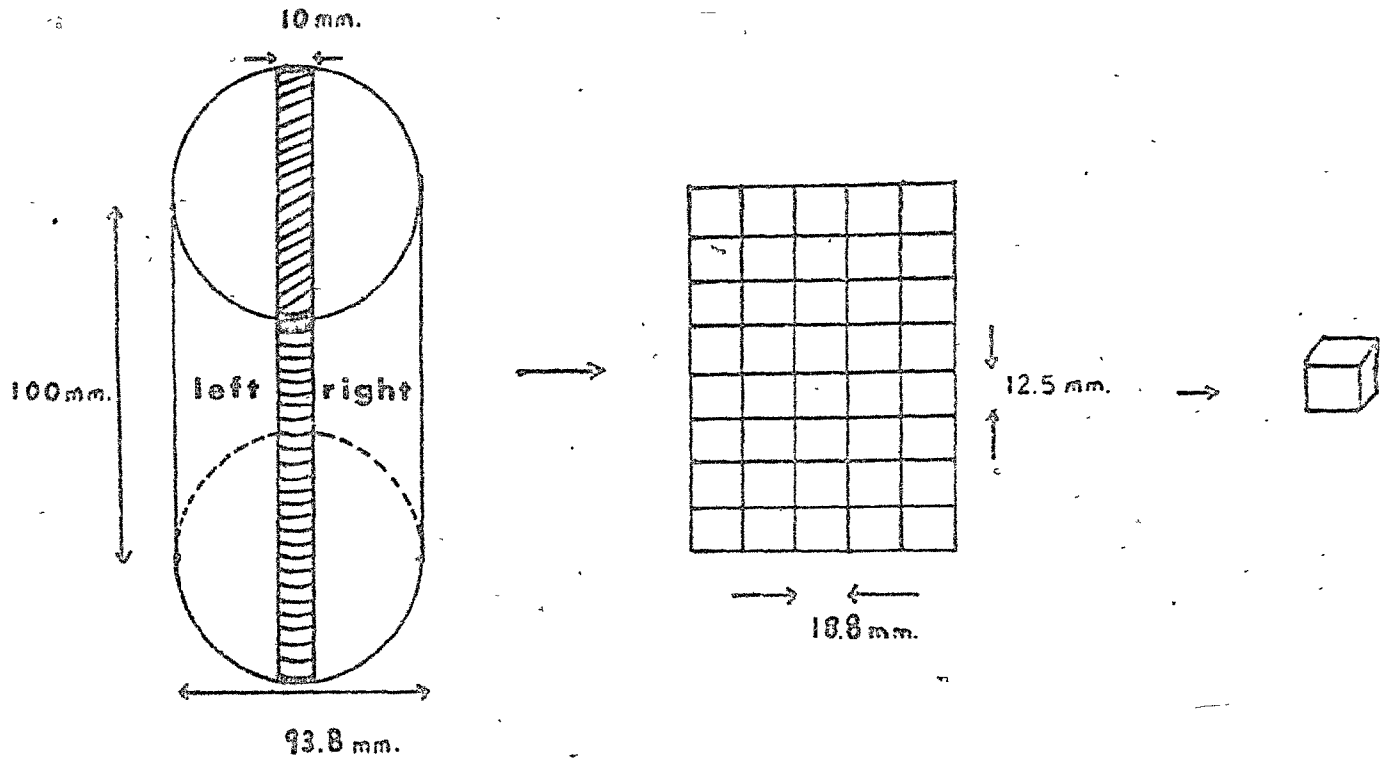

INGOT

CENTRELINE SLICE

CUBE

possible through the use of one of three techniques:

1) quantitative lineal metallography

2) density measurements

3) quantitative radiography

In this work density measurements were used to arrive at a quantitative measure of microporosity. This method was well established (27,29) for porosity measurements and the required apparatus was relatively easy to construct. Quantitative radiography was not employed because the required equipment was not available and density measurements were felt to be a reasonable alternative to the metallographic approach which involved the polishing of large numbers of porous samples.

A diagram of the apparatus used for density measurements is given in Figure 2.7 whereby the density is calculated using Archimedes' Principle. This technique measures porosity (blind pores) by comparing the weight of the sample in air and in another medium of known density, such as water. Pure ethanol can be used as an alternative. A sample calculation for porosity by this method is given

DENSITY APPARATUS

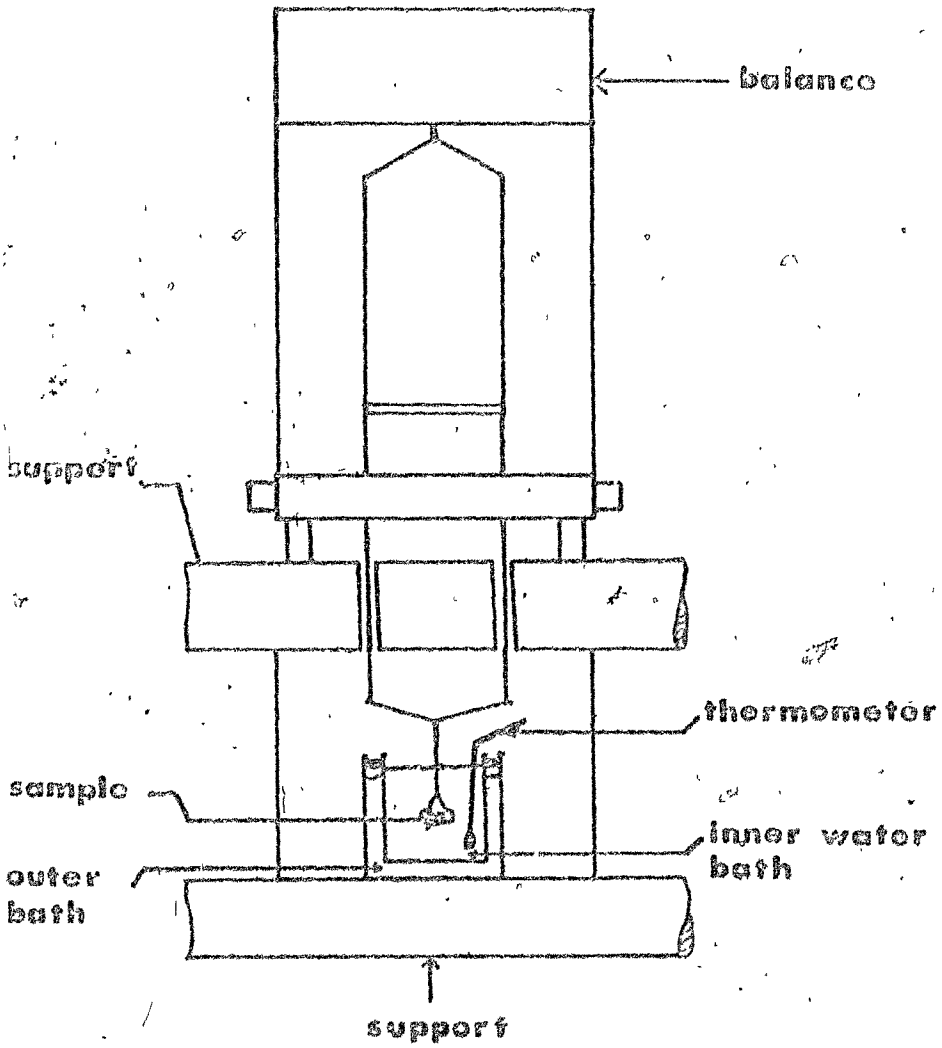

Figure 2.7 Density Apparatus

in Appendix II. Calibration of the apparatus to ensure accurate results was accomplished by two means. Firstly, the densities of pure Cu, Sn and Bi samples were measured and compared to known values [29], and then the apparatus was further checked by substituting pure ethanol for water. Identical results were obtained by each method (Table 2.5).

There were major difficulties in the density measurement technique; namely, a knowledge of the theoretical density of the alloy, and the entrapment of air bubbles on the sample surface during weighing. For the alloy used the theoretical density was dependent upon the copper content and could be calculated using a technique developed by two researchers at Alcoa [30]. A sample calculation using the technique appears in Appendix III. The accuracy of the calculation was checked by comparing it with the measured density of a rapidly chilled sample of the same alloy content. Values obtained by each method were found to be the same (Table 2.5). For each cast, only one theoretical density was calculated from the analysis of the alloy composition. Theoretical density was assumed constant throughout the entire cast, and this assumption is only valid if no macrosegregation occurs. To check the assumption, two slices were taken from the right face of two air melted ingots, casts A21 and A24 (Table 2.2). A grid similar to that

Table 2.5

Calibration of Density Apparatus

Part I Density of Pure Metals

Sample	Experimental Density gm/cm^3	Reported Density[29] gm/cm^3
Sn	7.2969 ± 0.0018	7.28
Cu	8.9261 ± 0.0011 *	8.92
Bi	9.8015 ± 0.0036	9.80

Part II Density of Quickly Frozen Sample

Sample	Experimental Density	Calculated Value[30]
Al - 4.5% Cu	2.7992	2.7985

* mean of 10 samples

made for the preparation of the density samples was constructed (Figure 2.6), and for each grid point two compositional analyses were made using the spectrograph as described in the earlier section. The results of these analyses are presented in Appendix IV, and mean results are presented in Table 2.6. Although microsegregation existed, both samples yielded the same copper amount, 4.73%. Only in the slowest cooled ingot did any amount of macrosegregation occur. The type was inverse, and as shown in Table 2.6 the copper content went as low as 4.58% at the centre to 4.83% at the outside. Even with this maximum amount of segregation, the density technique can yield porosity results to the nearest $\pm$ 0.1% as cited by other authors[27,28]. Macrosegregation was regarded as the major error in this technique with the error involved in the use of the density apparatus as secondary. Even so, to prevent the entrapment of air bubbles on the surface of the samples, the samples for density measurement were ground on 80 grit SiC paper to remove asperities and wetting agents (0.01% teepel) were added [28] to the distilled water in which the samples were weighed.

2.3.2 Metallographic Analysis

Each casting was sectioned as illustrated in Figure 2.6 with the opposite faces to the centreline slices used as

Table 2.6

Effect of Segregation in Al - 4.5% Cu *

Sample	Mean Values %Cu			
	Mean	Outside	Quarter Diameter	Center
A21**	4.73	4.78	4.74	4.62
A24***	4.73	4.83	4.71	4.58

* see Appendix IV

** cast at 825°C (1098K) into 25°C (298K) mould

*** cast at 825°C (1098K) into 400°C (673K) mould

samples for further examination. The left face was prepared for macro-examination by grinding smooth each sample on 80 grit SiC belts. Etching of the sample was carried out in caustic soda (0.1% NaOH) held at 60°C (333K) - 70°C (343K) for 3 - 5 minutes. The time of etching varied depending on the amount of eutectic present, because the role of the etch was to oxidize the $CuAl_2$. After etching in caustic soda, the samples were swabbed in a solution of 50% nitric acid in water.

From the right face of the section, samples were taken for microscopic examination. The method of selection followed a scheme by which samples were randomly selected from the chill, equiaxed and columnar zones. Selection also was made according to the absolute amount of porosity obtained from the density measurements.

All the samples were mounted in cold mount and hand ground on four Si-C papers, grit sizes 220, 320, 400 and 600 using water as the flow medium. Rough polishing was carried out using Brasso on a soft selvet cloth. After this operation, the samples were thoroughly cleaned in an ultrasonic cleaner before the final polish. The final polish was performed on a selvyt cloth using 0.3 micron alumina suspended in water. The samples were then cleaned in alcohol

and dried. During the grinding and the polishing steps, light pressure was employed to prevent the pores from being distorted.

For each sample dendrite arm spacing measurements were made, making use of a Quantiment Television Monitor microscope (Q.T.M.) A lineal intercept method was employed by which the number of interarm spacings was counted in a fixed distance. A starting point was set and the number of intercepts was counted in 5 mm lengths in four mutually perpendicular directions from the point. To faciliate the counting, the sample image was projected on to a television screen at 10X. A sample calculation using this procedure is shown in Appendix V1.

2.3.3 Scanning Electron Microscopy

This technique was employed to supply three - dimensional pictures of the micropores. For both the air and the vacuum melted samples displaying coarse porosity, 5 mm. high by 10 mm. diameter disks were cut. The disks were cold mounted and polished as described previously. Once polished they were removed from the mounts and used for S.E.M. examination.

2.3.4 Computer Modelling

An existing computer program[31] was used to calculate the local solidification time at the various nodal locations in the castings for the various air and vacuum runs. This program had been validated (i.e. parameters such as the heat transfer coefficients between the casting and the mould had been established) by experiment. The local solidification time is the time taken for the solidifying metal to go from the liquidus temperature to the solidus temperature. In the case of Al - 4.5% Cu the solidus temperature is actually the eutectic temperature. In addition the program was employed to calculate the times taken to reach certain fraction solids (As calculated by Scheil's Equation (Equation 1.9)).

CHAPTER III

RESULTS

The results from the experiments described in the previous chapter are presented here where the distribution, amount and type of porosity found is reported as a function of various solidification parameters.

3.1 TREATMENT OF EXPERIMENTAL DATA

A typical result making use of the density technique described in Section 2.3.1 is shown in Figure 3.1 where the percent porosity is given for every node or grid point of the centreline slice of the ingot. The specific case shown was one of the air castings, solidified under the casting conditions of 700°C (973K) pouring temperature, 25°C (298K) mould temperature and a gas content of 0.19 ml H_2 / 100 gm Al (S.T.P.). The density measurements for each casting, either air or vacuum, are presented in this manner in Appendix V. Values of porosity equal to or close to 100% represent those nodes where either piping was present or else sampling of the node, due to its size, was impossible.

Since it is rather difficult to make a comparison of the data as presented in this manner, the data was plotted

Figure 3.1 Typical porosity result in an ingot where percent porosity is given for every nodal point. Pouring temperature 700°C (973K), Mould temperature 25°C (298K), Hydrogen concentration 0.19 ml H_2/100 gm Al (S.T.P.), Atmospheric pressure.

Experimental Data

Pour temperature - 700°C (973K)

Mould temperature - 25°C (298K)

Pressure - 760 torr (1.01×10^5 Pa)

Gas Level - 0.19 ml H_2 gm Al (S.T.P.)

0.9648	100	100	100	1.6044
0.9791	1.1899	100	1.2221	0.9791
0.9684	1.3257	1.6044	1.3757	0.8755
0.8362	1.2328	1.2149	1.1435	0.8254
0.7683	1.0363	1.0327	1.0756	0.7075
0.6003	0.9148	1.0041	0.9326	0.5860
0.5324	1.0184	0.8398	0.7611	0.5789
0.1572	0.4145	0.4324	0.4753	0.1358

to produce distribution profile graphs as shown in Figure 3.2. The ingot represented in Figure 3.2 is the same as that in Figure 3.1. In producing these graphs, three assumptions were made:

1) Porosity at the mould wall is zero.

2) The values of porosity, are those at the centre of each individual sample.

3) Linearity of porosity exists between samples.

In addition, using the results as shown in Figure 3.1 and given in Appendix V, the mean amount and standard deviation of porosity in each ingot was calculated with the results presented in Table 3.1 for the air melts, and Table 3.2 for the vacuum melts. As seen in these tables, the deviation about the mean amount of porosity can be quite significant. Therefore great care should be taken in choosing a representative sample within an ingot in order to determine a mean porosity value.

3.2 POROSITY DISTRIBUTION PROFILES

3.2.1 Air Castings

The air melt experiments were designed to study

Table 3.1

Mean Values of Porosity in Air Castings

Melt Temp. °C (K)	Mould Temp. °C (K)	Initial Gas Content ml H_2 / 100 gm Al (S.T.P.)	Mean Value of Porosity %	Standard Deviation %
700 (973)	25 (298)	0.19	0.9	0.4
700 (973)	25 (298)	0.30	0.8	0.4
700 (973)	70 (343)	0.19	0.8	0.3
700 (973)	240 (513)	0.19	0.6	0.4
825 (1098)	25 (298)	0.46	1.1	0.6
825 (1098)	70 (343)	0.46	0.9	0.5
825 (1098)	250 (523)	0.46	1.1	0.7
825 (1098)	400 (673)	0.46	2.9	0.9
950 (1223)	25 (298)	0.45	3.1	1.0
950 (1223)	70 (343)	0.45	2.7	0.9
950 (1223)	250 (523)	0.45	3.5	1.1
825 (1098)*	25 (298)	0.23	0.9	0.5
825 (1098)*	70 (343)	0.23	0.6	0.4
825 (1098)*	250 (523)	0.23	1.4	0.5

* Grain Refined

the effect of various casting and solidification conditions on the amount, type and distribution of microporosity in an ingot. A result typical of those found at the lower superheats and hence faster rates of solidification is shown in Figure 3.2. For this case of a sample cast at a low pouring temperature, 700°C (973K); into a cold steel mould, 25°C (298K); with an initial gas content of 0.19 ml H_2 / 100 gm Al (S.T.P.); the pattern is such that one can readily identify contours of equal porosity, ie "isopores", which are perpendicular to the expected direction of heat transfer from the solidifying melt and whose magnitude increases from the outside to the inside of the cast.

At these low superheats, mould temperature has very little effect on the mean amount or distribution of microporosity. As illustrated in Figures 3.3 and 3.4 an increase in the mould temperature from 70°C (343K) to 240°C (513K) does not affect the distribution of porosity obtained. For each of the casts outlined in Figures 3.2 - 3.4 the mean amount of porosity was essentially constant at about 0.7 % (Table 3.1).

In addition, for these conditions of solidification the effect of initial gas content was minimal. With the

same superheat as before and a mould temperature of 25°C (298K), an increase in the initial gas content from 0.19 to 0.30 ml H_2 / 100 gm Al (S.T.P.) has no affect on the distribution profile as illustrated in Figure 3.5 or on the mean amount of porosity as shown in Table 3.1.

When the rates of solidification became slower, as a result of using higher pouring temperatures (825°C, 1098K; 950°C, 1223K) the pattern of porosity changed. As shown in Figure 3.6, pouring the liquid metal at 825°C (1098K) into a steel mould held at 25°C (298K), yielded results where the centreline symmetry of the profile began to breakdown and the isopore position was less predicable. Nevertheless, the isopores still followed the expected heat flow pattern. The initial gas content in this case was 0.46 ml H_2 / 100 gm Al (S.T.P.). When the mould temperature was increased to 250°C (323K) with the same casting conditions, the pattern (Figure 3.7) became more erratic with the isopores being randomly distributed in the cast. A further increase in the mould temperature to 400°C (673K) yielded a pattern (Figure 3.8) where the isopores were distributed as circles about the centre of the cast. The highest porosity existed at the centre and decreased in magnitude towards the outside. There was also a simultaneous change in mean porosity as the mould temperature

Figures 3.2 - 3.10 Porosity profiles in atmospheric cast ingots under different casting conditions. The isopore values given are in percentages.

Figure 3.2 Porosity profile of ingot shown in Figure 3.1. In producing this graph, three assumptions were made: 1) porosity at the mould wall is zero. 2) The values of porosity are those at the centre of each individual sample. 3) Linearity of porosity exists between samples.

Pouring Temp.	700°C (973K)
Mould Temp.	25°C (298K)
Pressure	1 atm.
Gas Content	0.19 ml. H_2/100gm Al (STP)

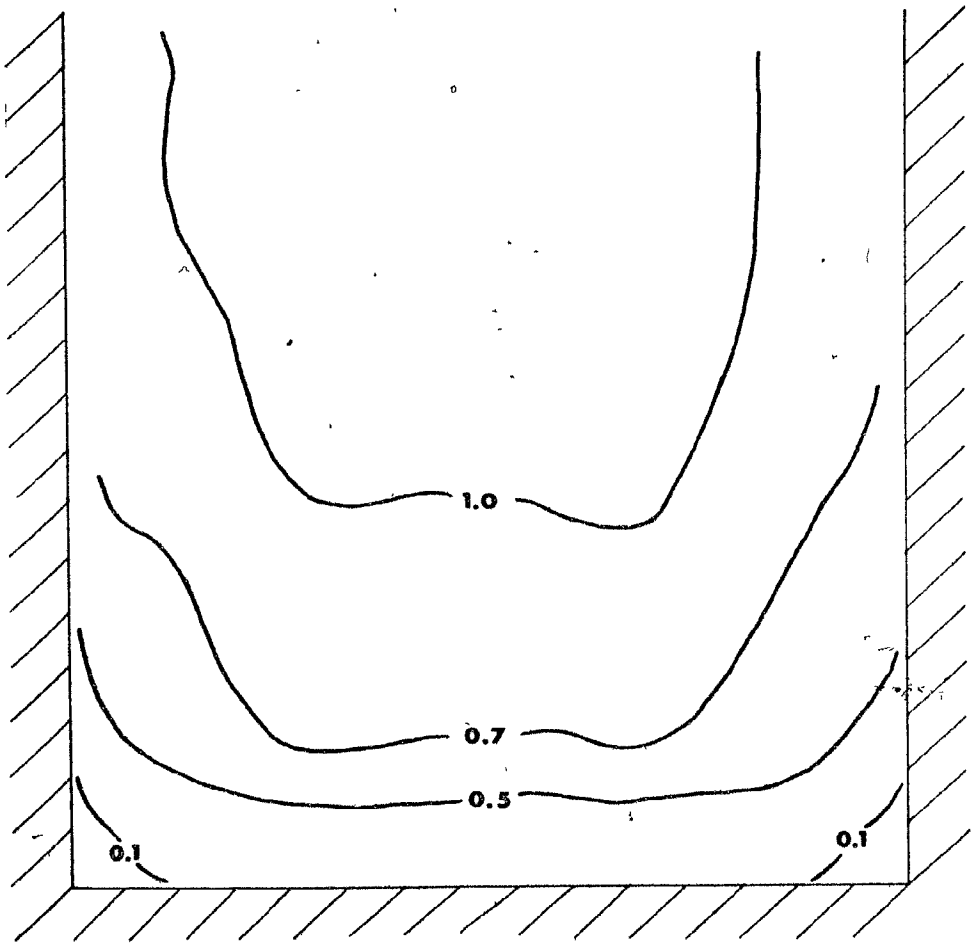

Figure 3.3 Effect of mould temperature on porosity distribution in an atmospheric cast ingot poured at low superheat. Pouring temperature 700°C (973K), Hydrogen Concentration 0.19 ml H_2/100 gm Al (S.T.P.), Mould temperature 70 °C (343K).

Pouring Temp.	700°C (973 K)
Mould Temp.	70°C (343 K)
Pressure	1atm.
Gas Content	0.19ml.H_2/100gm Al (STP)

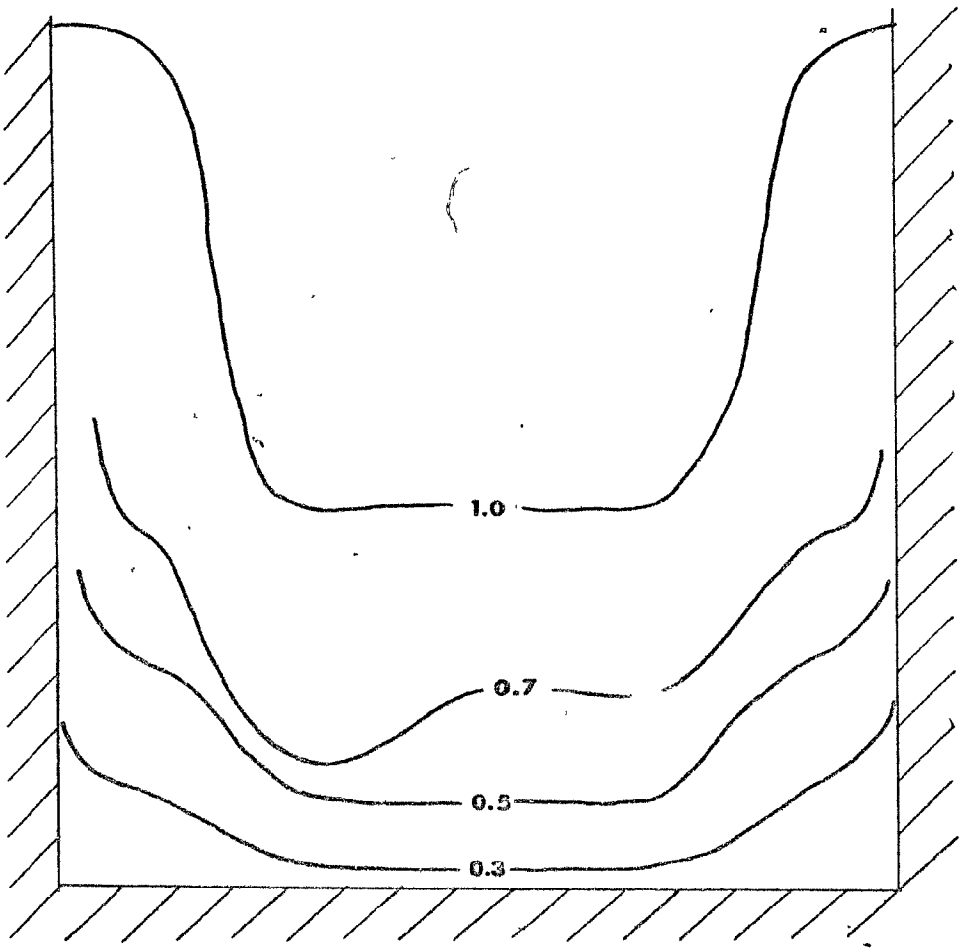

Figure 3.4 Effect of mould temperature on porosity distribution in an atmospheric cast ingot poured at low superheat. Pouring temperature 700°C (973K), Hydrogen Concentration 0.19 ml H_2/100 gm Al (S.T.P.) Mould temperature 240 °C (513K).

Pouring Temp.	700°C (973 K)
Mould Temp.	240°C (513 K)
Pressure	1 atm.
Gas Content	0.19 ml. H_2/100gm Al (S.T.P)

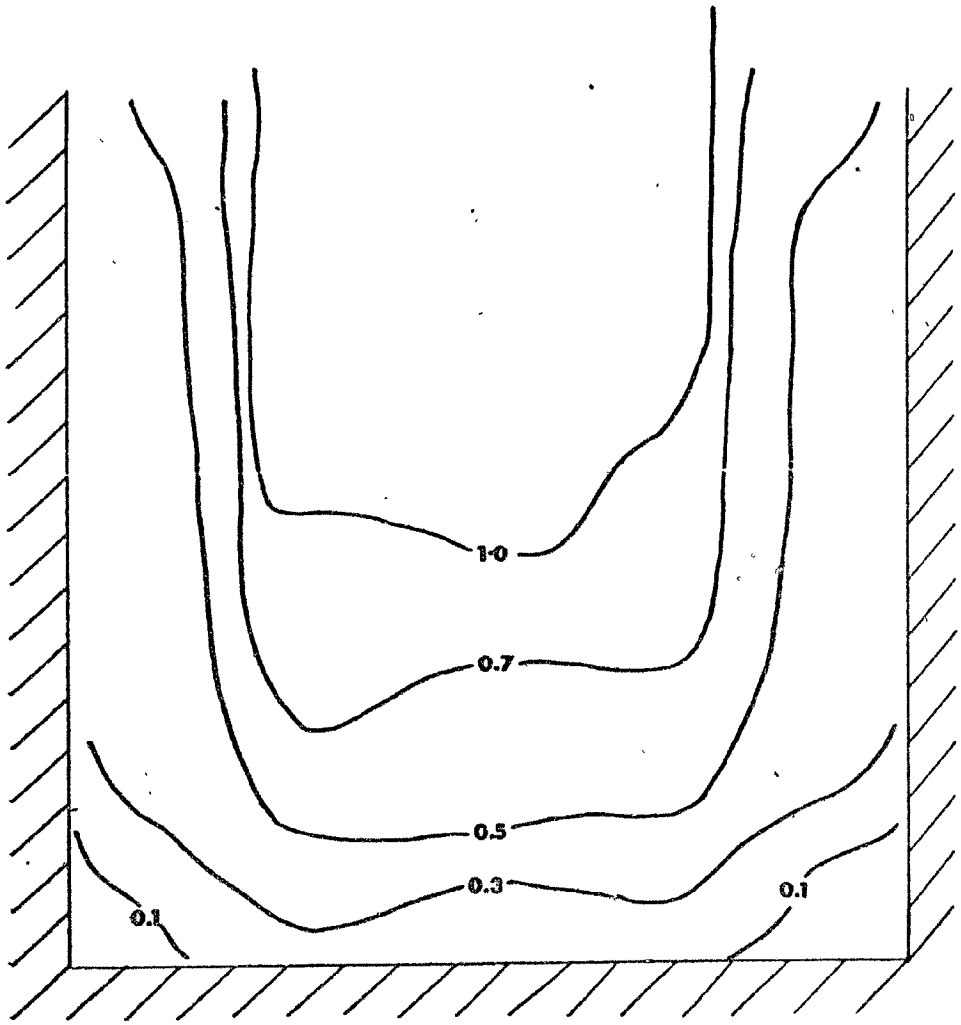

Figure 3.5 Effect of gas content on porosity distribution in an atmospheric cast ingot poured at low superheat. Pouring temperature 700°C (973K), Mould temperature 25°C (298K), Hydrogen Concentration 0.30 ml H_2/100 gm Al (S.T.P.).

Pouring Temp.	700°C (973K)
Mould Temp.	25°C (298K)
Gas Content	0.30 ml. H_2 / 100gm Al (S T P)
Pressure	1 atm.

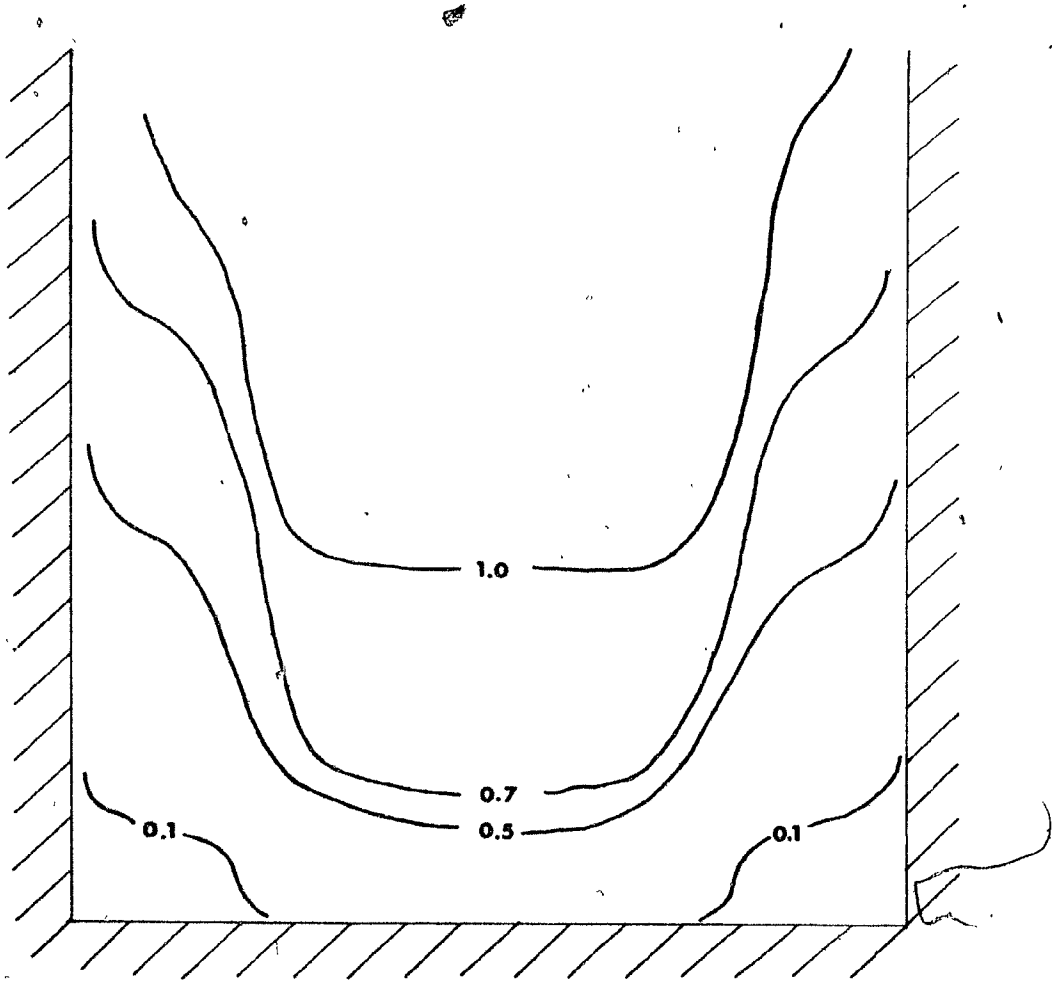

Figure 3.6 Porosity profile of atmospheric cast ingot poured at a higher superheat. Pouring temperature 825°C (1098K), Mould temperature 25°C (298K), Hydrogen concentration 0.46 ml H_2/100 gm Al (S.T.P.).

Pouring Temp.	825°C (1098 K)
Mould Temp.	25°C (298 K)
Pressure	1 atm.
Gas Content	0.46 ml. H_2/100gm. Al (S T P)

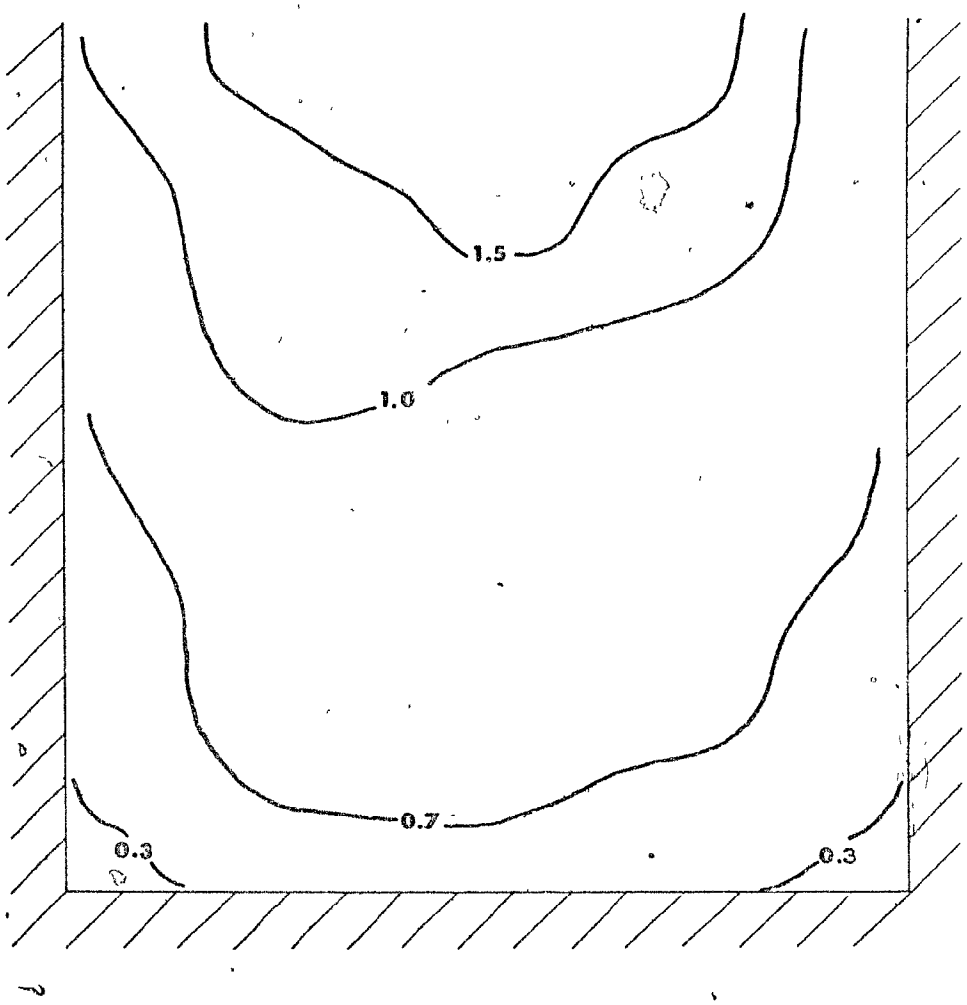

Figure 3.7 Effect of mould temperature on porosity distribution in an atmospheric cast ingot poured at high superheat. Pouring temperature 825°C (1098K), Mould temperature 250°C. (523K), Hydrogen concentration 0.46 ml H_2/100 gm Al (S.T.P.).

Pouring Temp.	825°C (1098 K)
Mould Temp.	250°C (523 K)
Pressure	1 atm.
Gas Content	0.46 ml. H_2 / 100gm. Al (S.T.P)

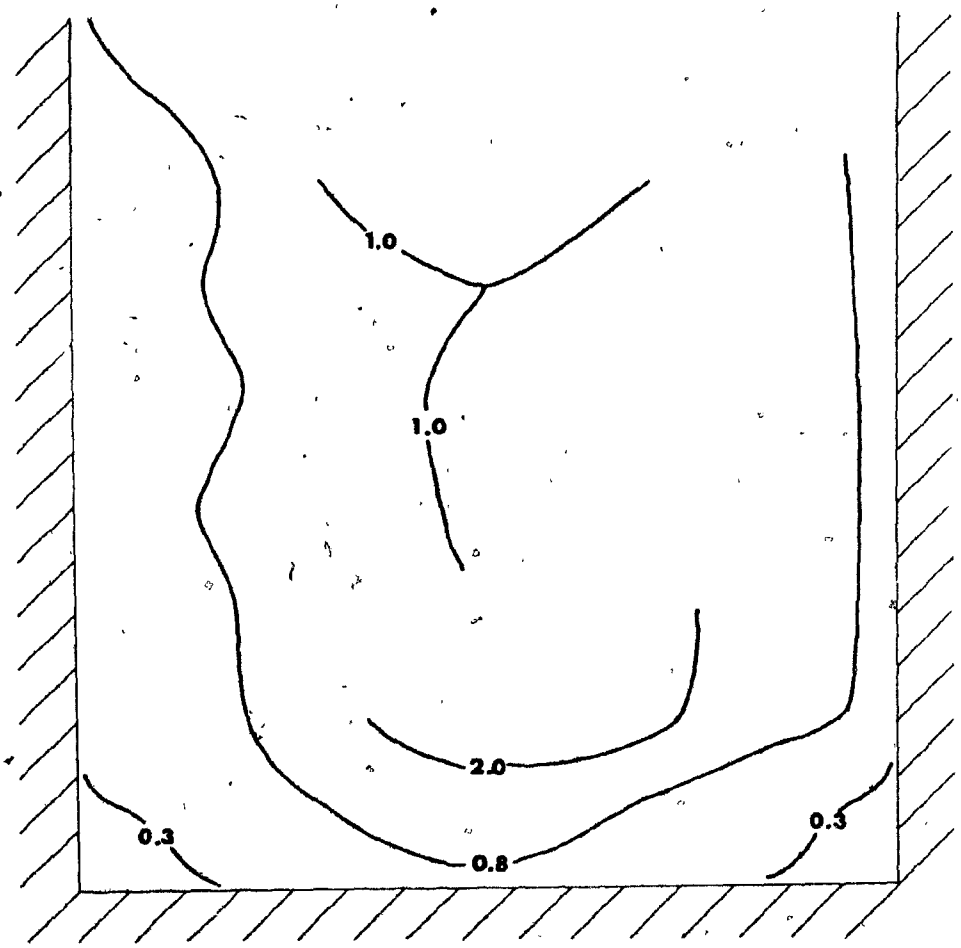

Figure 3.8 Effect of mould temperature on porosity distribution in an atmospheric cast ingot poured at high superheat. Pouring temperature 825°C (1098K), Mould temperature 400°C (673K), Hydrogen concentration 0.46 ml H_2/100 gm Al (S.T.P.).

Pouring Temp.	825°C (1098 K)
Mould Temp.	400°C (673 K)
Pressure	1 atm.
Gas Content	0.46 ml. H_2/100gm Al (STP)

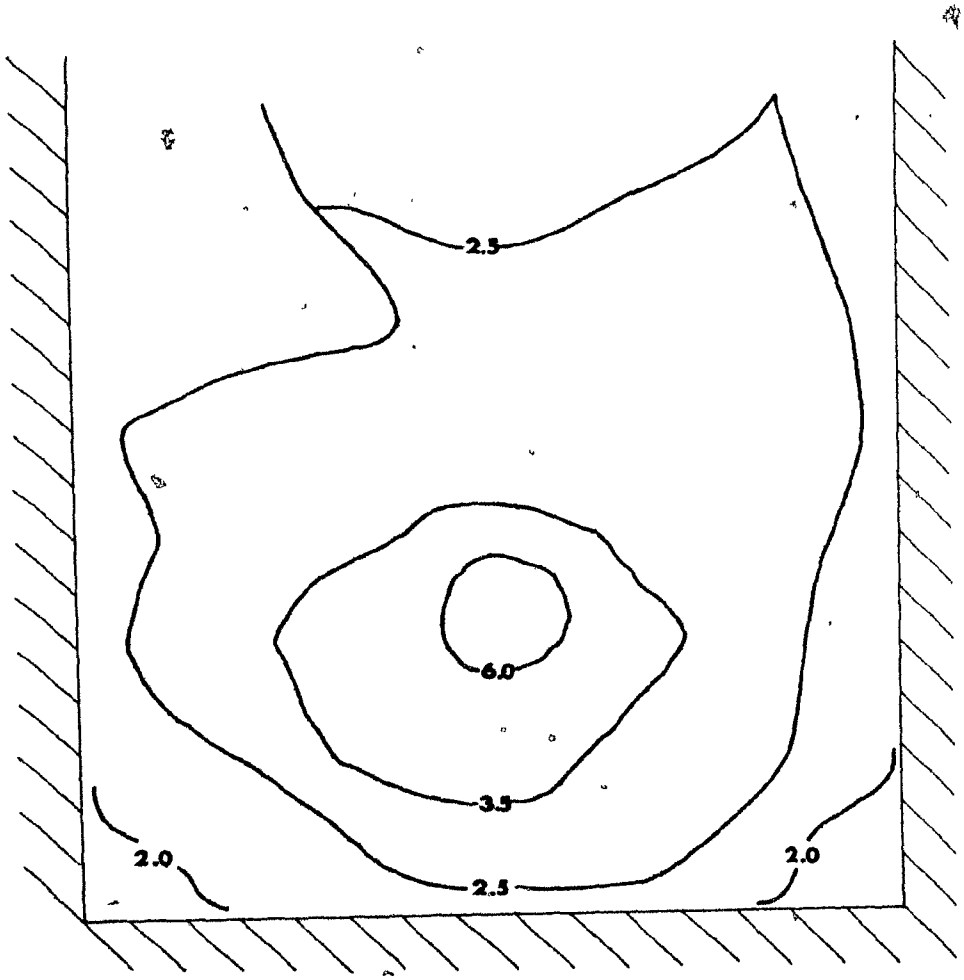

Figure 3.9 Effect of very high superheats on porosity distribution in an atmospheric cast ingot. Pouring temperature 950°C (1223K), Mould temperature 259°C (523K), Hydrogen concentration 0.45 ml H_2/100 gm Al (S.T.P.).

Pouring Temp.	950°C (1228 K)
Mould Temp.	250°C (523 K)
Pressure	1 atm.
Gas Content	0.45 ml. H_2/100gm Al (STP)

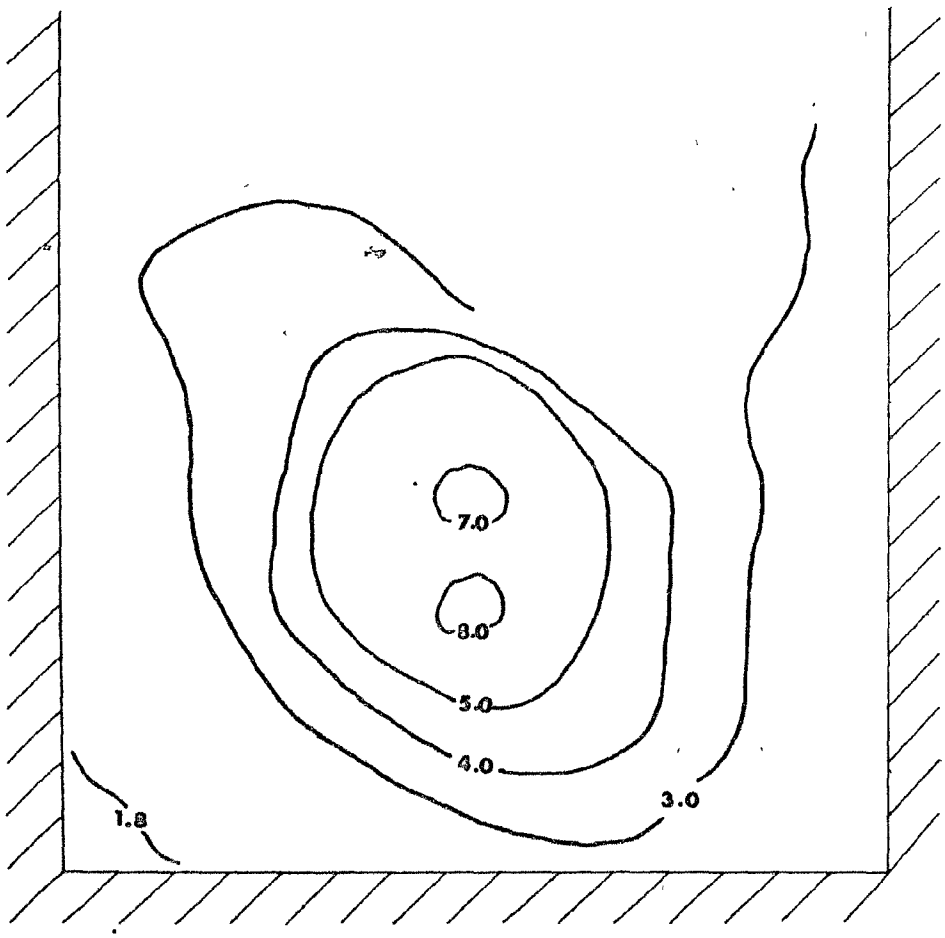

Figure 3.10 Effect of grain refining on porosity distribution in an atmospheric cast ingot poured at high superheat. Pouring temperature 825°C (1098K), Mould temperature 250°C (523K), Hydrogen concentration 0.23 ml H_2/100 gm Al (S.T.P.).

Pouring Temp. 825°C (1098K)
Mould Temp. 250°C (523K)
Pressure 1atm.
Gas Content 0.23 ml. H_2/100 gm Al (S.T.P)
GRAIN REFINED

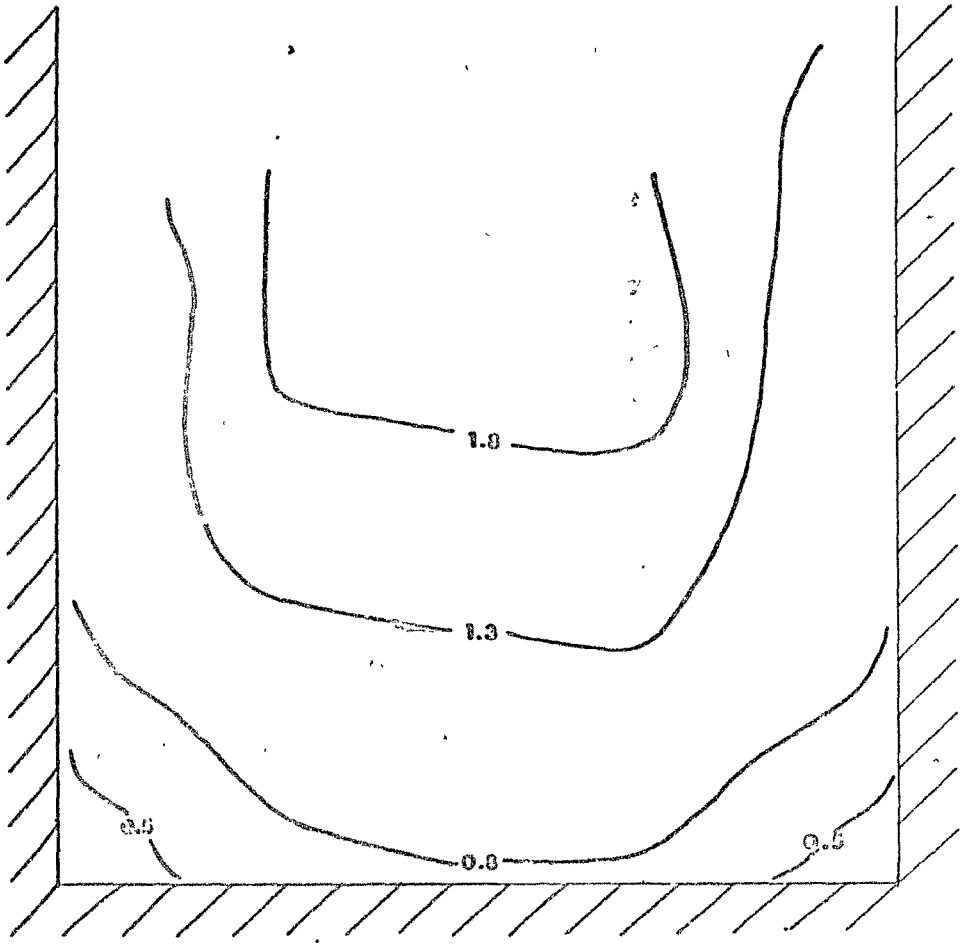

increased, ie. 1.0% at 250°C (523K) and 2.9% at 400°C (673K). The extreme case occured when the pouring temperature was increased to 950°C (1223K) with a 250°C (523K) mould temperature. The distribution then was such that porosity was concentric about the centre of the ingot (Figure 3.9); the same pattern as exhibited in Figure 3.8, but with higher centre and mean porosity (Table 3.1).

Several ingots were grain refined to determine if the grain size had any effect on the distribution and amount of porosity. As illustrated in Figure 3.10 for a cast poured at 925°C (1098K) into a 250°C (523K) mould, grain refining altered significantly the distribution of the pores but not the mean amount when compared to the non grain refined ingot (Figure 3.7). The distribution in the grain refined ingots reverted back to the type found at the lower superheats with the isopores being symmetric about the centre-line and following the expected position of the solidification front. However, the mean amount of porosity did not change.

3.2.2 Vacuum Castings

The effect of vacuum treatment on the aluminum alloy at 700°C (973K) and 0.25 torr (44.4 Pa) pressure was to bring about a sharp decrease in the hydrogen concentration of the melt. As shown in Figure 3.11 a 90 minute treatment

Figure 3.11 Vacuum degassing of hydrogen from Al - 4.5% Cu. Melt temperature 700°C (973K), Pressure over melt 0.25 torr (44.4 Pa), Area to volume ratio of liquid bath is 0.13 cm^{-1}.

VACUUM DEGASSING
of H_2 from Al - 4·5% Cu

Temperature of Melt	- 700°C 973 K
Pressure over Melt	- 0·25 torr 44·4 Pa
Type of Furnace	- Induction
Charge Weight	- 36 lbs (~14 kg)
A/V ratio	- 0·13 cm^{-1}

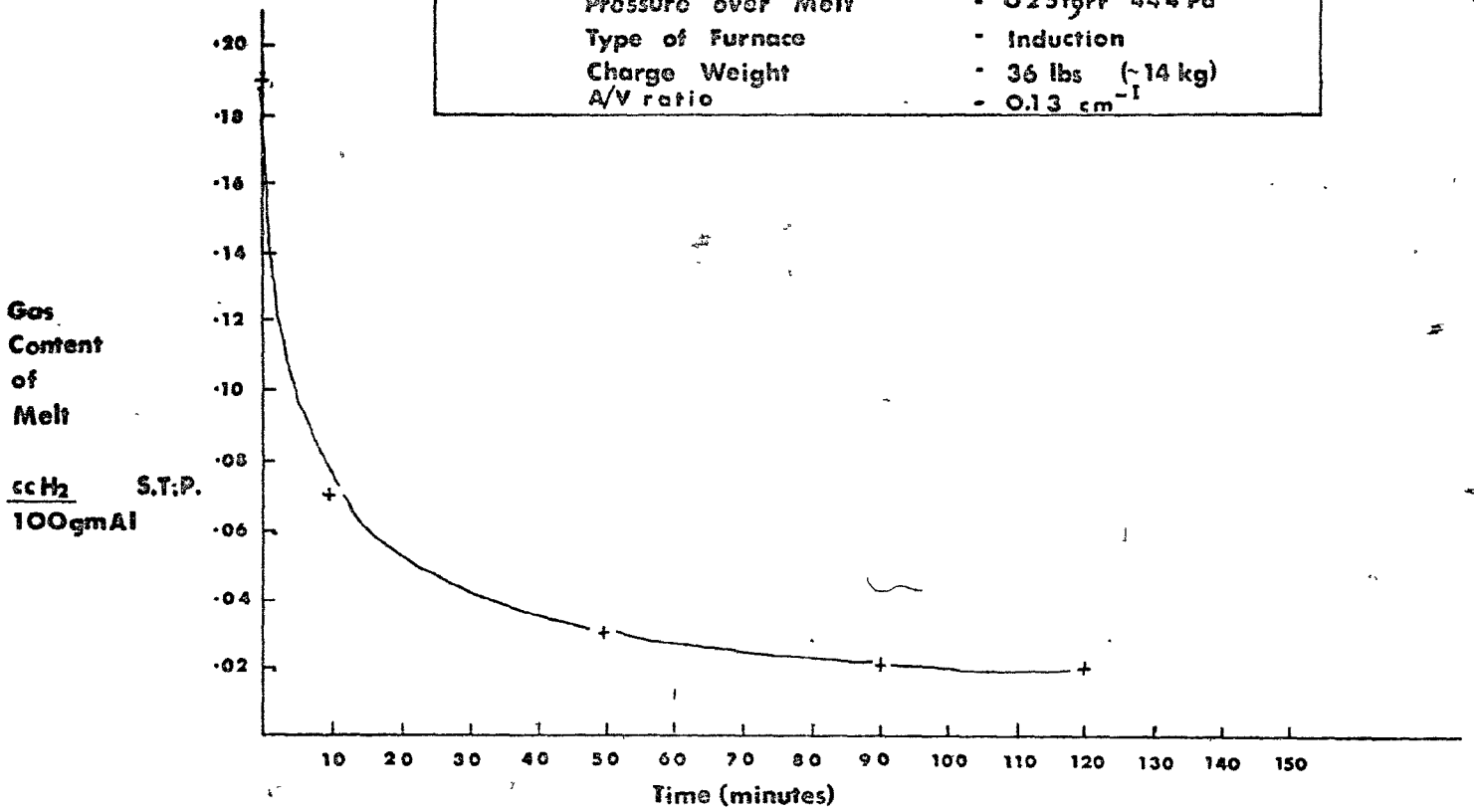

Table 3.2

Mean Values of Porosity in Vacuum Castings

Pouring Temp °C (K)	Mould Temp °C (K)	Pressure on Casting torr (Pascals)	Gas Content ml H_2/100 gm Al (S.T.P.)	Mean Value of Porosity %	Standard Deviation %
700 (973)	275 (548)	0.20 (26.6)	0.07	3.4	2.1
700 (973)	275 (548)	760 (1.01×10^5)	0.07	0.6	0.3
700 (973)	200 (473)	0.20 (26.6)	0.03	0.6	0.3
700 (973)	370 (643)	0.20 (26.6)	0.03	1.7	1.1
700 (973)	300 (573)	1.50 (200)	0.03	0.8	0.3
700 (973)	280 (553)	760 (1.01×10^5)	0.03	0.5	0.3
700 (973)	30 (303)	0.20 (26.6)	0.02	0.4	0.2
700 (973)	300 (573)	0.20 (26.6)	0.02	1.1	1.2
700 (973)	300 (573)	1.50 (200)	0.02	0.6	0.2
700 (973)	200 (473)	760 (1.01×10^5)	0.02	0.2	0.2
700 (973)	90 (363)	0.20 (26.6)	0.02	0.4	0.2
700 (973)	120 (393)	0.20 (26.6)	0.02	0.4	0.2
700 (973)	250 (523)	0.20 (26.6)	0.02	0.8	0.4
700 (973)	525 (798)	0.20 (26.6)	0.02	0.5	0.5
825 (1098)	275 (548)	0.35 (46.7)	0.14	4.4	5.0
825 (1098)	275 (548)	1.40 (187)	0.14	2.5	2.5
825 (1098)	275 (548)	100 (1.33×10^4)	0.14	1.5	1.4
825 (1098)	275 (548)	760 (1.01×10^5)	0.14	2.0	2.0

at these conditions reduced the hydrogen content from 0.19 ml H_2 / 100 gm Al (S.T.P.) to 0.02 ml H_2 / 100 gm Al (S.T.P.).

As in the atmospheric castings, a distribution of porosity within the ingot was found. Although the same trends occurred--a highly porous central region and a pattern of isopores more or less perpendicular to the heat flow direction--the vacuum cast results resembled air melts solidified at low freezing rates.

Lowering the hydrogen concentration of the melt and casting at atmospheric pressure did not alter significantly either the amount of distribution of porosity. As shown in Table 3.3, decreasing the gas content from 0.19 to 0.02 ml H_2 / 100 gm Al (S.T.P.) reduced the mean porosity from 0.6% to 0.2%. Yet, the distribution (Figure 3.12) was of the same type found under similar conditions of solidification, but at higher gas levels of 0.19 and 0.30 ml H_2 / 100 gm Al (S.T.P.) (Figures 3.2 and 3.5)

Table 3.4 illustrates the effect of pressure over the casting at various gas contents and pouring temperatures. For a low pouring temperature, 700°C (973K) and

Table 3.3

Effect of Initial Gas Content on Porosity

Pouring Temp. °C (K)	Mould Temp. °C (K)	Initial Gas Content ml H_2/100 gm Al (S.T.P.)	Applied Pressure torr (Pascals)	Mean Porosity %
700 (973)	25 (298)	0.19	760 (1.01 x 10^5)	0.9
700 (973)	25 (298)	0.30	760 (1.01 x 10^5)	0.8
700 (973)	70 (343)	0.19	760 (1.01 x 10^5)	0.8
700 (973)	240 (513)	0.19	760 (1.01 x 10^5)	0.6
700 (973)	275 (548)	0.07	760 (1.01 x 10^5)	0.6
700 (973)	280 (553)	0.03	760 (1.01 x 10^5)	0.5
700 (973)	200 (473)	0.02	760 (1.01 x 10^5)	0.2
700	275 (548)	0.07	0.20 (26.6)	3.4
700	300 (573)	0.02	0.20 (26.6)	1.1
825	250 (523)	0.46	760 (1.01 x 10^5)	1.1
825	275 (548)	0.14	760 (1.01 x 10^5)	2.0

an initial gas content of 0.07 ml H_2 / 100 gm Al (S.T.P.) decreasing the pressure from 1 atm (101.3KPa) to 0.20 torr (26.6Pa) resulted in an increase in porosity from 0.6% to 3.4%. The porosity distribution of the cast made at 0.20 torr (26.6Pa) (Figure 3.13) exhibited high central porosity in a pattern very similar to that found in the air melts at the higher superheats and mould temperature.

As the gas levels fell to 0.03 ml H_2 / 100 gm Al (S.T.P.) and below, the effect of decreasing the pressure over the casts was no longer significant. Two casts (Table 3.4) one at atmosphere and one at 1.50 torr (200.0Pa) yielded approximately the same mean amount of porosity. Yet, the distributions of porosity became more random at reduced pressure levels (Figure 3.14), similar to that obtained in the air casts solidified at the intermediate freezing rates. As the pressure increased to that of atmospheric pressure, the pattern (Figure 3.15) resembled that of similar air casts made at higher freezing rates.

In vacuum casting, the rate of solidification at the reduced gas levels had more effect on the amount and distribution than did the head pressure. Using a higher superheat of 825°C (1098K) increased the amount of porosity significantly (Table 3.4) but the effect of casting over a

Table 3.4

Effect of Pressure on Mean Porosity

Pouring Temp. °C (K)	Mould Temp. °C (K)	Gas Content ml H_2/100 gm Al (S.T.P.)	Applied Pressure Torr (Pascals)	Mean Porosity %
700 (973)	275 (548)	0.07	0.20 (26.6)	3.4
700 (973)	275 (548)	0.07	760 (1.01×10^5)	0.6
700 (973)	300 (573)	0.03	1.5 (200)	0.7
700 (973)	280 (553)	0.03	760 (1.01×10^5)	0.5
700 (973)	90 (363)	0.02	0.20 (26.6)	0.4
700 (973)	120 (393)	0.02	0.20 (26.6)	0.5
825 (1098)	275 (548)	0.14	0.35 (46.7)	4.4
825 (1098)	275 (548)	0.14	1.4 (187)	2.5
825 (1098)	275 (548)	0.14	100 (1.33×10^4)	1.5
825 (1098)	275 (548)	0.14	760 (1.01×10^5)	2.0

a large range of pressures of 1 atmosphere (101.3KPa) to 0.35 torr (46.6Pa) only yielded a 2-fold increase in mean porosity from 2.0% to 4.4%. The fact, that the casting in this series made at 100 torr (13.3KPa) resulted in a lower amount of porosity and displayed (Figure 3.16) fewer pockets of high porosity than that found at the higher pressure level (Figure 3.17), showed that although, the reduced pressure of 7 times did not affect porosity, the lower rate of heat extraction in the vacuum cast did.

It should also be noted that temperature resulted in a higher residual content. A gas level of 0.14 ml H_2/ 100 gm Al (S.T.P.) was obtained after 1.5 hours for a melt temperature of 825°C (1098K) and 0.35 torr (46.6Pa) pressure. (Table 3.2).

Even vacuum casting into a mould at higher pre-heated temperature can affect the porosity. Table 3.4 demonstrated this effect on the amount and distribution of porosity at reduced gas levels and pressure into moulds of different temperatures, for a pouring temperature of 700°C (973K). As the mould temperature increased from 90°C (363K) to 525°C (798K), no large change in mean porosity was found (Table 3.4), however, there was a change in the resulting distribution profile. At a low mould temperature of

Figures 3.12 - 3.19 Porosity profiles in vacuum cast ingots under different casting conditions. The isopore values given are in percentages.

Figure 3.12 Effect of reduced gas content on porosity distribution in an ingot cast under atmospheric pressure. Pouring temperature 700°C (973K), Mould temperature 200°C (473K), Hydrogen concentration 0.02 ml H_2/100 gm Al (S.T.P.)

Pouring Temp.	700°C (973 K)
Mould Temp.	~200°C (473 K)
Pressure	1 atm.
Gas Content	0.02 ml. H_2/100gm. Al (STP)

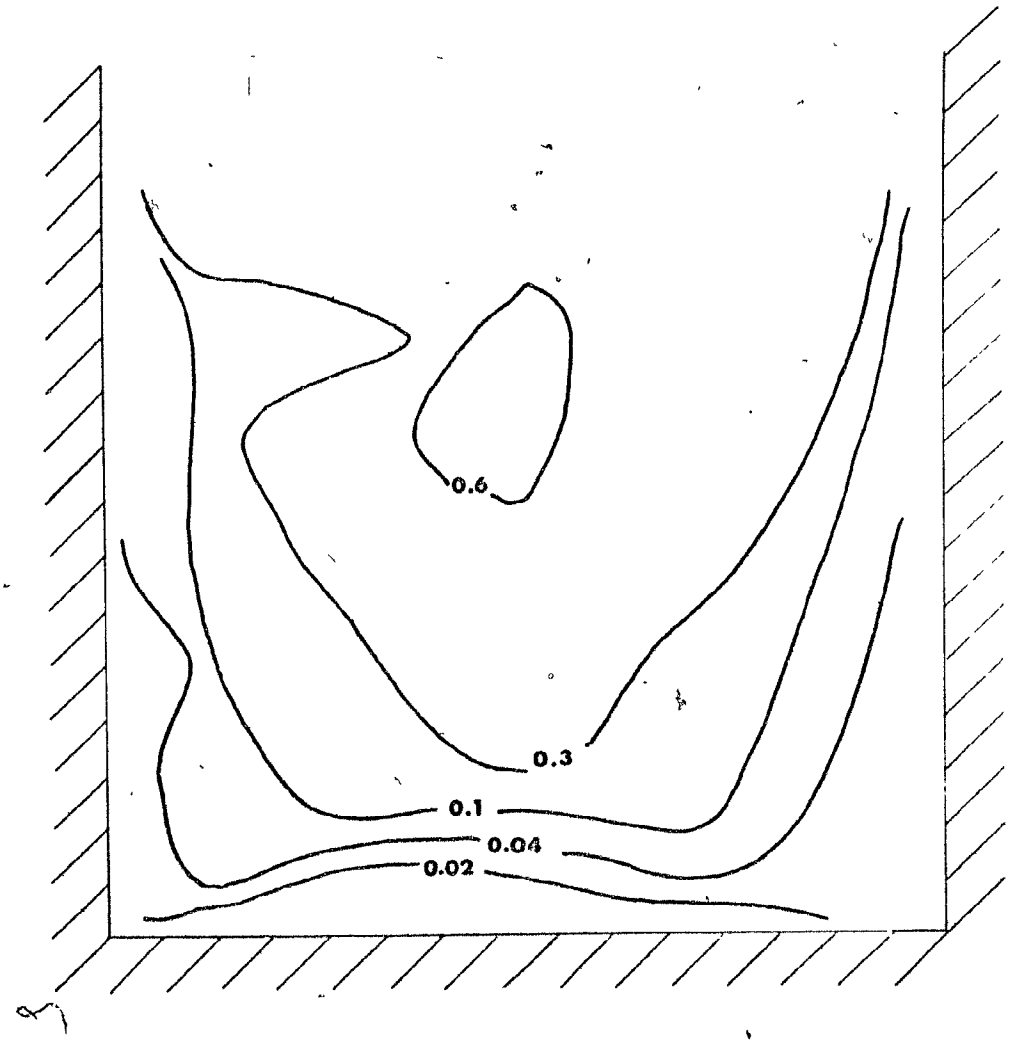

Figure 3.13 Effect of reduced pressure on porosity distribution in a cast ingot poured at low superheat. Pouring temperature 700°C (973K), Mould temperature 275°C (548K), Hydrogen concentration 0.07 ml H_2/100 gm Al (S.T.P.), Pressure over cast 0.20 torr (26.6Pa).

Pouring Temp.	700°C (973K)
Mould Temp.	275°C (548K)
Pressure	0.20 torr (26.6 Pa)
Gas Content	0.07ml. H_2/100 gm. Al (STP)

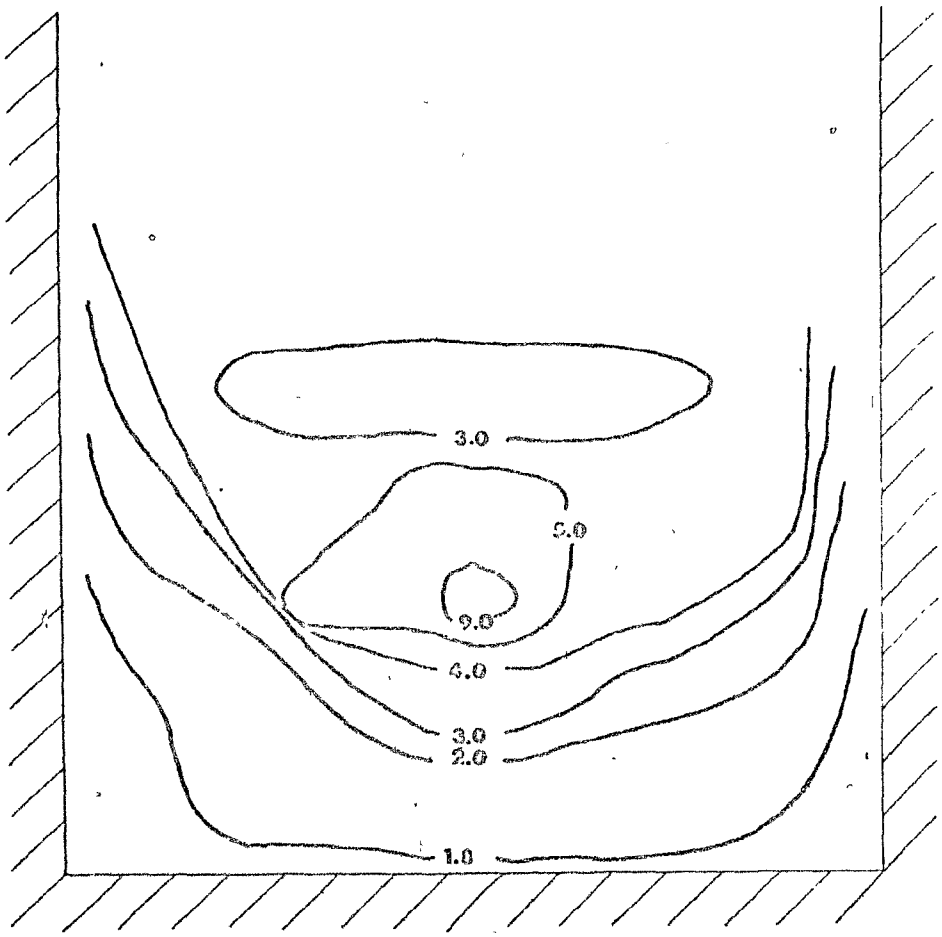

Figure 3.14 Effect of reduced pressure on porosity distribution. Pouring temperature 700°C (973K), Mould temperature 300°C (573K), Hydrogen Concentration 0.03 ml H_2/100 gm Al (S.T.P.), Pressure over cast 1.50 torr (200 Pa), Mean Porosity 0.7%.

Pouring Temp	700° C (973 K)
Mould Temp	300° C (573 K)
Pressure	1.50 torr (200 Pa)
Gas Content	0.03 ml H_2/100 gm Al (STP)

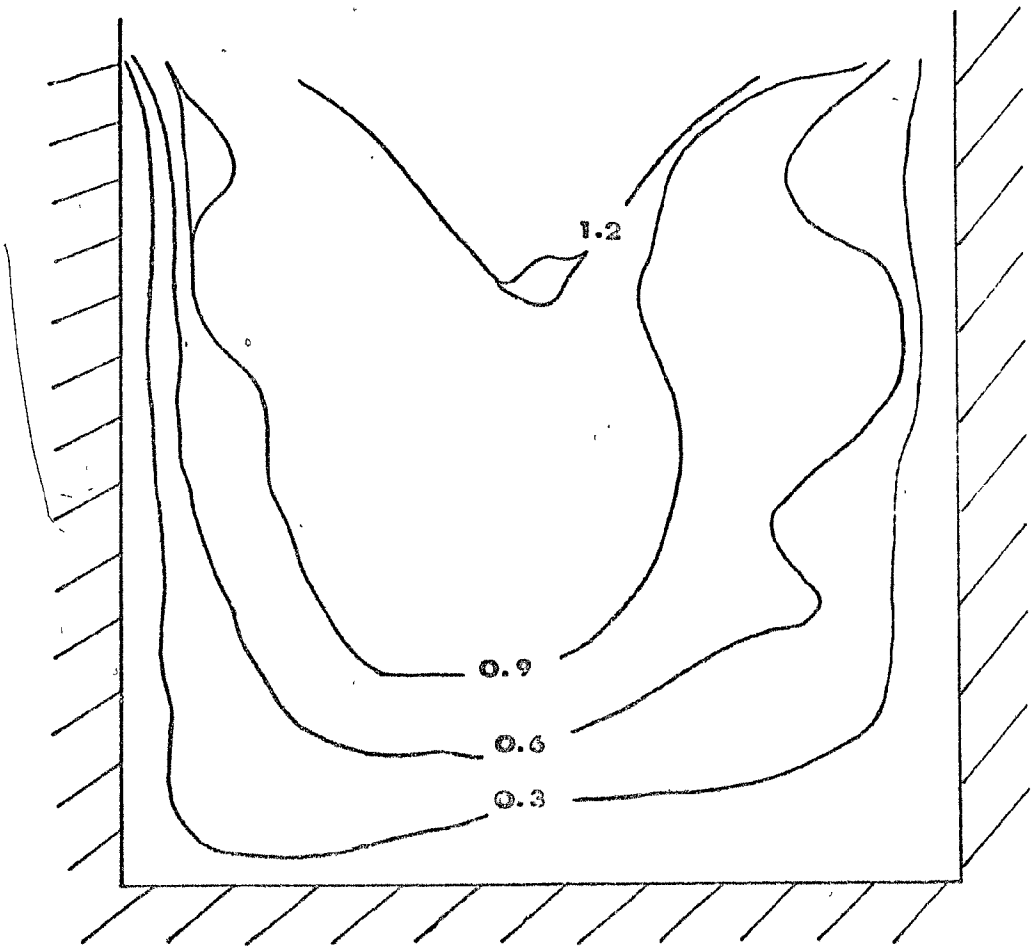

Figure 3.15 Effect of pressure on porosity distribution. Pouring temperature 700°C (973K), Mould temperature 280°C (553K), Hydrogen concentration 0.03 ml H_2/100 gm Al (S.T.P.) Pressure over cast 760 torr (101.3 KPa), Mean porosity 0.5%.

POURING TEMP	700°C (973K)
MOULD TEMP	280°C (553K)
PRESSURE	760 torr (101.3 KPa)
GAS CONTENT	0.03 ml H_2/100gm Al (S.T.P.)

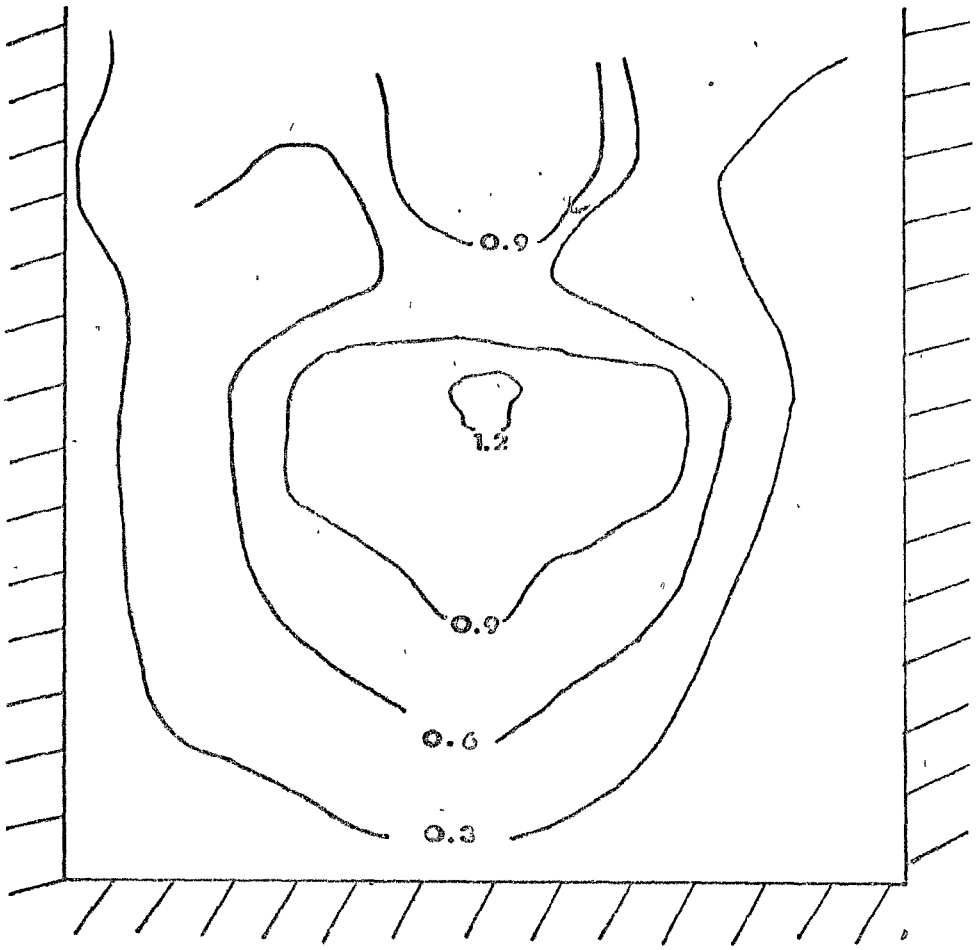

Figure 3.16 Effect of reduced pressure on porosity distribution in an ingot poured at high superheat. Pouring temperature 825°C (1098K), Mould temperature 275°C (548K), Hydrogen concentration 0.14 ml H_2/100 gm Al (S.T.P.), Pressure over cast 100 torr (13.3KPa).

POURING TEMP 825°C (1098 K)
MOULD TEMP 275°C (548 K)
PRESSURE 100 torr (13.3 KPa)
GAS CONTENT 0.14 ml/H_2 100 gm Al (STP)

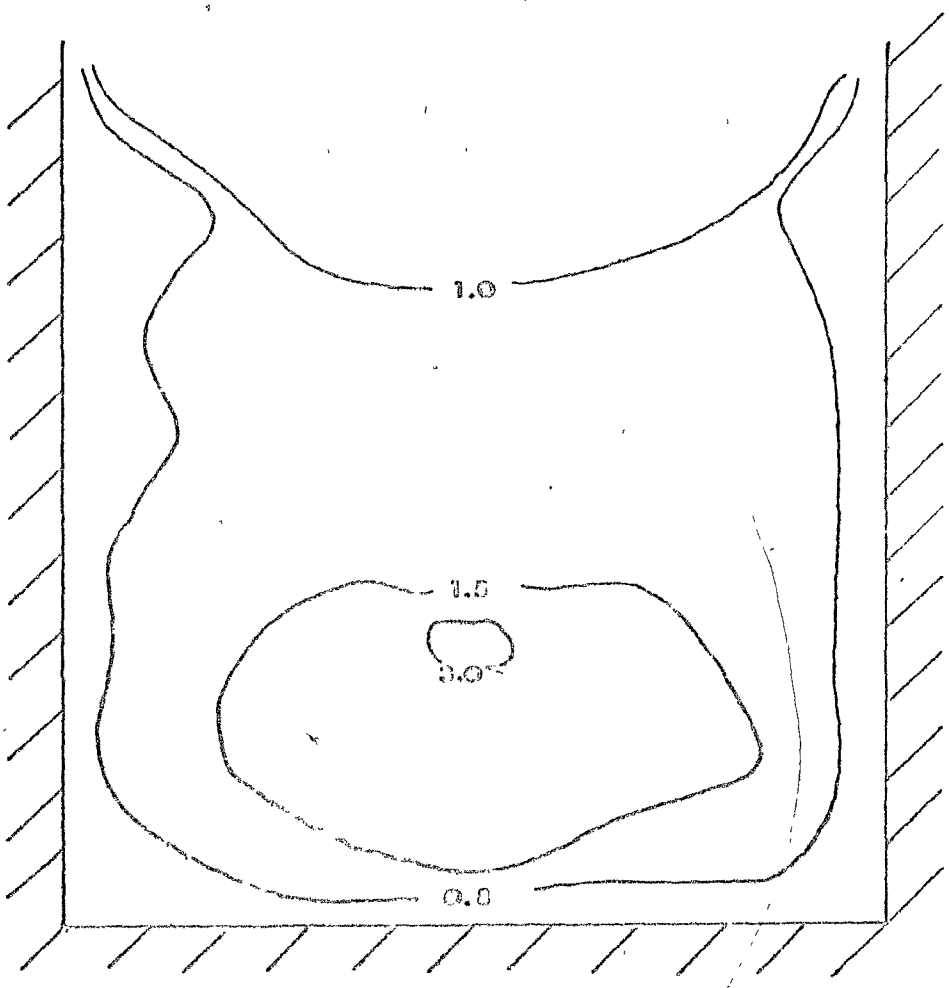

Figure 3.17 Porosity distribution in an ingot poured at high superheat. Pouring temperature 825°C (1098K), Mould temperature 275°C (548K), Hydrogen concentration 0.14 ml H_2/100 gm Al (S.T.P.), Pressure over cast 760 torr (101.1KPa).

POURING TEMP	825°C (1098K)
MOULD TEMP	275°C (548K)
PRESSURE	760 torr (101.3 KPa)
GAS CONTENT	0.14 ml H_2/100gm Al (S.T.P)

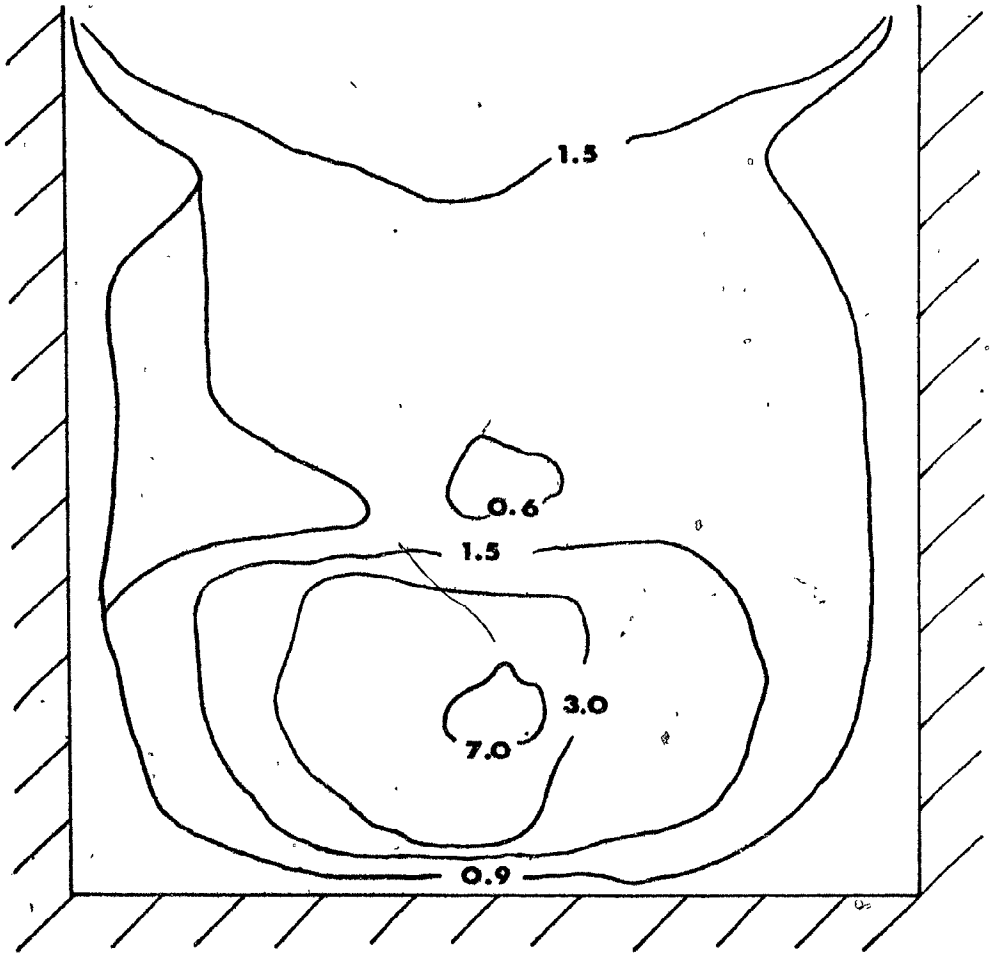

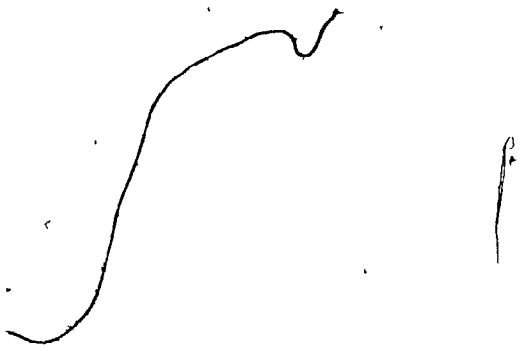

Figure 3.18 Effect of mould temperature on porosity distribution in an ingot poured under reduced pressure. Pouring temperature 700°C (973K), Hydrogen concentration 0.02 ml H_2/100 gm Al (S.T.P.), Pressure over cast 0.20 torr (26.6Pa), Mould temperature 90°C (363K), Mean Porosity 0.4%.

POURING TEMP	700°C (973K)
MOULD TEMP	90°C (363K)
PRESSURE	0.20 torr (26.6 Pa)
GAS CONTENT	0.02 ml H_2/100gm Al(S.T.P.)

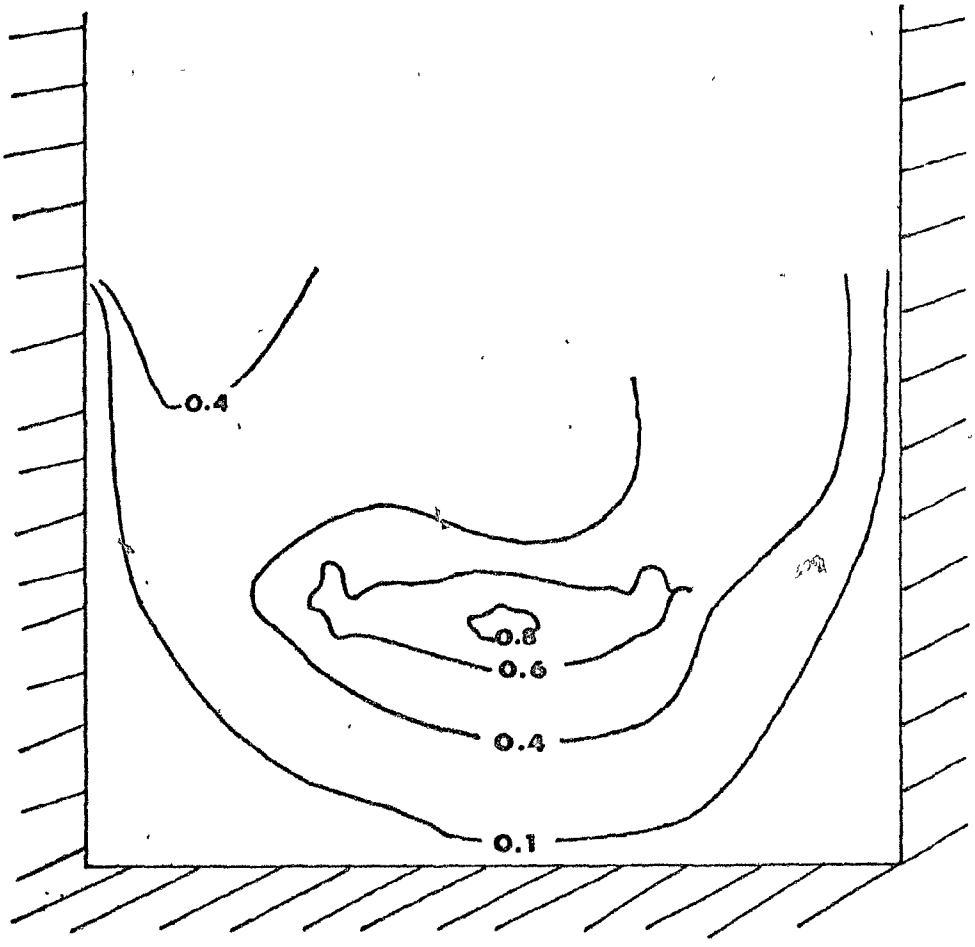

Figure 3.19 Effect of mould temperature on porosity distribution in an ingot poured under reduced pressure. Pour temperature 700°C (973K), Hydrogen concentration 0.02 ml H_2/100 gm Al (S.T.P.). Pressure over cast 0.20 torr (26.6Pa), Mould temperature 525°C (798K), Mean porosity 0.5%.

POURING TEMP	700°C (973K)
MOULD TEMP	525°C (798K)
PRESSURE	0.20 torr (26.6 Pa)
GAS CONTENT	0.02 ml H_2/100gm Al STP

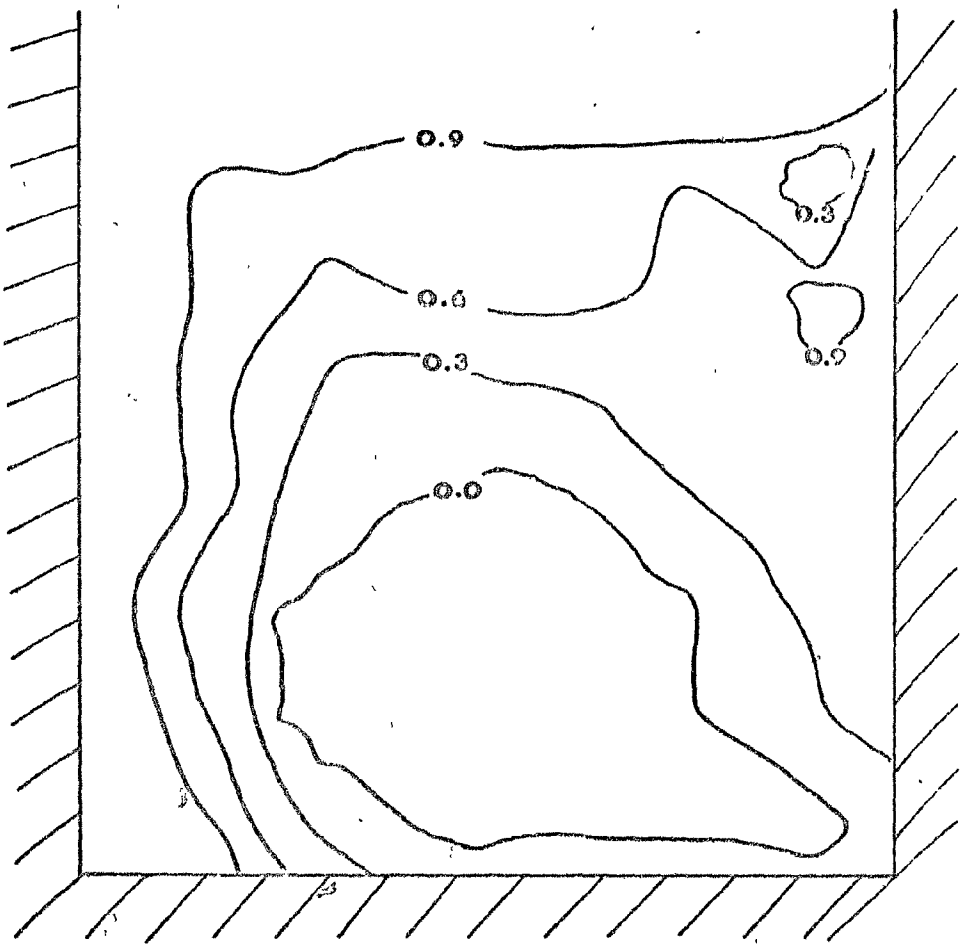

90°C (363K) the isopores (Figure 3.18) followed the expected position of the solid/liquid interface with the amount of porosity less at the mould walls. At a temperature of 525°C (798K) the profile (Figure 3.19) was very different yielding a sound centre with a very porous ingot surface (Figure 3.20).

3.3. RELATIONSHIP OF POROSITY TO STRUCTURE

Macroexamination and microexamination of the cast materials yielded some information about the nature of porosity and its distribution in the cast.

3.3.1 Macrostructure

At the outset, it is worth noting, that changes in the type of grain, eg columnar vs equiaxed, did not result in any abrupt change in either the amount or distribution of porosity. All changes were seen to be gradual.

A fine columnar or equiaxed structure (Figure 3.21) was typical of ingots that displayed low amounts of porosity. This type of structure was obtained either by casting at low superheat or else by grain refining the melt. The ingots which displayed the structure (Table 3.5) were cast at

Table 3.5

Grain Structure of the Castings

Group No.	Type of Grain Present	Sample *
1	Fine equiaxed	A41, A42, A43
2	Fine columnar	A11, A12, A13, A14,
	Fine equiaxed	V12, V24, V34
3	Mixture of Group 2	A21, A22, V23, V33,
	and Group 4	V31, V41
4	Coarse columnar	A23, A31, V11, V21, V22,
	Coarse equiaxed	V32, V42, V43, V44, V54
5	Coarse columnar	A24, A32, A33,
		V51, V52, V53

* Sample numbers are listed in Tables 2.2 and 2.3

700°C (973K) under atmospheric pressure, irrespective of the gas content, and those cast at 825°C (1098K) which were grain refined. For all these castings, the typical type of distribution profile (Figure 3.2), displayed isopores which followed the expected position of the solidification front and which were greatest in the last areas to solidify. In all of these ingots porosity was not visible to the naked eye.

As the structure became coarser as the direct result of slower freezing rates, the amount of porosity increased (Table 3.1). Porosity in these ingots was often of a layer type in microstructure (Figure 3.22) which could be detected without the use of a microscope. Etching in Keller's reagent of the vacuum and air samples revealed that the porosity occurred in the intergranular regions (Figure 3.23) in both coarse columnar or equiaxed structures.

A coarse equiaxed structure (Figure 3.24) produced a distribution profile where the position and the amount of the isopores tended to be unpredictable (Figure 3.6), while a coarse columnar structure (Figure 3.25), obtained at relatively slower freezing rates, yielded a porosity profile exhibiting very high central porosity and isopores that

formed concentric circles of decreasing magnitude from the centre of the cast.

The two types of structures described above were typical of the non-grain refined air melts at higher superheats of 825°C (1098K) and above. Also included with these casts (Table 3.5) were the vacuum casts-all those at 825°C (1098K) and the casts at 700°C (973K) cast under vacuum.

Along with these results was an observation made only with some vacuum casts. As illustrated by Figure 3.26, the larger and coarser equiaxed grains were associated with less porosity while the smaller grains in the centre exhibited higher amounts of porosity.

3.3.2 Microstructure

Examination of the microstructures of these castings which exhibited a fine columnar or equiaxed structure (Figure 3.21), revealed that the pores were interdendritic in nature (Figure 3.27), occurring on the same scale as the secondary dendrite arms. In some cases as exhibited by Figure 3.28 the pores were long and narrow occurring in the direction of the heat flow.

Figures 3.20 - 3.30 Macro and Micro examination of the cast materials.

Figure 3.20 Porous ingot surface of ingot described in Figure 3.19 X 3/4

Figure 3.21 Fine columnar and equiaxed structure, typical of ingots that displayed low amounts of porosity. Pour temperature 700°C (973K), Mould temperature 200°C (473K), Hydrogen concentration 0.02 ml H_2/100 gm Al (S.T.P.), Pressure ove cast 760 torr (101.3Pa) X 3/4

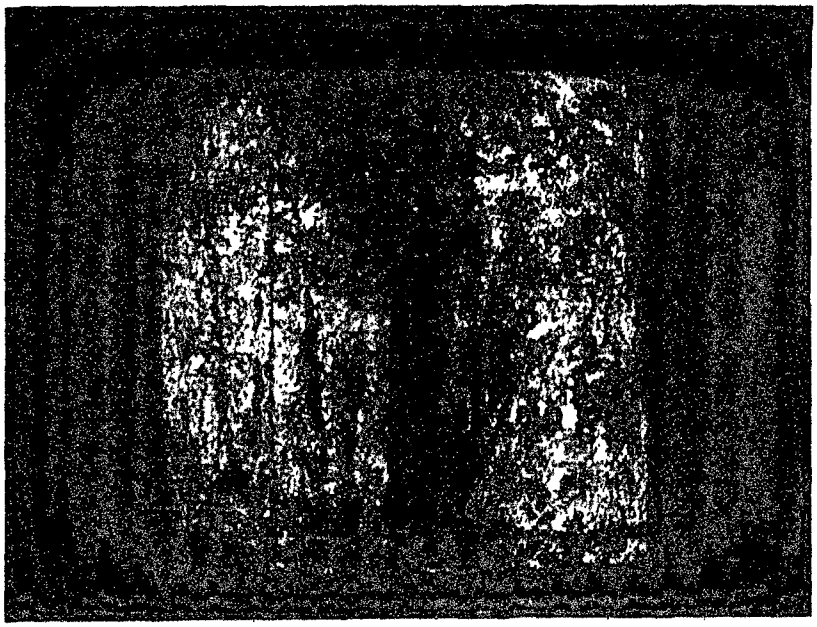

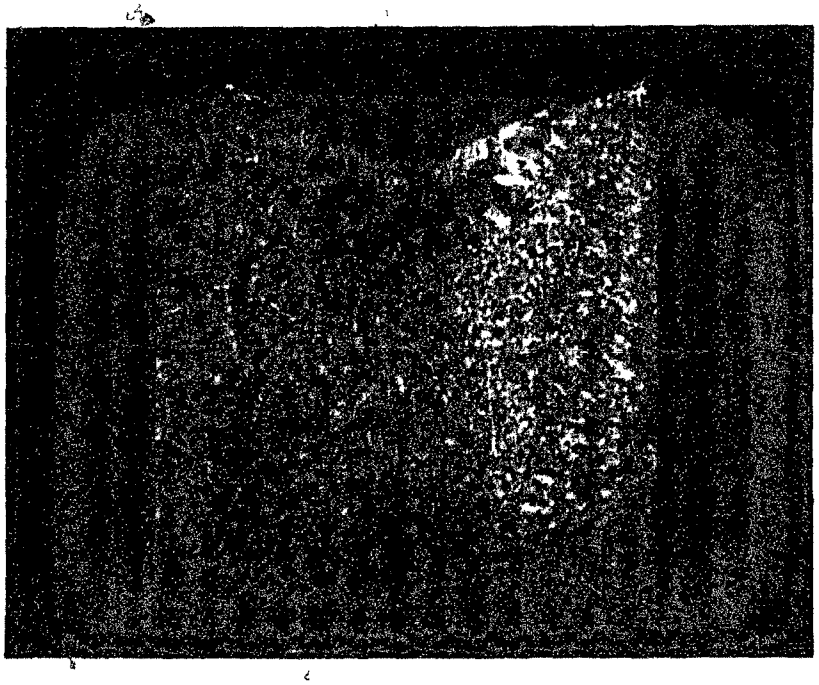

Figure 3.22 Micrograph of an atmospheric cast ingot showing a high degree of layer porosity. Pouring temperature 950°C (1223K), Mould temperature 250°C (523K). Unetched x 20

Figure 3.23 Micrograph of a region of layer porosity showing its intergranular nature. Pouring temperature 950°C (1223K), Mould temperature 250°C (523K). Dilute Keller's etch x 40

Figure 3.24 Macrostructure of an atmospheric cast ingot exhibiting coarse equiaxed grains in the centre. Pouring temperature 825°C (1098K), Mould temperature 25°C (298K). 0.1% NaOH etch X 9/10

Figure 3.25 Macrostructure of an atmospheric cast ingot exhibiting coarse columnar grains. Pouring temperature 950°C (1098K), Mould temperature 250°C (523K). 0.1% NaOH etch X 9/10

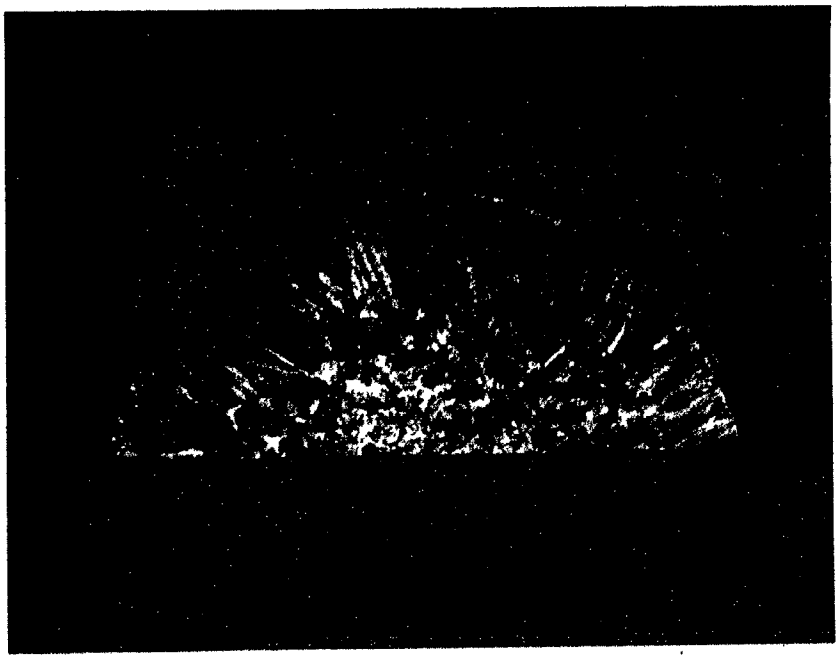

Figure 3.26 Macrostructure of a vacuum cast ingot exhibiting higher porosity in regions of smaller equiaxed grains. Pouring temperature 700°C (973K), Mould temperature 90°C (363K), Hydrogen concentration 0.02 ml H_2/100 gm Al (S.T.P.), Pressure over cast 0.20 torr (26.6Pa).

0.35%

055%

Figure 3.27 Microstructure of a vacuum cast ingot showing fine interdendritic porosity. Unetched x 170

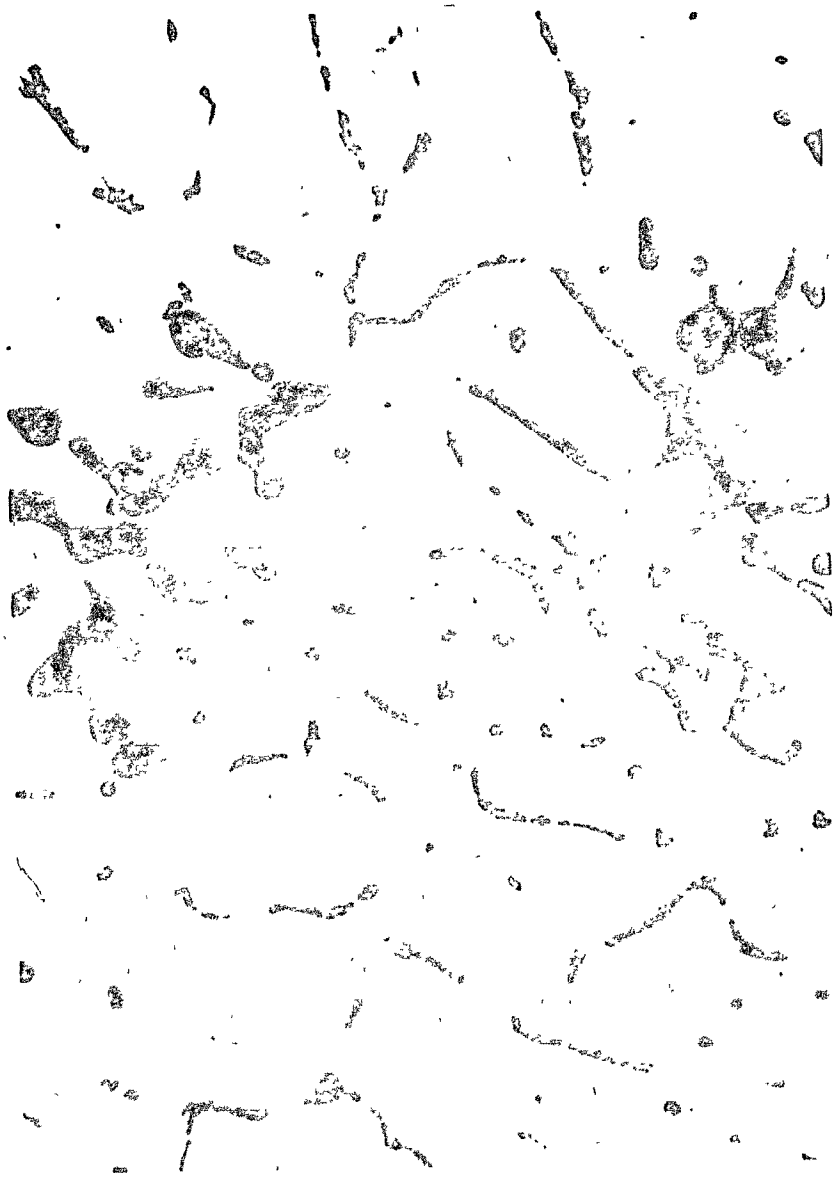

Figure 3.28 Microstructure of an atmospheric cast ingot showing fine interdendritic porosity in the direction of the heat flow. Unetched, X 170.

Figure 3.29 Scanning electron micrographs of a "hot tear" region showing the dendritic lining of the pore. a) X 84 b) X 168.

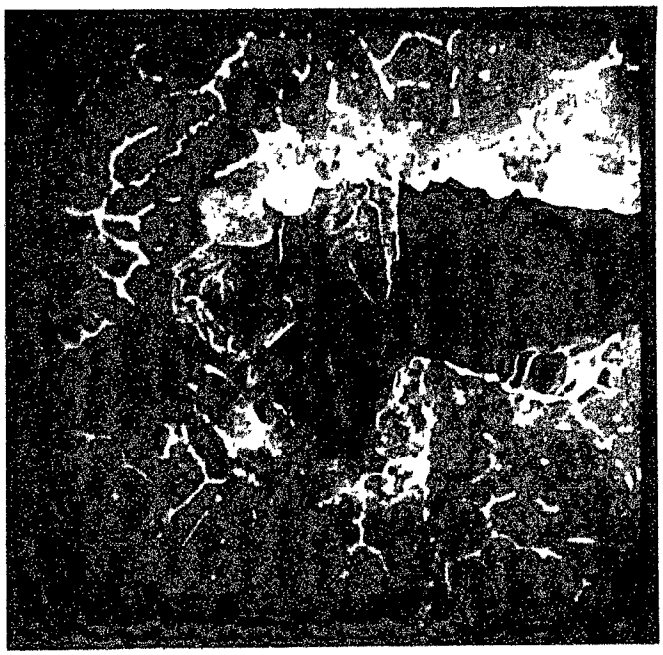

(a)

(b)

Figure 3.30 Scanning electron micrograph of a "gas type" pore a) X 42 b) X 168

(a)

(b)

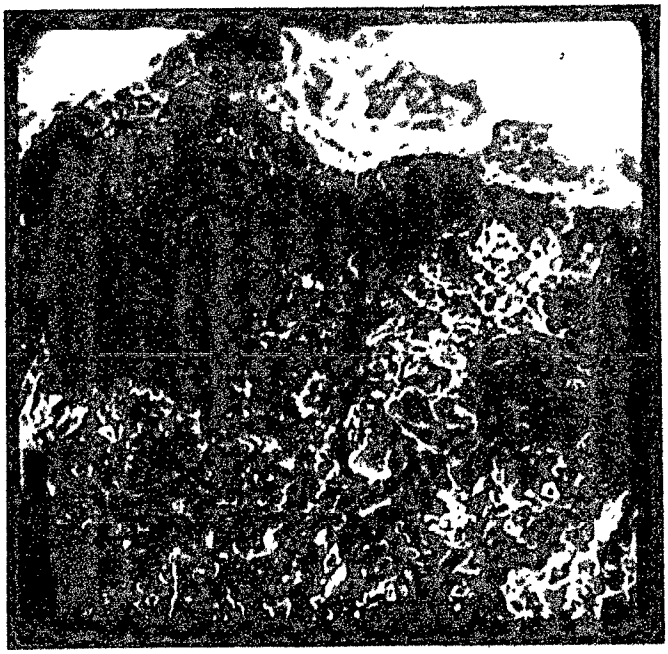

The intergranular pores (Figure 3.23) which were visible to the naked eye were examined further through use of the scanning electron microscope. Random samples of these pores were chosen from both the air and vacuum melts. This examination revealed two very different types of pores. One type exhibited a pore/metal interface that was lined with dendrites resembling a decanted or "hour out" interface (Figure 3.29). On closer inspection, the pore was seen to be on a size scale considerably greater than that of the secondary dendrite arms. A higher magnification (Figure 3.29b) of the same pore showed secondary dendrite arms with the area between the arms rich in eutectic.

The second type of pore took a different form, resembling a pore thought to be caused by dissolved or entrapped gas. The pore was circular in shape with dendrites protuding at the surface (Figure 3.30a). In Figure 3.30b the pore/metal interface is very rough and may well be lined with dross.

3.4 INFLUENCE OF SOLIDIFICATION PARAMETERS

An attempt was made to correlate the amount of porosity to the secondary dendrite arm spacing of the ingot on the grounds that this parameter is important in controlling

interdendritic solidification and consequently feeding. Two methods were used in the correlation. The secondary arm spacings were measured on several samples (Table 3.6), and an existing computer program [31] was used to compute the local solidification times at locations in the ingots from which the density samples were taken. The local solidification time, as stated beforehand, is the time required for a given location to cool from the liquidus to the solidus (eutectic) temperature, and it has been shown by many authors [33,34] to be the major factor in determining secondary arm spacings.

3.4.1 Secondary Dendrite Arm Spacing

Measurements of the secondary arm spacings agreed favourably with results obtained by others [34] on castings made under similar conditions as shown in Table 3.7. All results measured were in the 100 - 350 micrometre range, and as expected the castings made in air with the fastest freezing rates had the smallest arm spacings. For most cases no correlation could be made between the amount of porosity and the secondary arm spacings, as exhibited in Figure 3.31.

However, when the grain size was on the order of magnitude as the secondary dendrite arms, some correlation

Table 3.6

Dendrite Arm Spacings - Air Melts.

Position	Spacing µm.	Position	Spacing µm.	Position	Spacing µm.
A1118	73	A2418	180	A5347	211
A1117	145	A3148	175	A5348	189
A1133	128	A3127	171	A5332	161
A1136	121	A3147	169	A5357	
A1138	118	A3157	182	A5358	188
A4117	123	A3137	179		
A4118	90	A3117	180		
A4133	169	A3118	190		
A4134	179	A3128	154		
A4136	148	A3127	192		
A4138	117	A3158	310		
A4157	120	A3138	168		
A4158	100	A3335	175		
A4328	86	A3334	198		
A4348	94	A3317	172		
A4338	118	A3318	161		
A4318	84	A3336	172		
A4334	152	A3335	222		
A4335	146	A3338	164		
A4338	121	A3337	192		
A4358	86	A3328	171		

First three digits (ie. A11) signify the cast.

Last two digits (ie. 18) signify position in cast (see Appendix V).

Table 3.6 cont'd

Dendrite Arm Spacings - Vacuum Melts

Position	Spacing µm.	Position	Spacing µm.
V1118	206	V3127	168
V1128	177	V3437	286
V1138	184	V3438	217
V1137	187	V3448	260
V1135	174	V4418	172
V1136	213	V4437	230
V2137	213	V4436	270
V2138	187	V4438	155
V2128	222	V4428	174
V2118	377	V4336	215
V3137	308	V4338	225
V3135	196		
V3136	179		

Table 3.7

Secondary Dendrite Arm Spacings as a Function of Local Soldification Time in Al -4.5% Cu

Secondary Arm Spacing (μm.)	Local Solidification Time (seconds)
90 *	200 *
117 **	220 ***
175 **	390 ***

* Result taken from K.P. Young and D.H. Kirkwood [34]

** Result taken from Table 3.6

*** Local Solidification Time calculated from computer model [31]

could be made. Figure 3.32 demonstrates that even in the narrow range of 75 - 200 micrometres the percent porosity was directly related to the secondary dendrite arm spacings. The samples used in the correlation were chosen from the casts which exhibited a fine grain size either due to casting at low superheats or by grain refining the melt. Microexamination of the ingots showed that porosity was fine and interdendritic in nature (Figure 3.27), its size most likely a function of the secondary dendrite arm spacing.

3.4.2. Local Solidification Time

As stated in Chapter 2, an existing program [31] was used to calculate the local solidification times for each nodal location in the castings for the air melts. These values obtained agreed favourably with those found by others (Table 3.7) for similar dendrite arm spacing. Also, in the case of secondary dendrite arm spacing, porosity was only a function of local solidification times (Figure 3.33) in the ingots that displayed a fine - columnar and equiaxed structure and a fine interdendritic type of porosity.

In addition this variable was useful in determining the reasons for the types of distributions found. In a case

of a low superheat, the local solidification times increased from the outside to the inside (Figure 3.34) in the same manner as that exhibited in Figure 3.2. However, as the superheat increased, the local solidification time increased with a corresponding decrease in the temperature gradient (Figure 3.35). These factors will result in the formation of coarser grains which will be difficult to feed upon solidification.

Previous work [12,17] has stated the type of feeding was dependent upon the amount of fraction solid (Figure 1.8) where at low fraction solids (fs) mass feeding is prevalent and at a high fs interdendritic feeding is more possible. Therefore with use of the computer program, the time taken for each node to reach a specified fs was calculated. The fraction solids chosen were equally spaced between 0.00 and 1.00 fs. The fraction solid was calculated using Scheil Eqn (Eqn 1.9). Once calculated they were plotted against the corresponding porosity value of that node.

For a pouring temperature of 700°C (973K) into a 25°C (298K) mould, percent porosity was a linear function of time for very high fraction solids (Figure 3.36), while at a higher superheat 950°C (1223K) for the same mould temperature, the linearity disappeared at low fraction solids (Figure 3.37).

Figures 3.31 - 3.37 Influence of Solidification Parameters.

POROSITY
vs.
DENDRITE ARM SPACING

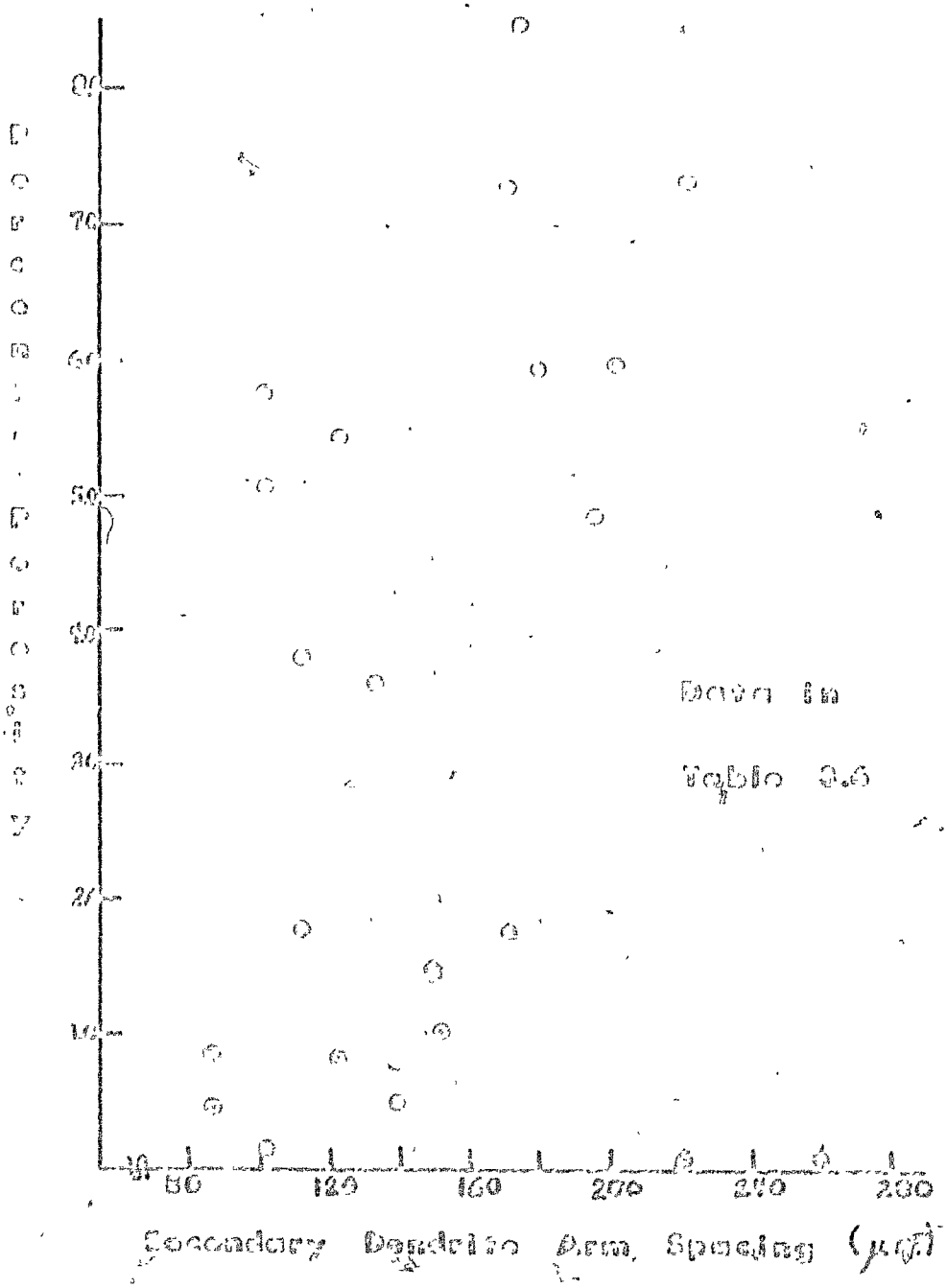

Beam 6m

Table 3.6

Figure 3.31 Percent porosity as a function of secondary dendrite arm spacing. Secondary dendrite arm spacing measurements appear in Table 3.6.

PERCENT POROSITY

vs.

DENDRITE ARM SPACING

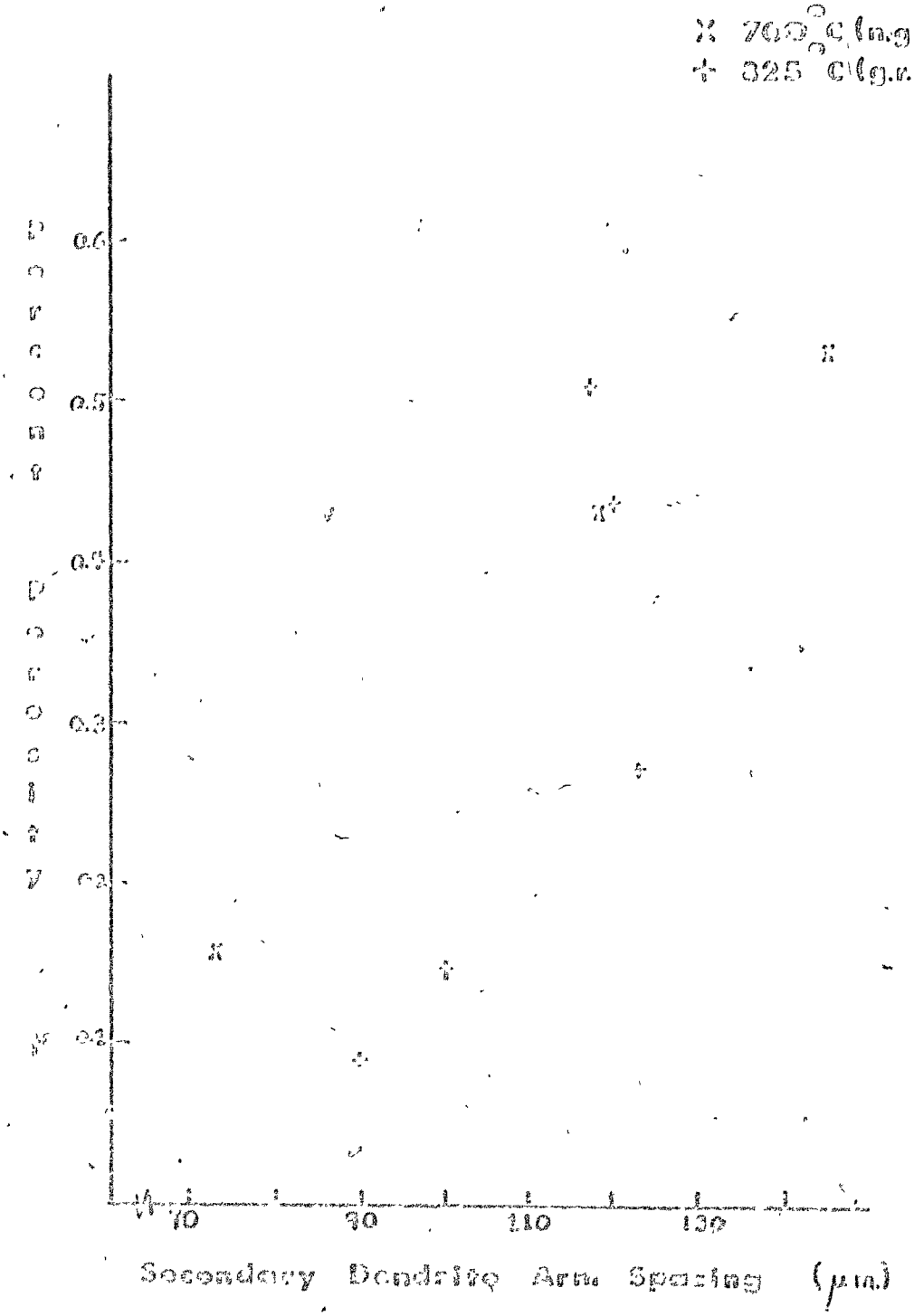

Figure 3.32 Percent porosity as a function of secondary dendrite arm spacing for ingots which displayed a fine grain structure.

PERCENT POROSITY

vs.

SECONDARY ARM SPACING

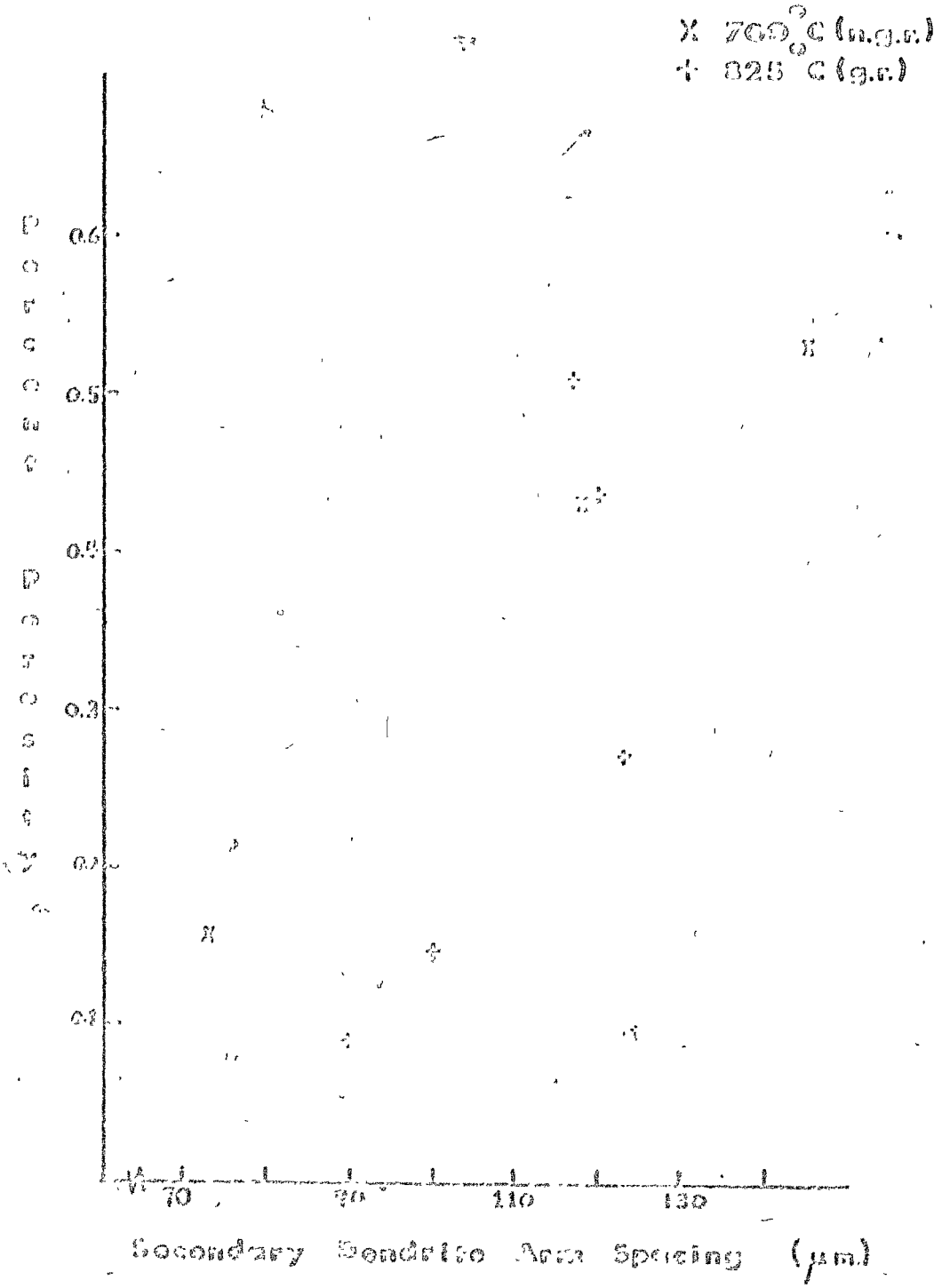

Figure 3.33 Percent porosity as a function of local solidification time (31). Pouring temperature 700°C (973K), Mould temperature 25°C (298K).

PERCENT POROSITY
vs.
LOCAL SOLIDIFICATION TIME

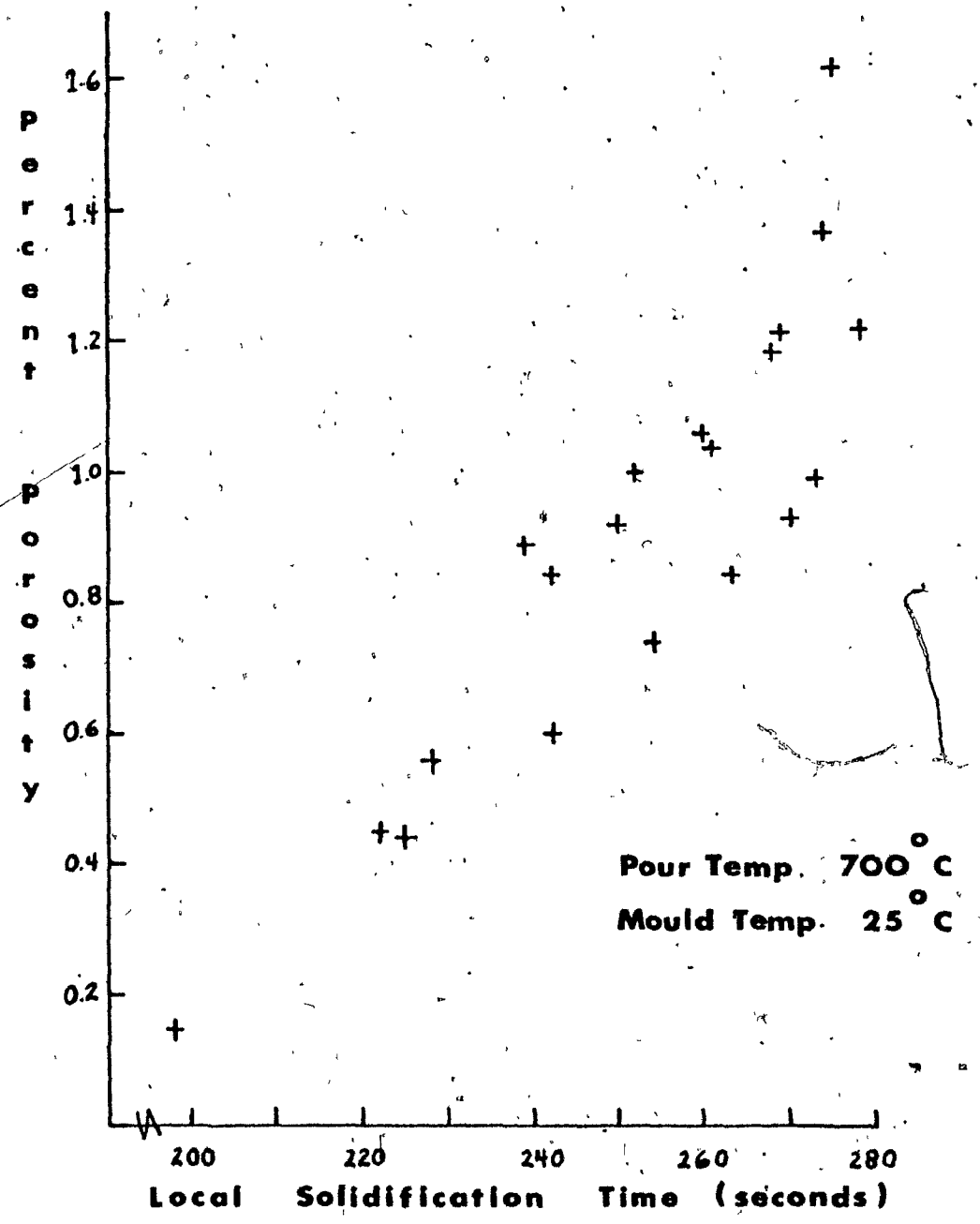

Figure 3.34 Local Solidification Time as a function of position in the mould. Pouring temperature 700°C (973K), Mould temperature 25°C (298K).

LOCAL SOLIDIFICATION TIME AS A FUNCTION OF POSITION IN THE MOULD.

Pour Temperature – 700°C (973 K)

Mould Temperature – 25°C (298 K)

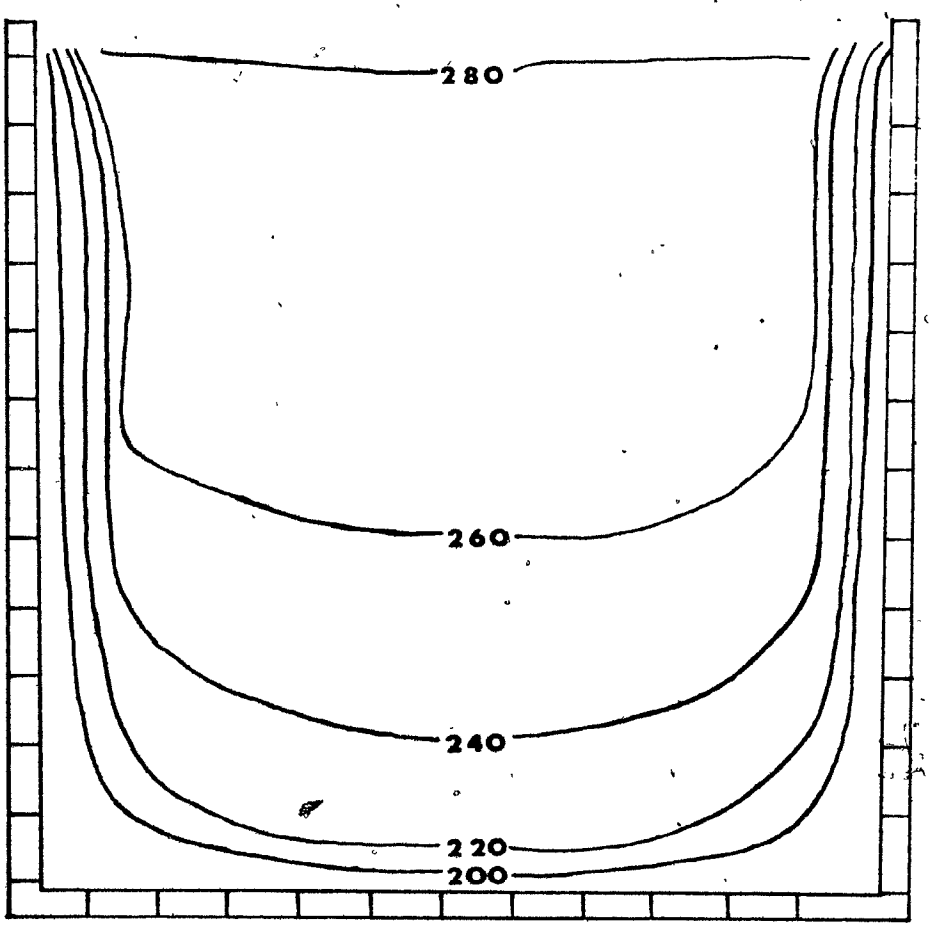

Figure 3.35 Local Solidification Time as a function of position in the mould. Pouring temperature 950°C (1223K), Mould temperature 25°C (298K).

LOCAL SOLIDIFICATION TIME AS A FUNCTION OF POSITION IN THE MOULD

Pour Temperature -950°C (1223K)

Mould Temperature - 25°C (298K)

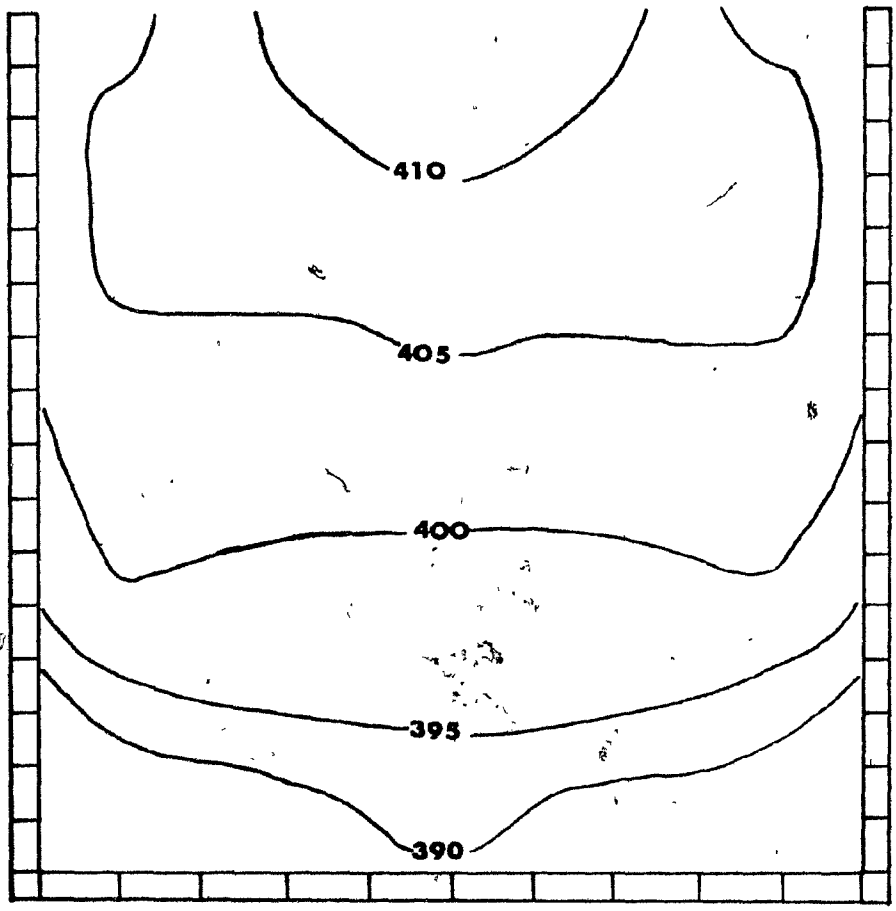

Figure 3.36 Percent porosity versus Solidification Time for various fraction solids. Pouring temperature 700°C (973K), Mould temperature 25°C (298K).

PERCENT POROSITY

VS.

SOLIDIFICATION TIME

Pour Temp 700°C (973K)

Mould Temp 25°C (298K)

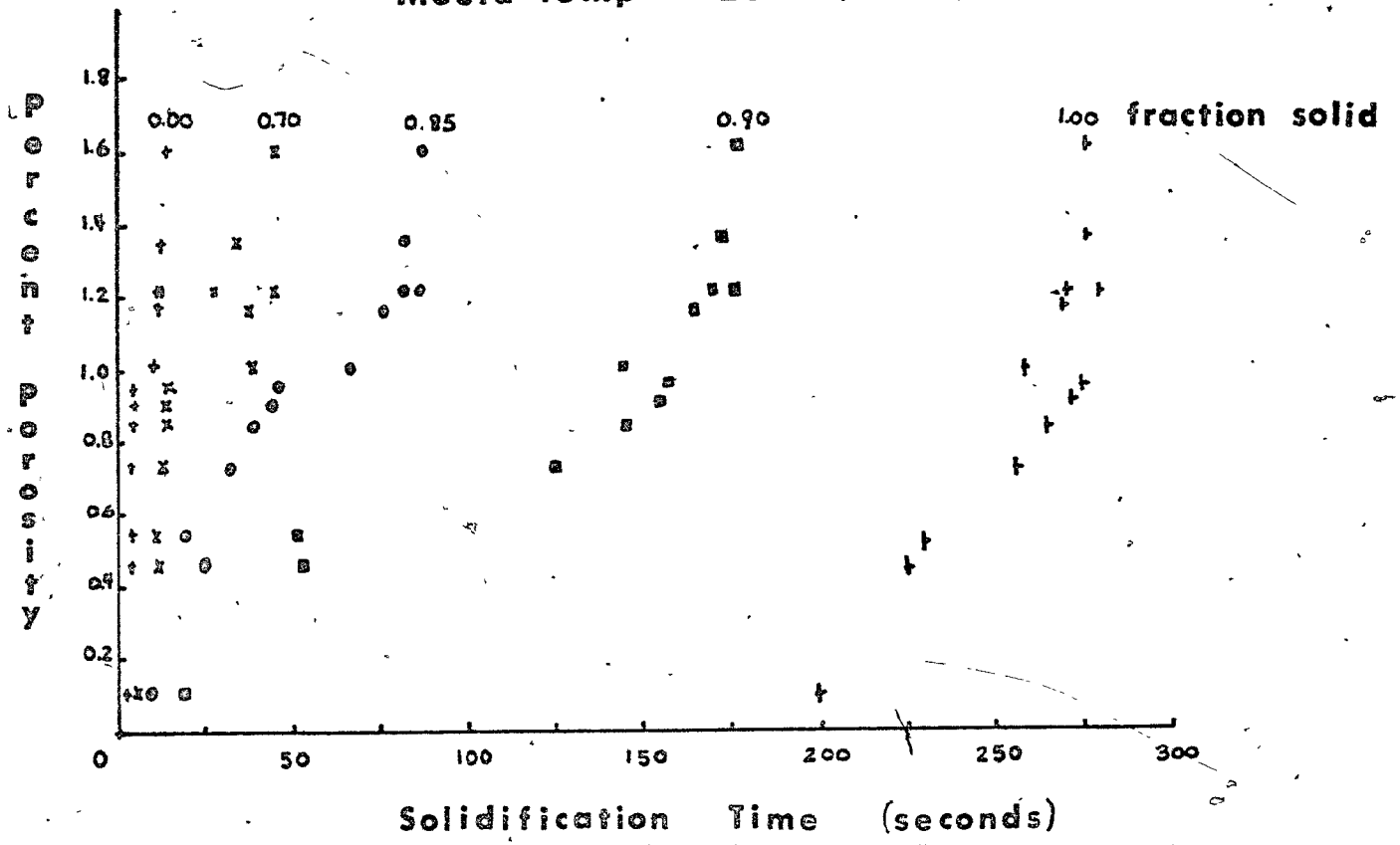

Figure 3.37 Percent porosity versus Solidification Time for various fractions solids. Pouring temperature 950°C (1223K), Mould temperature 25°C (298K).

PERCENT POROSITY

vs

SOLIDIFICATION TIME

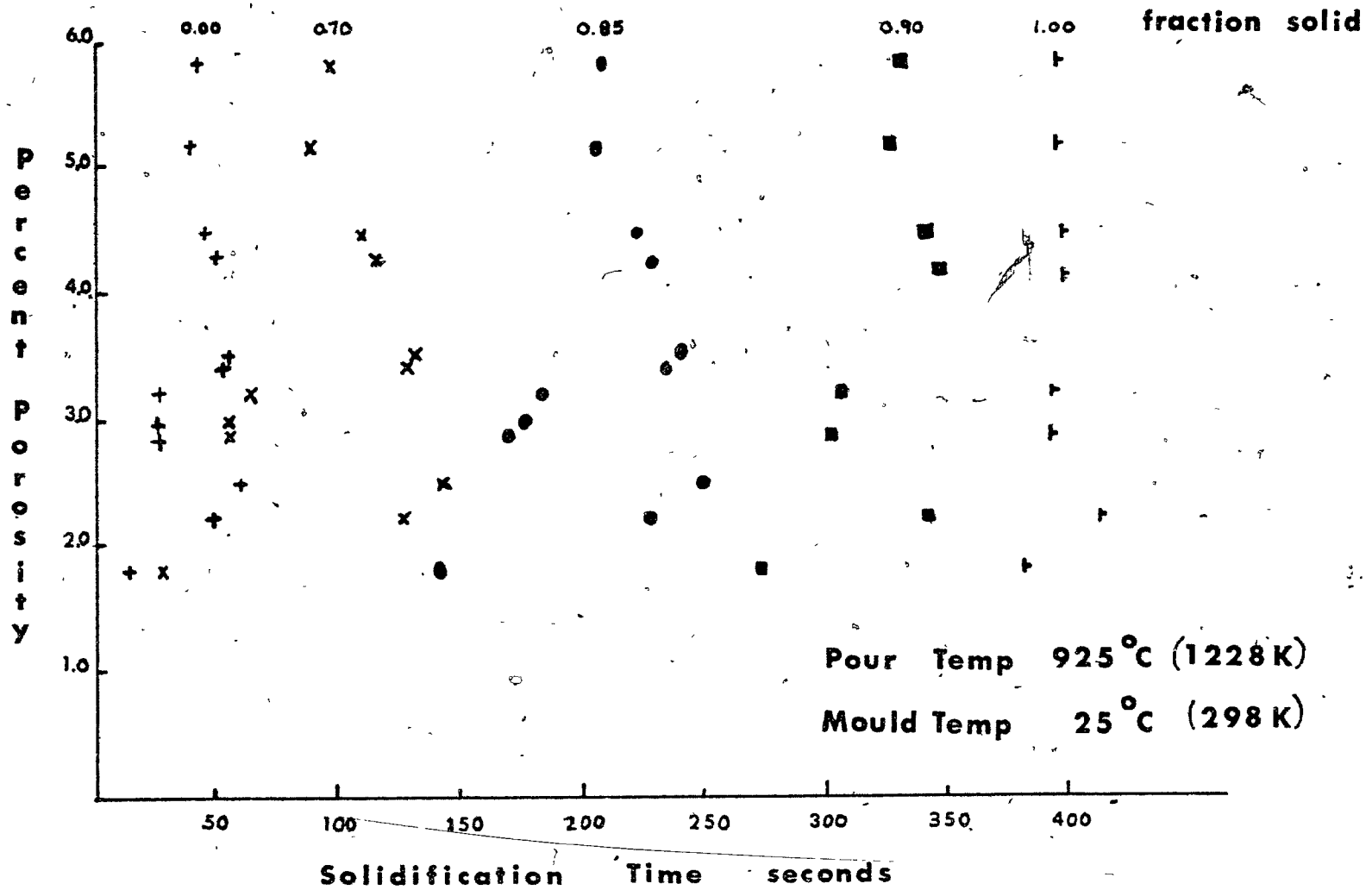

CHAPTER IV

DISCUSSION

4,1 MICROPOROSITY

The production of a sound cast structure is becoming of more importance to foundrymen today primarily because of the increasing demand for premium quality material. Information then, on how, where and why microporosity is formed is much desired. Previous research on microporosity in castings followed two distinct and different approaches. One approach was theoretical in nature as evidenced by the works by Campbell [7,12,18,21] and Piwonka and Flemings. [15] However, much of the theoretical work is difficult to analyse experimentally, and for this reason, little has been done to date to prove or disprove existing theories. On the other hand very empirical research has been done on this topic. The major aim of many of these works has not been primarily to explain pore formation but to find those techniques which can eliminate the problem. With this in mind the present work was undertaken to investigate pore formation in cast ingots. The work provides some fundamental research on microporosity where the amount, the type and the distribution of the pores can be related to theory.

4.1.1 Suitability of Al - 4.5% Cu to the study

Although the work involved a study of an Al - 4.5% Cu alloy, it is hoped that the results generated by this investigation can serve users of other metal and alloy systems. Several considerations were made in choosing this alloy for the study. As illustrated in Figure 4.1 the solubility of hydrogen in both solid and liquid aluminum is lower than that found in several other metal systems.

The problem of dissolved hydrogen in aluminum and aluminum base alloys arises because the solubilities of hydrogen in the liquid and solid are very much different (0.69 vs. 0.02 ml H_2 / 100 gm Al S.T.P.) (36). Since most commercial operations operate with hydrogen levels up to 0.2 ml H_2 / 100 gm Al (S.T.P.) for properly degassed melts, the effect of gas rejection is very important as a driving force behind pore formation. Even in cases where vacuum melting or other degassing operations reduce the hydrogen content in the liquid to values of about 0.02 ml H_2 / 100 gm Al (S.T.P.), this value is still of the same magnitude as the solubility of hydrogen in the solid below the solidus temperature.

Figure 4.1 Solubility of hydrogen in solid and liquid aluminum

SOLUBILITY OF HYDROGEN IN VARIOUS METALS

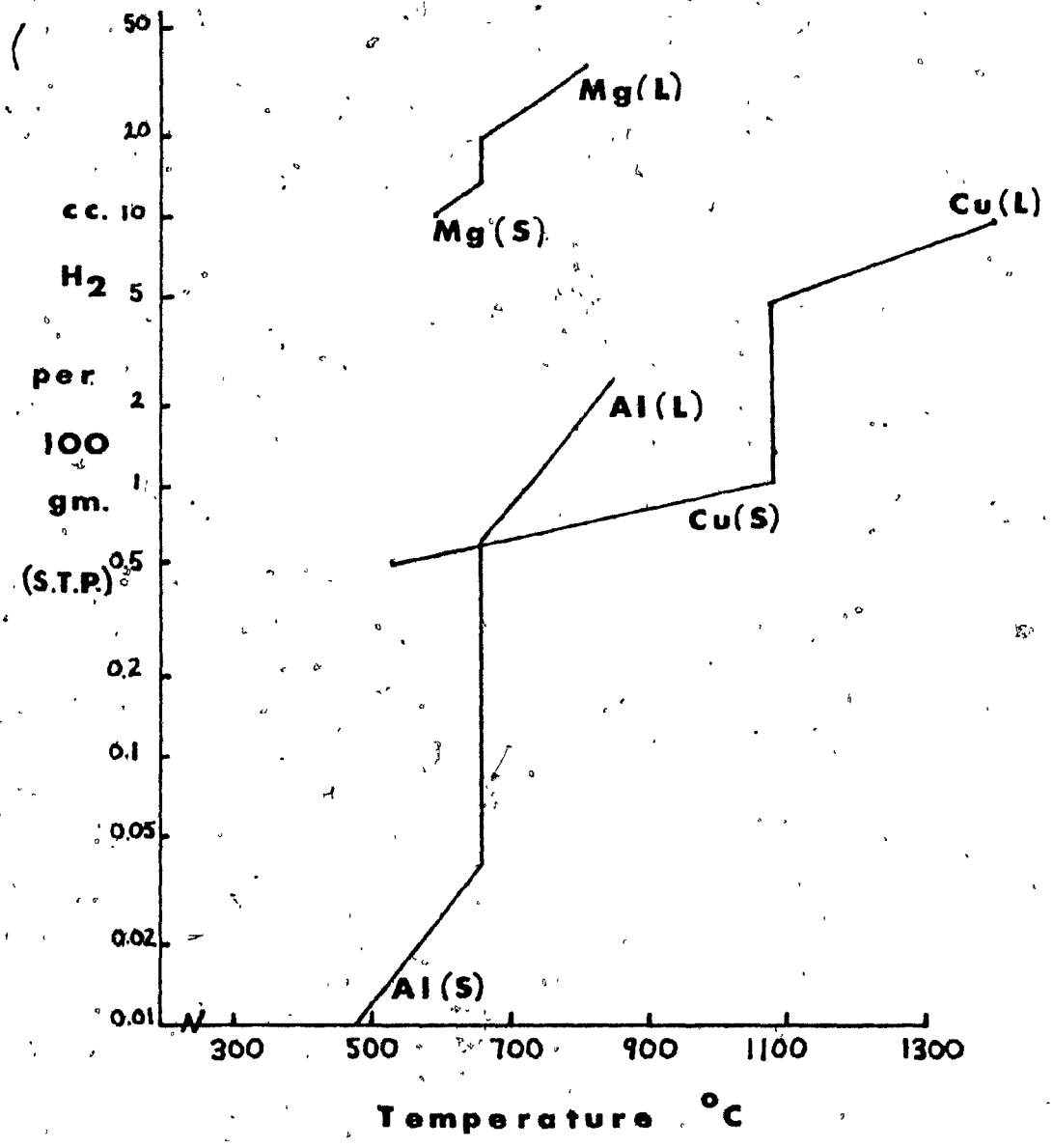

Figure 4.2 Effect of thermal conductivity on the solidification of a metal

EFFECT OF THE METAL'S THERMAL CONDUCTIVITY ON ITS SOLIDIFICATION[46]

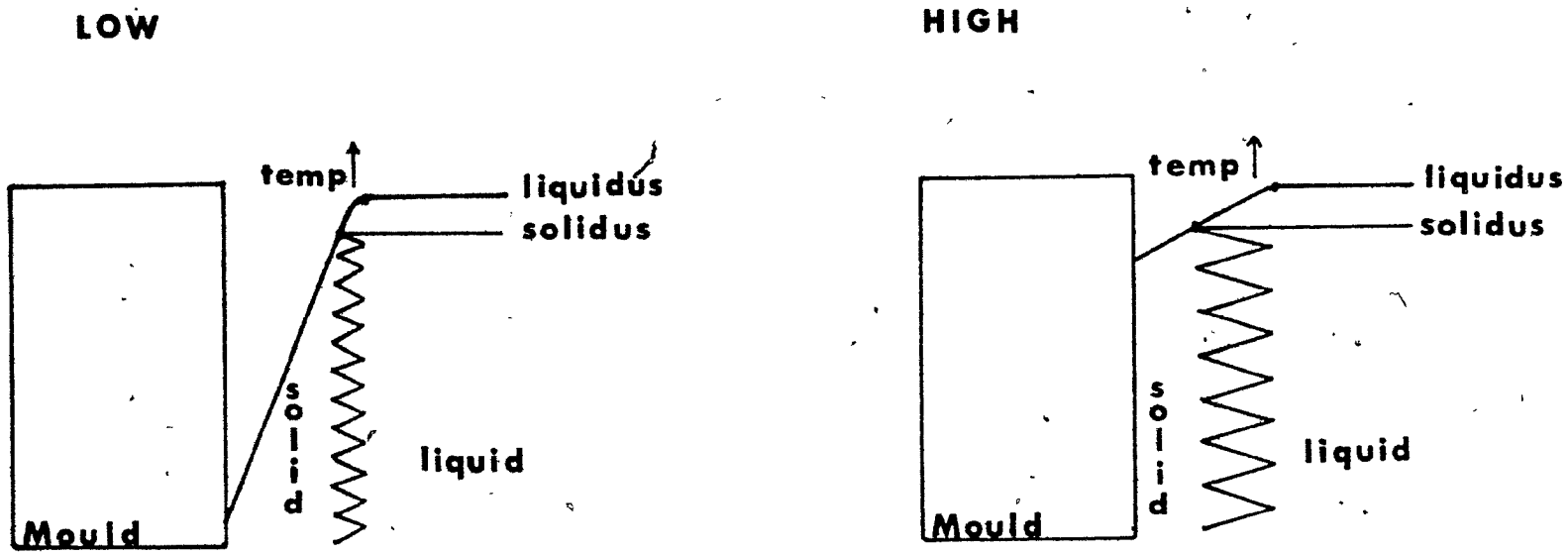

Figure 4.3 Effect of freezing range on the solidification of a metal.

EFFECT OF THE METAL'S FREEZING RANGE ON ITS SOLIDIFICATION FRONT (46)

SHORT

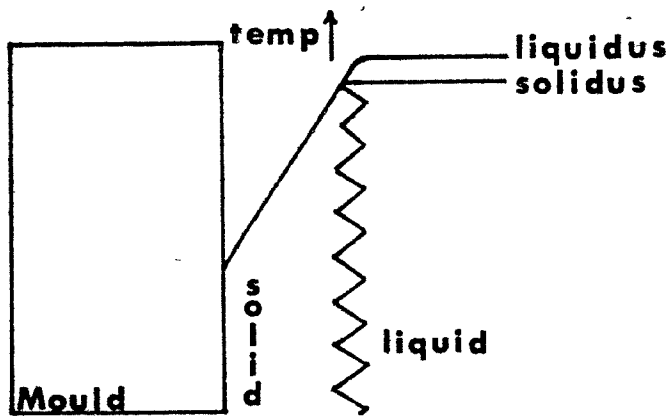

LONG

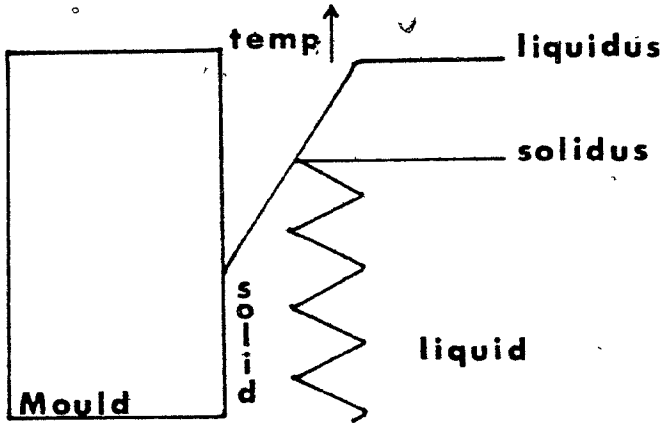

Compared to most metal and alloy systems, Al - 4.5% Cu has a relatively high thermal conductivity which as illustrated in Figure 4.2 results in low temperature gradients that give rise to a large mushy region. As mentioned previously the large mushy region is more difficult to feed, enhancing the possibility of pore formation. As a converse to this, metals displaying a low thermal conductivity allow steep temperature gradients to arise forming a short mushy zone which is easy to feed.

Al - 4.5% Cu solidifies over a long range of temperatures, approximately 100°C (100K) if the solidus temperature is considered as the eutectic temperature in non-equilibrium freezing. As in the case of a metal with a high thermal conductivity, the long freezing range results in a large mush zone (Figure 4.3) adding to the difficulties of feeding.

4.1.2 Sampling Techniques for Microporosity

At the outset of this work, the problem in selecting a representative sample for measurement of microporosity had to be overcome. As illustrated by the distribution profiles and quantitatively shown in Tables 3.1 and 3.2, where the standard deviation from the mean

can be as great as the mean value of porosity for the specific cast, the measured amount of porosity is a very strong function of position in the solidified product. Therefore the measurement of porosity in a series of ingots solidified under various casting conditions using a random sample process can yield meaningless results.

In the case of an open topped cylindrical ingot (Figure 4.4) as used in this work, a centreline slice was used because it provided a sample representative of all solidification conditions in the ingot. Since a cylindrical ingot was used any centreline slice should yield the same results, for as shown in Appendix V, most samples displayed symmetry about the centreline.

In the measurement of microporosity in more complex shapes the sampling techniques must obviously produce a representative sample. As illustrated in Figure 4.5, the casting of metal into either square, rectangular or spherical static moulds requires the use of different sampling procedures to produce representative samples. For a square ingot, one centreline slice as well as one surface slice is needed. For a rectangular ingot a surface and centreline slice parallel to both the x and y axes must be taken. And in the case of a sphere all that is needed is a slice

Figure 4.4 Sectioning of a cylindrical ingot to obtain a representative sample for the measurement of porosity.

SECTIONING OF A CYLINDRICAL INGOT - STATIC CAST AND OPEN TOPPED

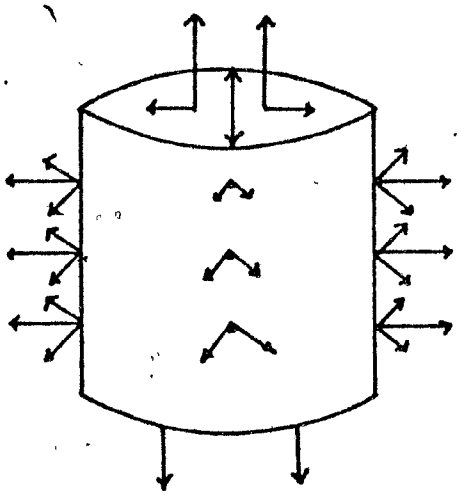

Open topped ingot showing directions of heat loss

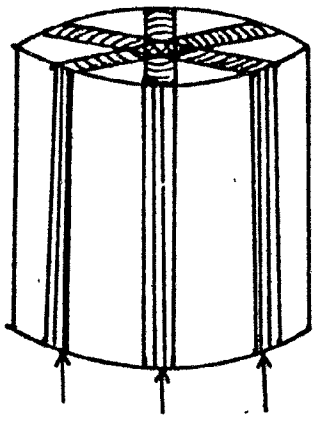

A, B and C are all representative samples

Figure 4.5 Sectioning of various types of ingots to obtain a reoresentative sample for the measurement of porosity.

SECTIONING OF VARIOUS TYPES OF STATIC CAST INGOTS

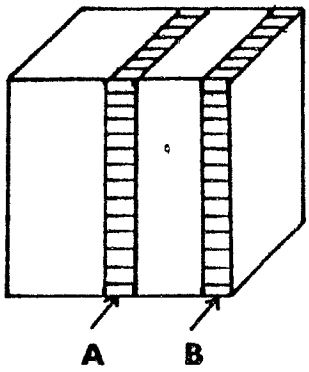

Square

Samples A, B

are required

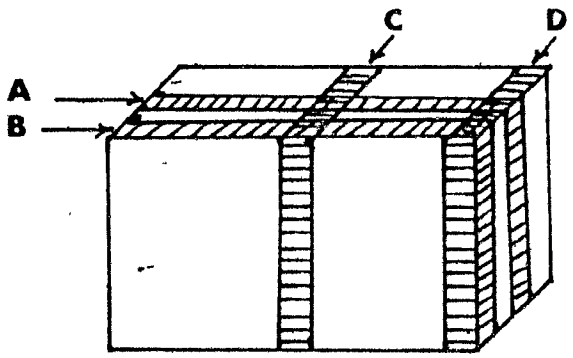

Rectangle

Samples A, B, C, D

are required

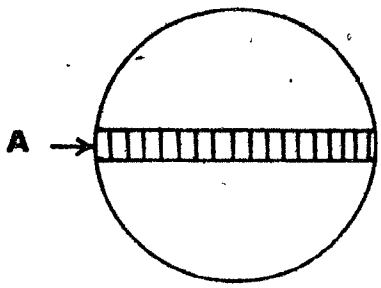

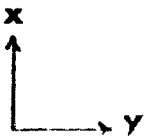

Sphere

Sample A

is required

along its diameter. It is therefore important to remember that before an ingot is sectioned for measuring microporosity, the ingot symmetry in relationship to the process of solidification must be considered.

4.2 RELATIONSHIP OF POROSITY TO STRUCTURE

The microporosity found in the castings, whether cast in air or in vacuum, was interdendritic in nature. As illustrated by the photomicrographs in Figures 3.26 and 3.27 the major difference from ingot to ingot was of scale. Fine interdendritic porosity was associated with ingots that displayed a fine grain structure, obtained by the use of low superheats or by grain refining. As illustrated in Figure 3.27 the interdendritic porosity was of a size the same order of magnitude as the secondary dendrite arms. Figure 3.22 shows the layer type of porosity that was obtained at slower rates of solidification. These pores existed in the intergranular regions of the cast and as evidenced by the scanning electron micrograph in Figure 3.29 each pore was associated with several secondary dendrite arms.

For gas levels of 0.19 - 0.46 ml H_2 / 100 gm Al (S.T.P.), and in some cases as low as 0.02 ml H_2 / 100 gm Al (S.T.P.), the amount and distribution of microporosity

was very sensitive to the initial casting conditions. Since the structure exhibited by the ingot is very dependent upon the casting conditions employed it should be possible to relate the amount and distribution of porosity in the ingot to the structure of the ingot.

4.2.1 Air Castings

In the castings made in air, the distribution, amount and type of porosity was found to be very dependent on the grain structure. If the particular cast underwent rapid solidification using low superheats or was grain refined, the resulting grain structure was of very fine columnar and equiaxed grains or just fine equiaxed grains (grain refined ingots) as shown in Figure 3.21. Porosity was very fine, and occurred in the interdendritic regions of the cast. Figure 3.2 shows a typical porosity profile where isopores follow the expected position of the solidification front, increasing in magnitude towards the centre of the cast. As expected, and shown by Figure 3.32, porosity was very dependent on the size of secondary dendrite arm spacing which has been shown to be a direct function of local solidification time [33,34]. Since Equation 1.5 demonstrated that the rate of cooling (dT/dt)

$$\frac{\Delta P}{\mu L'} \geq \propto \frac{dm}{dt} \qquad (1.5)$$

was an important parameter in calculating the driving forces for pore formation in the interdendritic regions, thus the fine porosity occurring under these conditions must be a result of poor interdendritic feeding. This is supported by the correlation of percent porosity and local solidification time. Figure 3.36 supports this conclusion because porosity is still a function of freezing rates even at a high fraction solid. Interdendritic feeding is the only type of feeding expected at these high fraction solids.

Slower rates of cooling such as those occurring at higher superheats, resulted in a coarser columnar and equiaxed structure, which in turn was associated with higher values of porosity. The type of porosity found in these castings was again the interdendritic type (Figure 3.22) although on a much larger scale than that found in the castings where the grain size was smaller. It can be seen by the scanning electron micrograph in Figure 3.29a, that these layer pores were lined with many secondary dendrite arms, and it is not surprising that for ingots produced under these conditions no correlation of percent porosity to secondary dendrite arm spacing (Figure 3.31) could be made. This type of porosity appeared to be the layer type as discussed by Campbell [37]. It could also be named as intergranular type for as revealed by etching in Figure 3.23, it

occurred in the intergranular regions of these casts.

In foundry terminology a term which comes close to describing this type of porosity is hot-tearing. Hot tearing [40] is usually referred to as fracture of metal just below or above the solidus temperature as a result of stresses which arise in the solidifying cast. The latter seems most likely the case for as seen in Figure 3.29b, the secondary dendrite arms appeared to be very smooth. If the tearing occurred in the metal below the solidus temperature, the surface should have exhibited signs of fracture.

The mechanism by which these pores formed can be explained by the structure present. Whether the structure was coarse columnar or equiaxed the layer type of porosity existed; however, the type of distributions found were different. Large superheats and high mould temperatures produced a coarse columnar structure (Figure 3.25) A typical distribution showing high concentric pockets of porosity was observed in Figure 3.9. The existence of this distribution can be explained by the mechanism in which a cast solidifies under these casting conditions. As illustrated in Figure 4.6 the coarse columnar grains will grow evenly from all directions. This fact is supported by Figure 3.35 which shows that the local solidification

Figure 4.6 Schematic illustration of the development of columnar grains in an ingot.

DEVELOPMENT OF COLUMNAR GRAINS IN AN INGOT

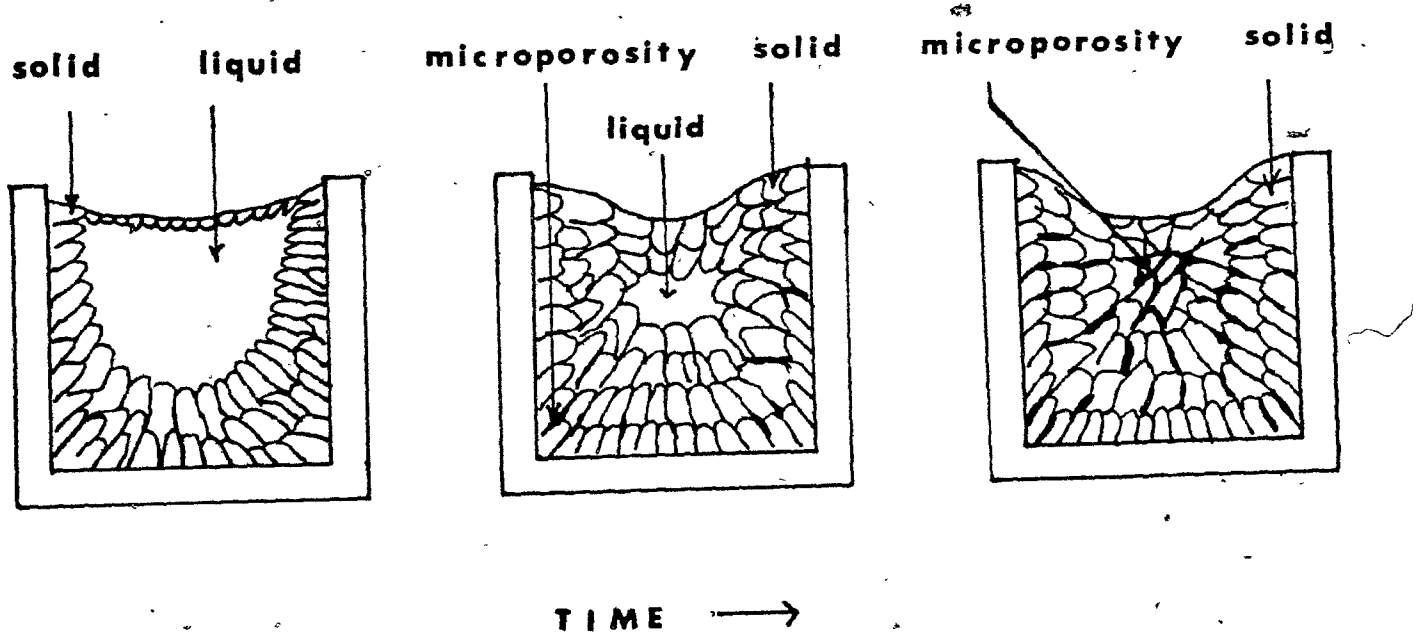

times are higher and the temperature gradients are lower; both facts which enhance the formation of coarse columnar grains. Pore formation will not be a problem until these columnar grains have grown to the centre of the cast. At this stage in the solidification the liquid metal will exist at the columnar grain boundaries and the last liquid feed reservoir will exist at the centre of the ingot. The resulting distribution profiles will then exhibit a very high centre porosity with concentric isopores decreasing in magnitude to the outside of the cast. (Figure 4.7)

At the other extreme, for an ingot that consists of coarse equiaxed grains - the result of using intermediate superheats and mould temperature - a rather simple explanation for the occurrence of layer porosity can be envisaged by regarding the mechanisms of formation of the equiaxed zone. Work on transparent model systems [38,39] has shown that the equiaxed zone builds up progressively during solidification, and if the density of the solid is greater than that of the liquid (as is the case with most metals) a considerable amount of equiaxed grain is deposited in the lower regions of the ingot by settling or sinking of grains formed early at the surface or from fragmented dendrite bits originating in the upper columnar zone (Figure 4.8). The grain to grain contact in the pile will,

Figure 4.7 Expected porosity profile of an ingot which solidified in a manner similar to that shown in Figure 4.6.

EXPECTED POROSITY PROFILE OF INGOT

WITH COARSE COLUMNAR GRAINS

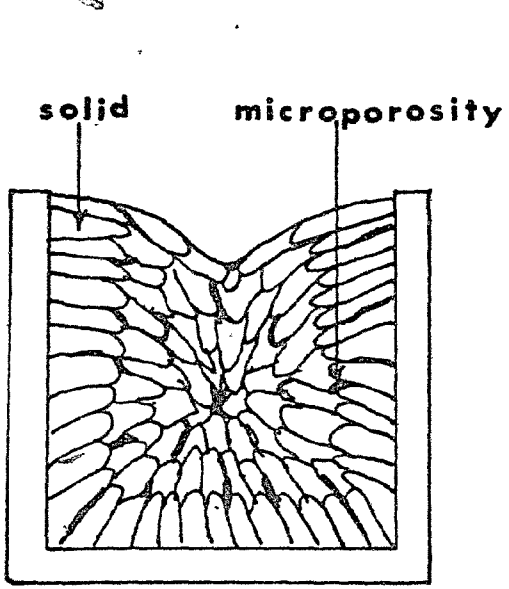

FINAL CAST SHAPE

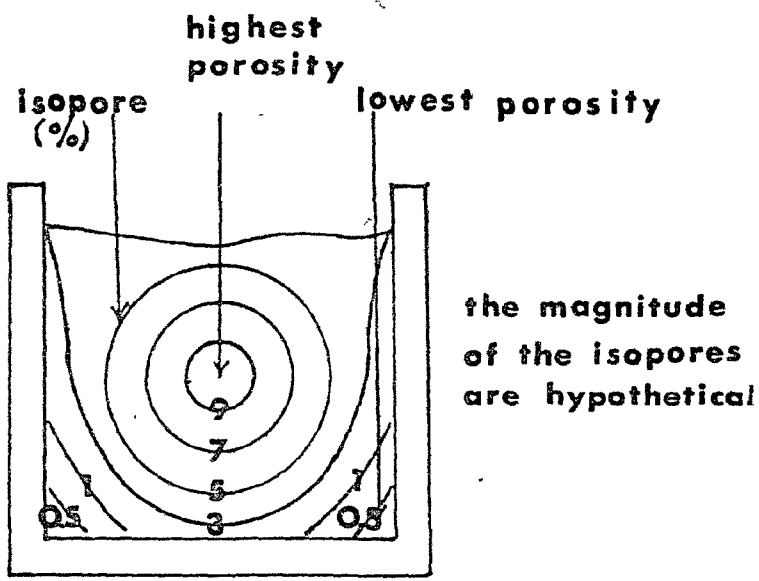

the magnitude of the isopores are hypothetical

EXPECTED POROSITY PROFILE

of course, be imperfect (Figure 4.8) and liquid pools or channels will remain between the equiaxed grains. Feeding of these intergranular liquid regions should be extremely difficult and solidification will result in the establishment of local tensile stresses which in turn aid pore formation. Since the packing of the grains is a random process, the resulting profile (Figure 4.9) should resemble some of the typical air casts that exhibit coarse equiaxed grains. (Figure 3.7).

On simple geometrical grounds it would be expected that a pile-up of large grains would be more imperfect and would result in larger and longer intergranular liquid channels than if the equiaxed grains were smaller. Therefore if the structure was one of fine equiaxed grains, better packing of the grains would be possible leading to a smaller amount of microporosity. As illustrated in Figure 3.10 grain refining results in a profile similar to that formed at low superheats. No erratic central porosity is noted. Since for this ingot, porosity is a function of secondary dendrite arm spacing (Figure 3.32) this porosity is suspected, although intergranular in nature, to be the result of poor feeding between small grains composed of only a few secondary arms growing from a central nucleus.

Figure 4.8 Schematic illustration of development of equiaxed grains in the centre of an ingot.

DEVELOPMENT OF EQUIAXED GRAINS IN AN INGOT

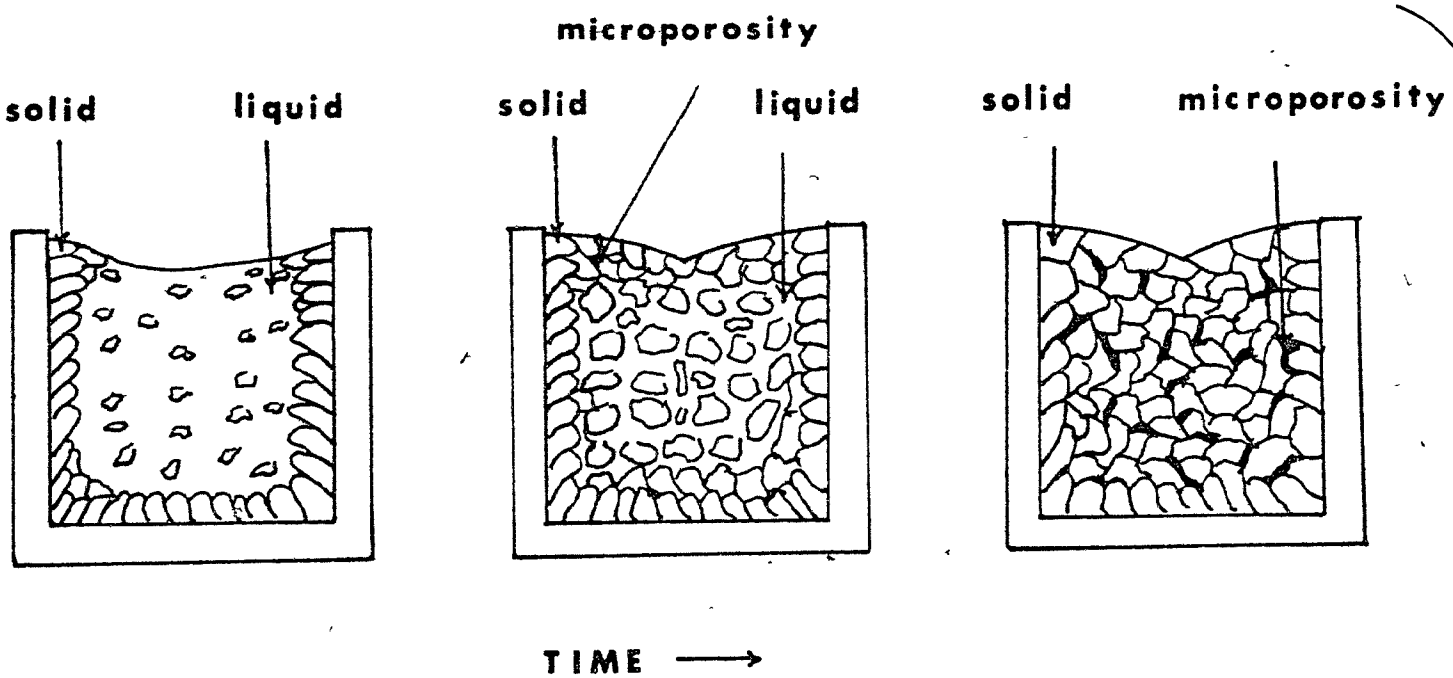

Figure 4.9 Expected porosity profile of an ingot which solidified in a manner similar to that shown in Figure 4.8.

EXPECTED POROSITY PROFILE OF INGOT WITH COARSE EQUIAXED GRAINS

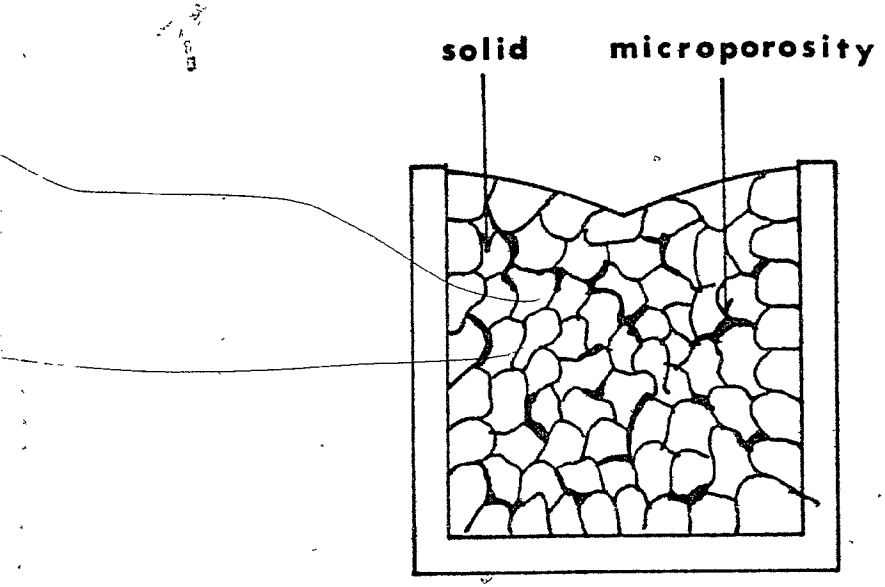

FINAL CAST SHAPE

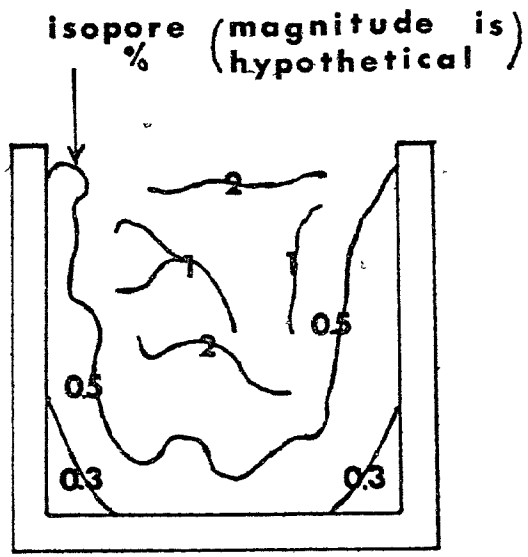

EXPECTED POROSITY PROFILE

In general, ingots contain mixtures of columnar and equiaxed grains and hence the porosity amount and distribution is probably most often caused by a combination of these two mechanisms.

4.2.2 Vacuum Casting

A distribution of microporosity also existed in the casts made in vacuum. The distribution tended to resemble those of atmospheric casting produced at slower freezing rates. For instance, as illustrated in Figure 3.15, the porosity profile made at the low superheat and reduced pressure resembled the air cast at a higher superheat (Figure 3.7). Correspondly the macrostructure exhibited coarse columnar or equiaxed grains (Figure 3.25).

As mentioned earlier the vacuum melting was employed to reduce the gas levels of H_2 in melt. At 700°C (973K) (Figure 3.11) a 1.5 hour treatment led to a gas level of 0.02 ml H_2 / 100 gm Al (S.T.P.) while for the same time period at 825°C (1098K), a gas content of 0.14 ml H_2 / 100 gm Al (S.T.P.) was attained. Degassing appeared to be a slower operation at the higher melt temperature. This result is logical because degassing rates are very dependent upon the equilibrium gas levels in the melt (Co) and at the

melt/gas interface (Ci). Since Co increases with melt temperature [36] the driving force for degassing (Ci-Co) is less at a higher superheat, and consequently degassing is a slower operation.

Casting at 700°C at atmospheric pressure but at reduced gas levels (due to vacuum degassing) did not significantly decrease the amount of porosity in the castings. Reducing the gas level from 0.19 to 0.02 ml H_2 / 100 gm Al (S.T.P.) for the same solidification conditions (Table 3.3) only resulted in a small decrease of mean porosity from 0.7% to 0.2%. In both cases, the macrostructures consisted of fine columnar and equiaxed grains (Figure 3.21) containing fine interdendritic porosity. These results suggest that gas rejection may not be the only way pores are nucleated. At low gas levels pore formation was only reduced and not eliminated thus suggesting that some other pore nucleant is present. This idea will be dealt with in detail later.

From the results on castings made at various levels of vacuum, the role of applied pressure was found to be insignificant in most cases. For example, a reduced gas level of 0.03 ml H_2 / 100 gm Al (S.T.P.), casting at 1.5 torr (50.9Pa) and at 1 atmosphere (101.3kPa) yielded approximately the same value of porosity (Table 3.9).

Nevertheless the reduction of pressure over the casting surface altered the structure of the ingot. Even at low pouring temperatures 700°C (973K), the structure changed from a mixture of fine columnar and equiaxed grains (Figure 3.21) at atmospheric pressure to a mixture of coarse columnar and equiaxed grains at 1.5 torr (50.9Pa) and less. This latter macrostructure was similar to that of one of the air melts cast at higher superheats (Figure 3.24). These castings at reduced pressure levels also exhibited an erratic pattern of isopores as illustrated in Figure 3.16, indicating that the distribution of pores was due to the random packing of these grains as described previously. Again, liquid pools or channels existed between the grains and upon solidification pore formation occurred. It is then easy to see why, at a gas level of 0.07 ml H_2 / 100 gm Al (S.T.P.) for a cast made at 0.20 torr (26.6Pa), pore formation occurred. Again as seen in the series cast at 825°C (1098K) at various pressure levels, the role of solidification which controlled the packing, overrode the effect of pressure. A 3000 fold decrease in pressure only resulted in a two fold increase in porosity. (Table 3.4)

In casting under vacuum the relative grain size was found to be important to the amount of porosity. As illustrated in Figure 3.26 more porosity was associated with the smaller grains. This observation can be explained by

again regarding the mechanism by which these casts solidify. As in the air castings, the formation of the equiaxed zone is a result of equiaxed grains being deposited at the lower regions of the cast, caused by the settling of grains, either formed at the surface or from fragmented dendrite bits (Figure 4.8). Smaller equiaxed grains for geometric reasons are expected to pack better.

If this mechanism of settling is considered similar to particles settling in an air chamber open both at the top and bottom of the chamber (Figure 4.10), the observation in the vacuum cast, where porosity was less in regions of larger grains, can then be explained. As illustrated in Figure 4.10a, if the top pressure (pressure over the cast) is less than bottom pressure (pressure due to gas rejection), the pressure will result in an upward driving force. This upward force will be counterbalanced by the weight (or size) of the grain, and as expected, the larger grains should compact more (with less porosity). This mechanism can also explain the observation found in the air casts where the smaller grains yielded less porosity. As shown by Figure 4.10b, if the top pressure (pressure over the cast) equals the bottom pressure (pressure due to gas rejection), the driving force due to a pressure drop should be zero. Therefore, compaction of the grains should be the same

Figure 4.10 Schematic of grains settling both in air and vacuum at various levels of gas concentration.

ILLUSTRATION OF GRAIN PACKING

VACUUM CAST

large grains
pack better

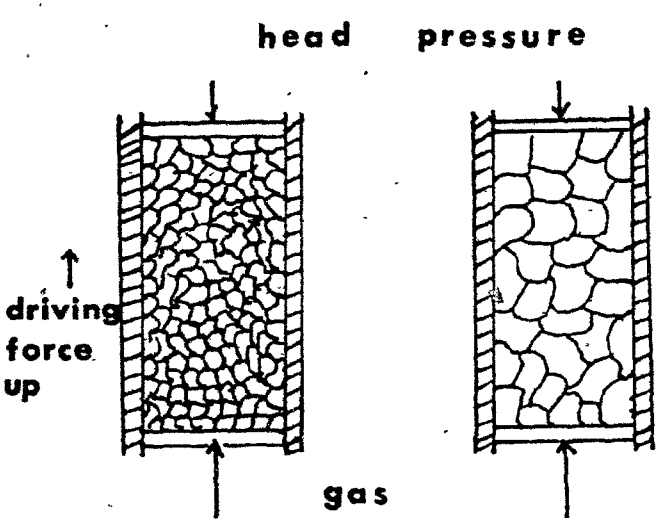

A

AIR CAST

small grains
pack better

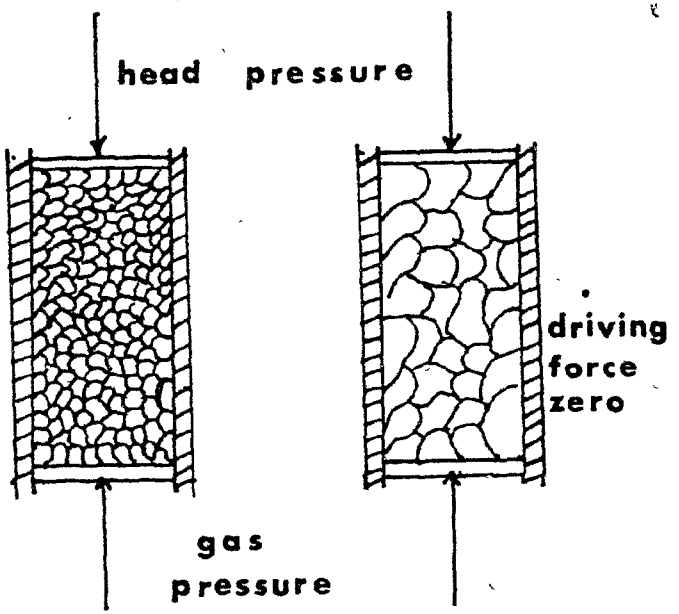

B

irregardless of grain size. However, the smaller grains should yield lower values of porosity due to the geometric reasons as discussed previously.

4.3 EFFECT OF CASTING VARIABLES ON PORE FORMATION

As mentioned in the introduction, there are several casting variables which can influence pore formation. Of these, the initial gas content, solidification rate and applied pressures are the most important. Each of these variables will be discussed making a correlation of the present results to previous work.

4.3.1 Initial Gas Content

Equation 1.2 as shown in Chapter I, indicated that gas rejection and unfed shrinkage are the driving forces behind pore formation. Recent research [7,21] has shown that pore formation is often the result of a gas-shrinkage interaction with unfed shrinkage playing a secondary role. However, unfed shrinkage cannot nucleate a pore [21] alone, and gas or some other pore nucleant such as inclusions is needed. It is known, however, that unfed shrinkage determines the final pore shape [6,7]. Work by Nishi et al [22] on directionally solidified Al - 4% Cu samples shows (Figure 4.11)

that the critical gas level required to nucleate a pore is 0.15 ml H_2 / 100 gm Al (S.T.P.). However, whether the pore shape is determined by shrinkage or gas depends on the solidification rate. For example, for a solidification rate of 60 cm/hr, the initial gas content must be above 0.41 ml H_2 / 100 gm Al (S.T.P.) to form a gas pore.

Since the rates of solidification used in this work range from 36 - 72 cm/hr (sample calculation in Appendix VII), the type of pore predicted and observed was the same. The gas levels of the air melts predict that for the levels 0.19 to 0.46 ml H_2 / 100 gm Al (S.T.P.), a pore will form but its shape will be of the shrinkage type, as was observed in Figures 3.22, 3.26. Thus, the present work confirms that of Nishi and Kurobuchi [22], even though the solidification was far from being unidirectional.

There are also discrepancies between the two works, in that air casting at reduced levels of gas 0.02 to 0.07 ml H_2 / 100 gm Al (S.T.P.) did not eliminate porosity, even though these values were far below the reported threshold level of 0.15 ml H_2 / 100 gm Al (S.T.P.) (Figure 4,11). Stating threshold values is quite possibly meaningless unless the cleanliness of the metal is also specified. As

Figure 4.11 Critical gas content to nucleate a pore and the rate of solidification required to form a shrinkage or gas type pore.

EFFECT OF GAS CONTENT AND SOLIDIFICATION SPEED ON PORE FORMATION

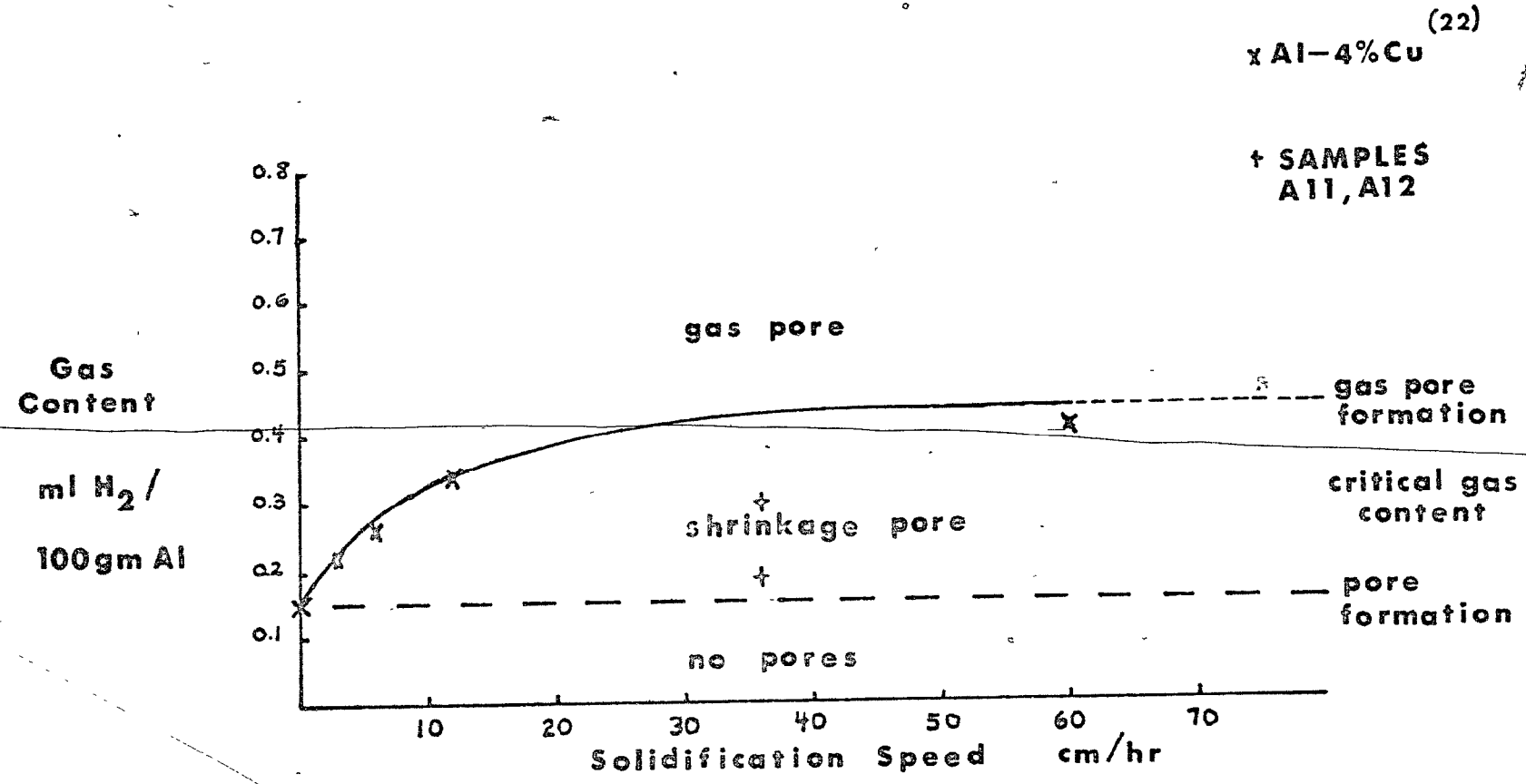

mentioned in the introduction, in nucleation theory gas or some other pore nucleant is needed to act as nucleation sites. In aluminum castings, inclusions such as Al_2O_3 can act as these sites. Thus if the liquid metal is dirty enough, even in the case of vacuum melting, pore formation can still occur when the initial gas level is far below the quoted threshold value (0.02 vs 0.15 ml H_2 / 100 gm Al (S.T.P.).

4.3.2 Solidification Rates

Much work to date has involved experiments whereby the rates of cooling and temperature gradients have been controlled for the purpose of finding optimum conditions which lower porosity by supressing pore formation. In this work, at the rates of cooling used (Figures 3.24 and 3.25), the solidification rate determines the amount of porosity by controlling the structure of the ingot produced.

To keep porosity to a minimum, the rate of solidification must be such that an open liquid reservoir of feed metal is possible. The slower freezing rates not only promoted the growth of large columnar grains which are hard to feed, but also allowed the top to freeze over (Figure 4.12) making feeding impossible.

Only in casting where the grain structure was fine, did the relative rate of solidification affect the amount of porosity. As illustrated by Figure 3.36 for a typical ingot fed interdendritically, the porosity increased as the rate of cooling decreased even at a time in the casting when the casting was almost 100% solid. In the slower rates of cooling where mass feeding was important the relationship broke down at low fraction solids (Figure 3.37).

4.3.3 Applied Pressures

Casting at reduced pressure levels has already been shown to be detrimental to ingot soundness, for as shown in steel castings [41], vacuum cast material is more porous. The reduction of pressure is very useful as a research tool since a pressure drop from 1 atmosphere (101.3 KPa) to 0.20 torr (26.6 Pa) represents a 3800 fold decrease. Since applied pressure over the casting acts to suppress pore formation, the decrease should enhance the possibility of pore formation.

This work revealed that the role of reduced pressure was two-fold. In one instance it allowed the ingot to solidify more slowly since the rate of heat extraction in

vacuum was less. This resulted in a coarser structure and a greater tendency to form layer porosity (Figure 3.22). In addition to the lower rates of solidification achieved by vacuum casting, there was also an increased tendency for pore formation due to the reduced driving force for feeding liquid metals into interdendritic channels. As shown in Eqn. 1.5 the ΔP

$$\frac{\Delta P}{\mu \bar{l}} \geq \propto \frac{dm}{dt} \qquad (1.5)$$

the pressure supplied at the channel opening is less in vacuum casting.

As shown in Table 3.4, casting at 0.03 ml H_2 / 100 gm Al (S.T.P.) at a pressure of 1.5 torr (200.0 Pa) did not alter the mean porosity from that obtained with identical casting conditions at atmospheric pressure. Yet the reduced pressure allowed for the formation of a coarser structure similar to that shown in Figure 3.24. This observation supports the work reported in Chapter I by Uram et al. [19] They found that casting at 17 atm. (1722.1 kPa) also did not affect the resulting amount of porosity.

4.4 HETEROGENEOUS AND/OR HOMOGENEOUS NUCLEATION OF PORES

Over the past twenty years, pore formation has been envisaged as a nucleation and growth process. Nucleation of a pore usually occurs early in solidification when pores are created by some external means (eg. air bubbles trapped in the cast stream); or late in the process of solidification at such a time when the liquid is completely surrounded by solidified metal, and pore formation is only possible by internal means. Previous authors[6,7] have referred to the first type as non-nucleation or heterogeneous nucleation and to the latter as homogeneous nucleation.

For the open-topped ingots used in these experiments there is evidence to support the fact that pore formation occurred late in solidification. Any pore formed early in solidification (as the result of air in the cast stream or reaction with moisture on the mould walls) likely had sufficient time to float out of the cast in front of the solidifying front. The conditions under which flotation would not be expected to occur are conditions of fast freezing or poor casting geometry. This latter condition was occassionally found in the vacuum casts when freeze-over of the top occurred (Figure 4.12).

Figure 4.12 Macrostructure of vacuum cast ingot where the top froze over. Pouring temperature 700°C (973K), Mould temperature 275°C (548K), Hydrogen Concentration 0.07 ml H_2/100 gm Al (S.T.P.), Pressure over cast 0.20 torr (26.6 Pa).

Except for those few vacuum casts, the distribution, type, and amount of porosity found in this work indicates that pore formation is the result of nucleation late in solidification - either homogeneous or heterogeneous. Since the distribution displayed a pattern of isopores dependent upon the casting conditions it is suggested that there is no barrier to nucleation and that the formation of a pore is both predictable and reproducible. This is also supported by the fact that, as predicted [22], shrinkage type pores were formed in air castings for the gas levels of 0.19 - 0.46 ml H_2 / 100 gm Al (S.T.P.). This ability to predict pore formation would not be expected if the only mechanism for pore formation were random heterogeneous nucleation early in solidification, eg. on gas bubbles introduced on casting or formed at the mould wall by a metal-mould reaction.

Although this work indicates that the majority of pores are nucleated late in solidification probably on some substrate, it would also appear that different nucleants have different degrees of effectiveness. This is indicated by the presence of porosity at a gas level of 0.02 ml H_2/100 gm Al (S.T.P.) far below the threshold values of 0.14 - 0.15 ml H_2/100 gm Al (S.T.P.) quoted.[22,42,43]. The nucleants in Nishi's experiments [22] were probably incapable of

nucleation at gas levels less than his reported value. Yet, considering that commercial grade materials were used in this study, the possibly that nucleation occurs at gas levels as low as 0.02 ml H_2/100 gm Al (S.T.P.) is a good one.

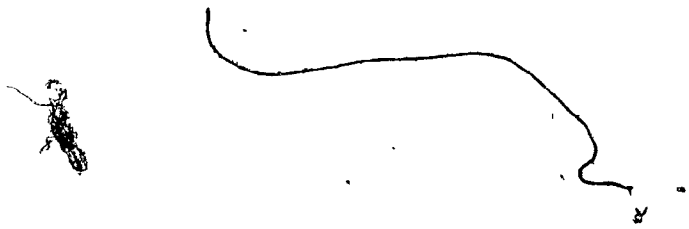

CHAPTER V

CONCLUSIONS AND SUGGESTIONS FOR FURTHER WORK

In investigating the formation of microporosity in castings, the chief aim was to study quantitatively the distribution of micropores in an ingot. By doing so, the questions which could be answered were:

1) Does microporosity follow a pattern?

2) What are the relevant variables and how do they "quantitatively" affect pore formation?

3) Is it possible to predict the amount of microporosity?

As a result of experimental evidence supplied by this investigation, it was possible to make general statements as to how the type, amount and distribution was related to the various solidification parameters. In general, the following conclusions can be made.

1) Porosity followed a definite reproducible pattern in the ingot. The pattern exhibited isopores (equal lines of porosity) with the position of the isopores being strongly dependent on the structure. In most cases these isopores

displayed symmetry about the centreline of the ingot.

2) Porosity was interdendritic in type, with the only difference from ingot to ingot being one of size. On one extreme, areas of low porosity were interdendritic in nature on the same scale as secondary dendrite arms, while at the other extreme, the areas high in porosity exhibited a layer type of porosity. The walls of these pores were lined with several secondary dendrite arms.

3) The distribution and type of porosity as well as the amount was sensitive to the structure.

a) A fine equiaxed and columnar structure achieved in the air castings by using low superheats or by grain refining, exhibited a type of porosity which was very fine and interdendritic. The distribution displayed isopores that followed the expected solidification front and whose magnitude increased from the outside to the inside of the cast.

b) A coarse columnar and equiaxed structure yielded a layer type of porosity. However both types of structure yielded a different porosity profile which was dependent upon the mode of solidification. Coarse equiaxed grains were associated with unpredictable patterns while coarse

columnar grains exhibited pockets of high porosity at the centre of the cast with the isopores forming concentric circles of decreasing value towards the mould wall.

4) At the rates of solidification used in the air melts, the gas levels 0.19 - 0.46 ml H_2 / 100 gm Al (S.T.P.) had no effect on the amount, type and distribution of micro-porosity in castings.

5) Vacuum degassing at 700°C (973K) and 0.20 torr (26.6Pa) pressure resulted in a rapid decrease of hydrogen level. A 50 minute treatment produced a level of 0.02 ml H_2 / 100 gm Al (S.T.P.). However, casting at these reduced gas levels did not eliminate porosity, even though the gas level was below the threshold value [22] for pore formation.

6) Casting under vacuum resulted in a coarser grain structure and the resulting porosity was of the layer type. Yet a sound cast could be obtained by vacuum casting as long as the gas level was decreased along with the pressure level. At 0.20 torr (26.6Pa) pressure, an unsound cast at 0.7 ml H_2 / 100 gm Al (S.T.P.) became a sound cast below 0.03 ml H_2 / 100 gm Al (S.T.P.).

7) Pore formation was the result of homogeneous nucleation

since a predictable reproducible pattern of pores could be observed. The use of an open top ingot allowed pores formed by heterogeneous nucleation to escape.

8) Although the pore was nucleated by gas or by inclusions present at the interface, the resulting pore was determined by the shrinkage of the alloy. Under the casting conditions used here, no gas bubble or pinhole type of porosity was observed.

SUGGESTION FOR FUTURE WORK

As a result of this investigation, the author feels the following areas should be further investigated.

1) With the use of same alloy, other solidification conditions should be employed. These could include a) casting at higher freezing rates into a mould designed to produce solidification in order to simulate D/C casting and b) casting at the same rates of solidification but altering the grain structure by different casting methods (ie. vibration casting).

2) Work could be done on other alloy systems to show that this investigation is not unique to the alloy used here.

3) A computer model could be developed to simulate pore

formation in the simplied casting shape as used here, and then the model's results could be compared to the results of this investigation.

4) Further metallography could yield more information as to the nature of the pores. Examination by the scanning electron microscope could supply more, information as to how the pores were nucleated.

5) The effect of cleanliness on pore formation could be investigated by casting of very clean spectrographic grade Al - 4.5% Cu alloys.

6) Another method of measuring porosity could be developed and quantified against the results here. For example, a metallographic technique which now supplies information about the shape of the pores could then be quantified.

REFERENCES

1. C. E. Ransley and H. Neufeld, Journal Institute of Metals, 74, (1948), 599.

2. A. K. Higgins, American Foundrymen's Society, "Symposium on Principles of Gating", (1950), 40-50.

3. M. C. Fleming, S. Z. Uram and H. F. Taylor, Modern Castings, Dec. 1960, 66-79.

4. R. W. Ruddle, "Applied Science in the Casting of Metals", Pergamon Press, Oxford, 1970, 417-442.

5. S. Engler, Z. Metallkde, 56, (1965), 327-335.

6. E. J. Whittenberger and F. N. Rhines, Trans. AIME., 194, (1952), 409-420.

7. J. Campbell, The British Foundryman, 4, (1969), 147-158.

8. T. S. Piwonka, Foundry, 8, (1966), 66.

9. B. Chauvelier, Fonderie, 154, (1958), 505.

10. R. J. Kissling and J. F. Wallace, Foundry, 2, (1963), 70.

11. R. Mehrabian, M. Keane and M. C. Flemings, Trans. AIME, 1, (1970), 1209.

12. J. Campbell, AFS Cast Metals Research Journal, 4, (1969), 1 - 8.

13. J. F. Wallace, "Fundamentals of Risering Steel Castings", Steel Founders Soc., Cleveland Ohio (1960).

14. N. P. Allen, Journal Institute of Metals, 49, (1932), 317 - 46, 51, (1933) 233-308, 52, (1934), 193-220.

15. T. S. Piwonka and M. C. Flemings, Trans. AIME, 236, (1966), 1157-1165.

16. W. D. Walther, C. M. Adam, H. F. Taylor, Trans. A.F.S., 64, (1956), 658-664.

17. J. Campbell, P.H.D. Thesis, University of Birmingham, Birmingham, 1967.

18. J. Campbell, Trans. A.I.M.E., 245, (1969), 2325-34.

19. S. Z. Uram, M.C. Flemings and H. F. Taylor, Trans. A.F.S., 66, (1958), 129-34.

20. B. Chamberlain and J. Sulzer, Trans. A.F.S., 46, (1964), 600-607.

21. J. Campbell, Trans. A.I.M.E., 239, (1967), 138-42.

22. S. Nishi and T. Kurobuchi, Journal Jap. Inst. of Metals, 24, (1974), 245-54.

23. N. S. Mahadevan, K. S. Sreenivase Murthy and M. R. Seshardi, Trans. A.F.S., 76, (1962), 77-84.

24. H. Rosenthal and S. Lipson, Trans. A.F.S., 63, (1955),301.

25. C. E. Ransley and D. E. J. Talbot, Journal Institute of Metals, 84, (1955-56) 445-52.

26. A. Sieverts, G. Zapf and H. Moritz, Z. Phys. Chem., 183, (1938), 19.

27. Fondeur, 243, (1973), 13-21.

28. R.W. Ruddle, The British Foundryman, 12, (1957), 605-615.

29. "Lange's Handbook of Chemistry", McGraw Hill Book Company, New York, (1973).

30. D. E. Kundle and L. A. Willey, Journal of Materials, 1, (1966), 226.

31. S. Argyropoulos, N. Christodoulou, R. Torres-Sanchez , Dept. of Mining and Metallurgical Eng., McGill University, Montreal, (1976), Unpublished Work.

32. H. H. Willard, L. L. Merritt, J. A. Dean, "Instrumental Methods of Analysis", Van Nostrand, Princeton, (1965).

33. M. C. Flemings, Trans. A.I.M.E., 5, (1974), 2121-34.

34. K. P. Young and D. H. Kirkwood, Trans. A.I.M.E., 6A, (1975), 197-205.

35. K. Alker, Giesserei, 61, (1974), 693-696.

36. W. Claus, Z. Metallkunde, 21, (1929), 268.

37. J. Campbell, Trans. A.I.M.E., 242, (1968), 1464-1465.

38. K. A. Jackson, J. D. Hunt, D. R. Uhlmann and T. P. Seward, Trans. A.I.M.E., 236, (1966), 149-158.

39. B. Chalmers, J. Australian Inst. Metals, 35, (1926), 255.

40. R. W. Ruddle, "The Solidification of Castings", The Institute of Metals, London, 1957.

41. D. E. Parsons, Trans. A.F.S., 71, (1963), 433-54.

42. C. E. Ransley and D. E. J. Talbot, Z. Metallkunde, 46, (1955), 328.

43. M. F. Jordan, G. D. Denyer and A. N. Turner, Journal Institute of Metals, 91, (1962-63), 48-53.

44. J. Szekely and N. J. Themelis, "Rate Phenomena in Process Metallurgy", Wiley, New York, 1971.

45. A. K. Biswas and W. G. Davenport, "Extractive Metallurgy of Copper", Pergamon Press, Oxford, 1976.

46. R. W. Heine, C. R. Loper and P. C. Rosenthal, "Principles of Metal Casting", McGraw Hill Book Company, New York, 1967.

Appendices

Appendix	Title	Page
I	Rate of bubble rise in liquid aluminum	166
II	Sample calculation of porosity	167
III	Calculation of Theoretical Density	168
IV	Segregation results in Al - 4.5% Cu	169
V	Experimental Data Air Vacuum	173 174 187
VI	Dendrite arm spacing measurement	205
VII	Solidification Rates in the Castings	206

Appendix I

Rate of bubble rise in Liquid Aluminum

All bubbles of a diameter of 1 cm. or less will rise out of the melt at a velocity determined by Stokes' Law.

$$ut = \frac{db^2}{18\mu} g\rho \qquad (44)$$

for aluminum

μ = 0.011 gm/cm-sec

ρ = 2.7 gm/cm^3

g = 980 cm/sec^2

ut is the terminal velocity

db is the bubble diameter

Diameter of the bubble (cm.)	Terminal Velocity (cm/sec)	Reynold's Number
1.0×10^{-4}	1.6×10^{-5}	0.39
5.0×10^{-4}	4.0×10^{-4}	1.96
1.0×10^{-3}	1.6×10^{-3}	3.92
5.0×10^{-3}	4.0×10^{-2}	19.6
1.0×10^{-2}	1.6×10^{-1}	39.2
5.0×10^{-2}	4	196
1.0×10^{-1}	16.	392
5.0×10^{-1}	400	1960
1.0	1600	3920

Appendix II

Sample Calculation of Porosity

Each sample was weighed in air and in water (0.01 % teepol), to obtain the sample's density.

$$\text{Sample Density} = \frac{\text{Mass in air}}{\text{Mass in air-Mass in Water}} \times \text{Density of Water}$$

The density of water was taken from book values [32].

Using the sample's density the percent porosity was calculated with a knowledge of the theoretical density (see Appendix III)

$$\text{Percent Porosity} = \frac{(\text{Theoretical Density-Sample Density})}{\text{Theoretical Density}} \times 100$$

Appendix III

Calculation of Theoretical Density [30] for alloy of 4.32% Cu, 0.12% Fe, and 0.10% Si, and rest Al.

Assume 100 gm sample.

Element	1/Density (cm^3/gm)	Amount Present (gm)	Volume (cm^3)
Cu	0.1116	4.32	0.4821
Fe	0.1271	0.12	0.0152
Si	0.4292	0.10	0.0429
Total A			0.5402
Al	0.3705	95.46	33.2679
Total B			33.9011

$$\text{Theoretical Density} = \frac{100 \text{ gm}}{\text{Total B}} = 2.7854 \text{ gm/cm}^3$$

Appendix IV

Segregation Results

Cu, Fe and Si values of Samole A21; samole A21 cast at 825°C (1098K) into 25°C (298K) mould.

Grid Position (Appendix V)	Cu %	Fe %	Si %
11	4.76	0.12	0.09
12	4.82	0.11	0.09
13	4.76	0.11	0.10
14	4.70	0.11	0.11
15	4.76	0.12	0.13
16	4.56	0.11	0.15
17	4.61	0.11	0.10
18	4.61	0.12	0.09
21	4.73	0.11	0.10
22	5.09	0.13	0.12
23	5.04	0.12	0.13
24	4.53	0.10	0.13
25	4.78	0.11	0.12
26	4.36	0.10	0.14
27	5.03	0.12	0.17
28	4.68	0.12	0.10
32	4.86	0.12	0.11
33	4.64	0.10	0.12
34	-	-	-
35	4.48	0.08	0.12
36	4.73	0.11	0.13
37	4.70	0.11	0.15
38	4.84	0.12	0.12

A21 cont'd

Grid Position	Cu %	Fe %	Si %
41	4.88	0.12	0.12
42	5.00	0.12	0.13
43	4.54	0.10	0.10
44	4.99	0.12	0.13
45	4.53	0.10	0.12
46	4.65	0.10	0.12
47	4.89	0.11	0.12
48	4.73	0.10	0.09
51	4.79	0.12	0.09
52	4.98	0.12	0.11
53	4.94	0.12	0.12
54	4.87	0.12	0.13
55	4.68	0.10	0.12
56	4.65	0.12	0.10
57	4.62	0.11	0.08
58	4.57	0.10	0.08

Appendix IV cont'd

Segregation Results

Cu, Fe and Si values of Sample A24; sample A24 cast at 825°C (1098K) into 400°C (673K) mould.

Grid Position	Cu %	Fe %	Si %
11	4.81	0.12	0.11
12	4.80	0.12	0.11
13	4.96	0.12	0.11
14	4.88	0.12	0.11
15	4.89	0.12	0.11
16	4.95	0.11	0.11
17	4.71	0.11	0.11
18	4.51	0.10	0.10
21	4.71	0.11	0.11
22	4.50	0.11	0.11
23	4.67	0.11	0.12
24	4.51	0.11	0.12
25	4.57	0.11	0.11
26	4.53	0.11	0.10
27	4.63	0.10	0.10
28	4.69	0.11	0.10
32	4.57	0.11	0.11
33	4.48	0.10	0.10
34	4.46	0.11	0.10
35	5.04	0.12	0.11
36	4.57	0.12	0.11
37	4.49	0.10	0.10
38	4.48	0.10	0.10

A24 cont'd

Grid Position	Cu	Fe	Si
	%	%	%
41	5.08	0.13	0.13
42	5.09	0.13	0.11
43	4.48	0.11	0.10
44	4.44	0.11	0.10
45	4.61	0.11	0.11
46	4.45	0.10	0.10
47	4.61	0.10	0.10
48	4.91	0.11	0.10
51	4.85	0.11	0.14
52	4.86	0.11	0.12
53	4.89	0.11	0.11
54	4.97	0.12	0.11
55	4.89	0.12	0.11
56	4.93	0.12	0.10
57	4.81	0.11	0.10
58	4.74	0.11	0.10

Appendix V

Experimental Data

For each casting the value of percent porosity is given for every nodal point. In addition, the pour temperature, the mould temperature, initial gas content and pressure over the cast is given. The format for these results is shown below.

Pour temperature - ^{o}C (K)

Mould temperature - ^{o}C (K)

Initial Gas Content - ml H_2/100 gm Al (S.T.P.)

Pressure over cast - torr (Pascals)

Grid

11	21	31	41	51
12	22	32	42	52
13	23	33	43	53
14	24	34	44	54
15	25	35	45	55
16	26	36	46	56
17	27	37	47	57
18	28	38	48	58

AIR MELT EXPERIMENTS

Experimental Data

Pour temperature - 700°C (973K)

Mould temperature - 25°C (298K)

Pressure - 760 torr (1.01×10^5 Pa)

Gas Level - 0.30 ml H_2/100 gm Al (S.T.P.)

2.3219	100	100	100	1.0303
0.7298	1.3917	100	1.2378	0.8157
0.7012	1.3309	100	1.3416	0.7513
0.6475	1.2378	1.3452	1.2701	0.6189
0.5438	1.0840	1.0697	1.0876	0.5366
0.4114	0.9373	0.9946	0.8980	0.3864
0.2540	0.6905	0.8193	0.6941	0.2826
0.0787	0.1968	0.2791	0.3578	0.0823

Experimental Data

Pour temperature - 700°C (973K)

Mould temperature - 70°C (343K)

Pressure - 760 torr (1.01×10^5 Pa)

Gas Level - 0.19 ml H_2/100 gm Al (S.T.P.)

0.9326	100	100	100	0.9898
0.9076	1.3900	100	1.4043	0.8505
0.8433	1.4472	100	1.4651	0.8433
0.7826	1.2864	1.2971	1.2578	0.7540
0.7111	1.0541	1.0255	1.0220	0.7075
0.5825	0.8648	0.9362	0.8683	0.5860
0.4395	0.7361	0.6325	0.6932	0.4824
0.1572	0.3145	0.3824	0.3395	0.2573

Experimental Data

Pour temperature - 700°C (973K)

Mould temperature - 240°C (513K)

Pressure - 760 torr (1.01×10^5 Pa)

Gas Level - 0.19 ml H_2/100 gm Al (S.T.P.)

0.4896	100	100	100	0.5681
0.4002	1.2900	100	1.2650	2.9980
0.3895	1.4401	1.5080	1.1470	0.3430
0.3109	1.1077	1.1578	0.9326	0.3145
0.3430	0.8040	0.9148	0.8254	0.2895
0.3680	0.7861	0.6754	0.7075	0.3538
0.3109	0.5825	0.6718	0.5967	0.3037
0.1036	0.3538	0.2895	0.3037	0.0464

Experimental Data

Pour temperature - 825°C (1098K)

Mould temperature - 25°C (298K)

Pressure - 760 torr (1.01×10^5Pa)

Gas Level - 0.46 ml H_2/100 gm Al (S.T.P.)

1.1385	100	100	100	0.9697
0.9446	1.0307	100	1.1026	0.8548
0.9266	1.1960	1.4617	1.0846	2.8839
0.8512	1.1098	0.7363	1.0559	0.7650
0.7219	2.2231	0.9912	2.0363	0.9338
0.7865	1.8316	1.7023	1.6305	0.6608
0.6177	1.2067	1.4474	0.9446	0.4453
0.2945	0.4633	0.6177	0.4669	0.3412

Experimental Data

Pour temperature - 825°C (1098K)

Mould temperature - 70°C (343K)

Pressure - 760 torr (1.01×10^5 Pa)

Gas Level - 0.46 ml H_2/100 gm Al (S.T.P.)

0.5423	0.8620	100	0.8224	0.9984
0.5890	0.7039	100	0.6213	0.6428
0.5459	0.9805	1.0667	0.9553	0.4741
0.5136	1.7418	2.2195	1.5263	0.5207
0.3627	1.4904	1.5910	1.5407	0.4777
0.3160	1.7095	1.2103	1.3432	0.3699
0.4561	1.0271	1.3612	0.9168	0.4489
0.4022	0.2335	0.2837	0.2442	0.2981

Experimental Data

Pour temperature - 825°C (1098K)

Mould temperature - 250°C (523K)

Pressure - 760 torr (1.01×10^5 Pa)

Gas Level - 0.46 ml H_2/100 gm Al (S.T.P.)

0.8763	100	100	100	0.4382
0.6644	0.9446	100	1.0235	0.3986
0.7506	1.4006	1.0343	1.4258	0.6213
0.6141	0.9302	1.1026	1.6341	0.6249
0.7829	1.3791	0.8620	1.2714	0.9877
0.5854	1.8711	1.1672	2.2195	0.7327
0.5782	1.7203	3.8249	2.1549	0.8907
0.3053	0.7147	0.9841	0.7398	0.2945

Experimental Data

Pour temperature - 825°C (1098K)

Mould temperature - 400°C (673K)

Pressure - 760 torr (1.01×10^5 Pa)

Gas Level - 0.46 ml H_2/100 gm Al (S.T.P.)

2.2438	100	100	100	2.1864
2.4234	2.4952	3.5112	2.4413	2.5059
2.6208	2.6101	1.4234	2.3587	2.5921
2.8326	2.8183	3.1486	2.7178	2.9008
2.5167	3.2742	5.6760	3.0086	2.5849
2.6424	4.2364	6.0207	3.6261	2.4880
2.3300	3.4717	3.9025	2.9008	2.4413
1.9710	2.2869	2.7824	2.8398	1.9423

Experimental Data

Pour temperature - 950°C (1223K)

Mould temperature - 25°C (298K)

Pressure - 760 torr (1.01×10^5 Pa)

Gas Level - 0.45 ml H_2/100 gm Al (S.T.P.)

2.3423	3.4057	100	4.6343	4.1996
3.0464	3.0931	4.1996	3.3051	2.0441
2.3351	3.2979	2.6441	3.3123	2.0765
2.8740	3.3518	2.5291	3.2440	2.1734
3.1290	3.3338	3.5781	3.6320	2.0765
2.9027	5.3240	4.3253	3.5278	2.0908
3.8655	4.9181	5.7910	5.3671	1.8501
2.1160	3.6535	3.2368	2.2022	1.6418

Experimental Data

Pour temperature - 950°C (1223K)

Mould temperature - 70°C (343K)

Pressure - 760 torr (1.01×10^5Pa)

Gas Level - 0.45 ml H_2/100 gm Al (S.T.P.)

2.6045	100	100	100	2.6117
2.4249	3.1721	3.2691	2.6261	2.1914
2.4644	3.3087	1.7639	2.7303	2.8129
2.5974	3.5314	2.1052	2.9351	2.5650
2.2812	5.0366	3.8691	3.7577	2.3459
1.7567	2.9818	3.4703	3.3230	2.2920
1.5160	3.0428	5.1121	3.0500	1.8860
1.2682	1.7136	2.4069	1.7747	1.6130

Experimental Data

Pour temperature - 950°C (1223K)

Mould temperature - 250°C (523K)

Pressure - 760 torr (1.01×10^5 Pa)

Gas Level - 0.[illegible]5 ml H_2/100 gm Al (S.T.P.)

2.5794	3.3338	100	4.7852	3.5817
2.9782	2.7698	3.6607	3.6463	3.0464
3.0500	3.9086	2.9494	3.4272	3.0177
2.8416	4.0020	5.9779	3.7829	2.8776
2.9243	4.9181	7.3179	4.4618	2.8632
2.2992	4.9504	8.6838	4.4187	2.5902
3.3733	3.0464	6.0546	4.2355	2.3459
1.8070	2.6512	3.1434	2.7590	2.0154

Experimental Data

Pour temperature - 825°C (1098K)*

Mould temperature - 25°C (298K)

Pressure - 760 torr (1.01×10^5 Pa)

Gas Level - 0.23 H_2/100 gm Al (S.T.P.)

2.8256	100	100	100	1.0281
1.2187	1.1252	100	1.1648	0.9239
0.8952	1.1504	1.9772	1.2079	0.7837
0.6183	1.1684	1.5494	1.2546	0.7765
0.6435	1.0246	1.2403	1.1072	0.7118
0.4350	0.8808	1.0102	0.9455	0.6723
0.2732	0.7406	0.9347	0.8017	0.4386
0.0899	0.4098	0.5105	0.4961	0.1474

*Grain Refined

Experimental Data

Pour temperature - 825°C (1098K)*

Mould temperature - 70°C (343K)

Pressure - 760 torr (1.01×10^5Pa)

Gas Level - 0.23 ml H_2/100 gm Al (S.T.P.)

1.6788	100	100	100	2.5021
0.3990	2.0203	100	1.1360	0.4350
0.4422	0.9814	100	1.0030	0.4062
0.4925	1.1504	1.1432	0.8448	0.3811
0.4674	1.0246	0.9958	0.9383	0.3595
0.4206	0.7981	0.6938	0.7621	0.3056
0.3487	0.7046	0.6687	0.6758	0.2624
0.1115	0.3703	0.3128	0.3703	0.0467

* Grain Refined

Experimental Data

Pour temperature - 825°C (1098K)*

Mould temperature - 250°C (523K)

Pressure - 760 torr (1.01×10^5 Pa)

Gas Level - 0.23 ml H_2/100 gm Al (S.T.P.)

4.3642	5.2522	100	2.8975	1.3193
2.2864	1.7759	2.3044	1.8370	0.9455
1.1360	1.9197	1.8334	1.9808	0.9383
1.2043	1.8262	1.8298	1.9916	0.9562
2.0599	1.9197	1.5926	1.6716	0.9131
0.8988	1.2978	1.3085	1.3553	0.8233
0.7873	1.0929	1.2762	1.1468	0.8053
0.5105	0.8017	0.8556	0.8125	0.5680

* Grain Refined

VACUUM MELT EXPERIMENTS

Experimental Data

Pour temperature - 700°C (973K)

Mould temperature - 275°C (548K)

Pressure - 0.20 torr (26.6Pa)

Gas Level - 0.07 ml H_2/100 gm Al (S.T.P.)

100	100	100	100	100
100	4.3583	100	100	100
4.5337	100	6.6502	10.0559	5.5579
3.8068	1.3931	2.5104	2.8076	3.3412
2.5749	4.4908	5.5974	5.6761	4.8596
1.5865	5.1390	9.4471	7.5419	2.7682
1.2856	1.9159	3.4952	3.1872	1.4110
0.6410	1.4146	1.5936	2.1738	1.2749

Experimental Data

Pour temperature - 700°C (973K)

Mould temperature - 275°C (548K)

Pressure - 760 torr (1.01×10^5Pa)

Gas Level - 0.07 ml H_2/100 gm Al (S.T.P.)

100	100	100	100	100
100	100	100	100	100
0.6124	0.4978	100	0.6554	0.3474
0.3581	0.5587	1.3644	0.4692	0.3402
0.3760	0.6876	0.6446	0.4799	0.5193
0.3975	0.9168	0.8344	0.8272	0.2937
0.3259	0.6804	0.7950	0.6912	1.1711
0.2149	0.3152	0.3402	0.2722	0.1576

Experimental Data

Pour temperature - 700°C (973K)

Mould temperature - 200°C (473K)

Pressure - 0.20 torr (26.6Pa)

Gas Level - 0.03 ml H_2/100 gm Al (S.T.P.)

100	100	100	100	100
19.0625	100	100	100	25.6725
0.9792	100	1.1047	0.7926	0.6205
0.9756	0.8536	0.5129	0.7568	0.4591
0.7783	0.7675	0.6312	0.7532	0.4770
0.3802	0.5523	0.7388	0.6994	0.3300
0.2439	0.6384	0.9325	0.7962	0.2654
0.1686	0.3874	0.6205	0.5488	0.1506

Experimental Data

Pour temperature - 700°C (973K)

Mould temperature - 370°C (643K)

Pressure - 0.20 torr (26.6Pa)

Gas Level - 0.03 ml H_2/100 gm Al (S.T.P.)

100	100	100	100	100
14.7586	100	100	100	1.1585
1.2194	1.1082	2.2022	1.5458	1.3450
1.1872	1.7610	3.1741	2.3851	1.6004
1.1226	2.1268	5.3404	2.8513	1.5996
1.0760	1.9332	3.7085	2.4173	0.9110
0.8393	1.2015	1.6964	1.4311	0.8106
0.3085	0.6420	0.9361	0.9182	0.4125

Experimental Data

Pour temperature - 700°C (973K)

Mould temperature - 300°C (573K)

Pressure - 1.50 torr (200 Pa)

Gas Level - 0.03 ml H_2/100 gm Al (S.T.P.)

8.5862	100	100	100	0.7101
0.9505	0.8716	3.0091	0.7819	0.5882
0.9469	0.9792	1.2481	0.7747	0.6886
0.7783	1.3019	1.0473	0.8393	0.6456
0.6671	1.3019	1.3486	0.8357	0.4735
0.5954	1.1620	1.2015	0.7209	0.4089
0.5093	0.7424	0.7568	0.5703	0.3049
0.4555	0.3228	0.2403	0.2008	0.1435

Experimental Data

Pour temperature - 700°C (973K)

Mould temperature - 280°C (553K)

Pressure - 760 torr (1.01×10^5 Pa)

Gas Level - 0.03 ml H_2/100 gm Al (S.T.P.)

0.6994	0.7101	100	0.4519	0.3336
1.1441	0.3945	100	0.3228	0.2367
0.4089	0.5021	0.7604	0.3551	0.2690
0.3587	0.9684	1.2266	0.9397	0.2331
0.3407	0.9971	1.0437	0.9361	0.1506
0.3623	0.7388	0.9505	0.7245	0.2403
0.3013	0.5344	0.7281	0.4735	0.2188
0.1793	0.2654	0.3228	0.2403	0.0897

Experimental Data

Pour temperature - 700°C (973K)

Mould temperature - 30°C (303K)

Pressure - 0.20 torr (26.6Pa)

Gas Level - 0.02 ml H_2/100 gm Al (S.T.P.)

100	100	100	100	100
100	100	100	100	100
0.4763	0.5408	3.7459	3.8569	0.9598
0.3760	0.5945	0.4906	0.5694	0.6339
0.3832	0.5049	0.4154	0.6124	0.4727
0.3080	0.3832	0.4297	0.5049	0.2937
0.2328	0.3689	0.4405	0.3259	0.1970
0.0931	0.3366	0.4297	0.2722	0.0824

Experimental Data

Pour temperature - 700°C (973K)

Mould temperature - 300°C (573K)

Pressure - 0.20 torr (26.6Pa)

Gas Level - 0.02 ml H_2/100 gm Al (S.T.P.)

1.9875	100	100	100	1.1711
0.6124	1.0242	3.7709	1.0278	1.4432
0.6052	1.3071	1.4611	1.2606	1.3895
0.4763	1.6724	7.0943	2.0627	0.5945
0.5085	1.2856	2.2275	1.5363	0.5694
0.5515	1.3071	1.7906	1.0851	0.5766
0.3796	0.7736	0.9454	0.6912	0.4047
0.1934	0.2650	0.2614	0.2614	0.1862

Experimental Data

Pour temperature - 700°C (973K)

Mould temperature - 300°C (573K)

Pressure - 1.5 torr (200 Pa)

Gas Level - 0.02 ml H_2/100 gm Al (.S.T.P.)

100	100	100	100	100
100	100	100	100	100
1.0171	0.6804	0.9275	0.8881	0.6016
0.7234	0.5408	0.6554	0.5229	0.6733
0.7019	0.8272	0.8129	0.7592	0.5049
0,5909	1.0063	0.9275	0.6267	0.3832
0.3939	0.6912	0.5587	0.5551	0.2686
0.2256	0.4297	0.4297	0.2686	0.0251

Experimental Data

Pour temperature - 700°C (973K)

Mould temperature - 200°C (473K)

Pressure - 760 torr (1.01×10^5 Pa)

Gas Level - 0.02 ml H_2/100 gm Al (S.T.P.)

0.1719	100	100	100	0.4226
0.3725	0.4692	100	0.4656	0.1826
0.1039	0.2435	0.6697	0.2650	0.2901
0.1003	0.5479	0.6339	0.3474	0.1074
0.1110	0.3832	0.4942	0.3653	0.0788
0.0430	0.2722	0.3760	0.2757	0.0394
0.0537	0.1540	0.3008	0.1612	0.0358
0.0394	0.0072	0.0215	0.0430	-0.0036

Experimental Data

Pour temperature - 700°C (973K)

Mould temperature - 90°C (363K)

Pressure - 0.20 torr (26.6Pa)

Gas Level - 0.02 ml H_2/100 gm Al (S.T.P.)

100	100	100	100	100
100	100	100	100	100
4.9998	0.3942	100	0.5054	0.6416
0.4480	0.3190	0.2258	0.4158	0.5591
0.2867	0.3190	0.2402	0.5519	0.4122
0.1864	0.6200	0.8387	0.6738	0.1434
0.0717	0.3799	0.5699	0.4480	0.0359
-0.0466	0.0789	0.2473	0.1075	0.0000

Experimental Data

Pour temperature - 700°C (273K)

Mould temperature - 120°C (393K)

Pressure - 0.20 torr (26.6Pa)

Gas Level - 0.02 ml H_2/100 gm Al (S.T.P.)

100	100	100	100	100
0.4839	100	100	2.5770	0.3011
0.6272	0.4086	0.4731	0.4086	0.3656
0.6057	0.4014	0.2509	0.3727	0.3656
0.3118	0.3763	0.3692	0.3548	0.3441
0.2545	0.5699	0.5304	0.5734	0.2186
0.2007	0.4122	0.5125	0.3907	0.5914
0.0466	0.1469	0.2509	0.0394	0.0036

Experimental Data

Pour temperature - 700°C (973K)

Mould temperature - 250°C (523K)

Pressure - 0.20 torr (26.6Pa)

Gas Level - 0.02 ml H_2/100 gm Al (S.T.P.)

100	100	100	100	100
0.5018	1.0322	4.6127	1.9247	1.4014
1.6989	0.7634	0.9605	0.9892	1.3118
0.6667	0.8279	1.1756	1.3333	0.8172
0.5340	0.7849	0.9355	1.0322	0.6416
0.5412	0.9856	1.4372	1.0752	0.5197
0.3333	0.7562	1.0609	1.1792	0.4767
0.0681	0.2294	0.4660	0.5089	0.2294

Experimental Data

Pour temperature - 700°C (973K)

Mould temperature - 525°C (798K)

Pressure - 0.20 torr (26.6Pa)

Gas Level - 0.02 ml H_2/100 gm Al (S.T.P.)

100	100	100	100	100
1.1398	0.8674	0.6882	0.6200	0.3226
1.0250	0.5806	0.6021	0.5591	0.9032
0.9713	0.2975	0.1613	0.4516	0.6774
1.0179	0.0609	-0.2796	0.1183	0.5770
0.6416	-0.2186	-0.5663	-0.3118	0.3799
0.9032	-0.2724	-0.8351	-0.7383	0.2688
1.8351	0.3118	-0.8351	-0.8422	-0.1362

Experimental Data

Pour temperature - 825°C (1098K)

Mould temperature - 275°C (548K)

Pressure - 0.35 torr (46.7 Pa)

Gas Level - 0.14 ml H_2/100 gm Al (S.T.P.)

100	100	100	100	100
3.0733	4.1277	4.2532	6.1503	12.2360
1.1727	23.7905	2.3920	1.4237	1.7393
1.1978	1.7536	5.8705	1.0651	1.7106
1.5492	1.0902	0.4411	1.2731	2.2557
0.7603	15.9656	2.8689	8.9295	1.0113
1.2229	10.3532	9.0156	8.5064	1.3914
0.4841	4.1779	5.1246	2.7039	1.5492

Experimental Data

Pour temperature - 825°C (1098K)

Mould temperature - 275°C (548K)

Pressure - 1.40 torr (187Pa)

Gas Level - 0.14 ml H_2/100 gm Al (S.T.P.)

9.2738	100	100	100	4.4791
3.3100	5.3721	9.9695	3.3638	1.2408
3.3495	0.8858	0.8678	1.0687	1.1978
1.8325	0.5379	0.5057	0.4662	1.0220
1.0687	0.1076	0.1865	0.4734	1.2767
1.1153	1.4058	1.5958	0.9575	1.2229
1.3986	3.0016	3.7762	1.7931	2.4135
1.3197	7.4126	8.7287	4.5185	1.2014

Experimental Data

Pour temperature - 825°C (1098K)

Mould temperature - 275°C (548K)

Pressure - 100 torr (1.33×10^4 Pa)

Gas Level - 0.14 ml H_2/100 gm Al (S.T.P.)

9.0443	100	100	100	2.1158
0.5917	1.9903	1.8361	1.3305	0.7674
0.7997	0.8607	0.8140	0.8858	1.1583
0.8714	0.9073	1.9365	0.9503	0.9647
1.1727	1.1978	0.7136	1.1978	0.9754
0.9467	1.7464	3.1845	2.7721	0.8965
1.1260	2.1051	1.9293	2.9048	1.3592
0.6383	1.3663	1.7895	0.8929	0.8140

Experimental Data

Pour temperature - 825°C (1098K)

Mould temperature - 275°C (548K)

Pressure - 760 torr (1.01×10^5Pa)

Gas Level - 0.14 ml H_2/100 gm Al (S.T.P.)

5.0565	100	100	100	10.0878
0.7495	1.4954	1.5421	1.4883	0.5738
0.9611	0.8392	0.8894	0.9073	1.0328
0.9431	0.8320	0.6527	0.8427	1.0687
1.0758	0.9682	0.6168	1.1547	1.1583
1.1081	3.1056	4.9848	2.5569	1.7321
0.9467	3.8981	7.4018	2.4565	1.0256
0.8248	2.6932	4.4540	1.5707	0.5917

Appendix VI

Sample Calculation of Dendrite Arm Spacing Measurement.

For each sample, the number of dendrite arm intercepts was counted for a fixed distance.

In a 20 mm. distance for sample 1138, the number of intercepts equalled 170.

Therefore the dendrite arm spacing was

$$= \frac{20 \text{ mm}}{170} = 0.118 \text{ mm} = 118 \mu \text{m}$$

Appendix VII

Solidification Rates in the Castings

Assumptions:

1) For a 10 cm high by 10 cm diameter cylindrical cast, the distance over which solidification occurred was 5 cm.

2) The local solidification times varied between 250 and 500 seconds [31].

Sample Calculation:

At a local solidification time of 250 seconds, the rate of solidification was

$$\frac{5 \text{ cm.}}{250 \text{ seconds}} \times \frac{3600 \text{ seconds}}{1 \text{ hr.}} = 72 \text{ cm/hr}$$

Since the local solidification times varied between 250 and 500 seconds, the solidification rates varied between

$$36 - 72 \text{ cm/hr}$$

These are very approximate values, as the solidification rate at any location within the ingot is certainly not constant throughout freezing.